7-5-2023 1:00 PM

Shedding Light on Hearing in Coma: Investigating the Applicability of Functional Near-infrared Spectroscopy for Assessing Auditory Function and Aiding Prognosis in Patients with Acute Disorders of Consciousness

Reza Moulavi Ardakani, *Western University*

Supervisor: Owen, Adrian M., *The University of Western Ontario*
Co-Supervisor: Debicki, Derek B., *The University of Western Ontario*
A thesis submitted in partial fulfillment of the requirements for the Master of Science degree in Neuroscience

Abstract

There is a critical need for a bedside neuroimaging tool to aid in the prediction of functional recovery outcomes for patients with acute disorders of consciousness (DoC) following severe brain injury. Current neurobehavioral examinations and prognosis tools have limitations in predicting good outcomes, leading to potential mistreatment or premature withdrawal of life support. Functional near-infrared spectroscopy (fNIRS) is a viable candidate for such purposes due to its portability and cost-effectiveness. Auditory processing, viewed as a multi-level and multifaceted brain function, could provide a sensitive and specific marker of residual cognitive function in unresponsive patients. This study aimed to investigate the effectiveness of fNIRS for hierarchical assessment of auditory function and evaluate its applicability for predicting recovery outcomes in acute DoC. The capability of fNIRS for such an application was demonstrated by validating it against fMRI in a healthy population and cross-validating it in an entirely unresponsive patient with cognitive-motor dissociation. An innovative fNIRS-focused method was developed to quantify patients' auditory function, and a data-driven method was explored to improve the sensitivity and specificity of auditory scores. Using these analytical tools, a direct association was found between auditory function and recovery outcome in a small patient cohort. Based on the study's findings, the crucial role of methodological considerations in the use of fNIRS was discussed, and specific modifications in the stimulus and optical montage designs were suggested to enhance the method's reliability.

Keywords

Functional near-infrared spectroscopy; functional neuroimaging; auditory processing; speech; language; severe acute brain injury; disorders of consciousness; coma; withdrawal of life-sustaining therapy; functional recovery outcome; prognosis; intensive care unit; Guillain-Barré syndrome

Summary for Lay Audience

“What happens next?” This is the first question on everyone's mind when someone falls into a coma. Predicting the functional recovery outcome for comatose patients is a critical yet challenging question, even for critical care professionals. These predictions play an important role in decisions made for patients by medical professionals and loved ones, especially when deciding whether to withdraw life support.

Currently, established neurologic examinations and prognosis tools have some limitations, especially in determining if an adequate functional recovery is possible. Advanced neuroimaging methods can help assess the degree of preserved brain function in unresponsive patients.

Depending on its severity, brain injury may not damage the brain's ability to hear sounds but may damage regions involved in recognizing speech and extracting meaning from it. Therefore, we can determine the extent of damage by assessing brain activity in response to stimuli with different acoustic and linguistic features and using the assessment results to predict recovery outcomes. fNIRS is a portable method that can be used at the bedside for comatose patients whose transfer to imaging departments is risky. It uses red light to measure changes in blood oxygenation and estimate the activity in the brain's regions.

This research used fNIRS to record the brain responses of thirty healthy participants and eight unresponsive patients while listening to specific stimuli. The method was found to be suitable for detecting healthy participants’ brain responses. Using the reference activation maps from the healthy participants, we could detect preserved auditory function in an entirely unresponsive patient who suffered from an autoimmune condition that rendered her paralyzed but did not damage her brain function. Additionally, the degree of preserved auditory function in the patient cohort was found to be a predictor of their functional recovery outcome. We concluded that fNIRS has the capacity to be used as a tool aiding prognosis, for which further improvements in the method and its validation in larger patient cohorts are essential.

To my father
whose will-to-be should've survived sever brain injury
and my mother
who's my why-to-be

Acknowledgment

I wish to express my profound gratitude to my supervisors, Dr. Adrian Owen and Dr. Derek Debicki. Their trust, support, patience, and guidance have been pivotal throughout my journey at Western University. Adrian enriched my understanding of the scientific endeavor and the life of a scientist, while Derek epitomized the pinnacle of kindness and professional integrity. I extend my thanks to BrainsCan for their grant to Dr. Debicki, which underpinned my research. Special appreciation goes to their assistants, Dawn Pavich and Kim Masseo, for their consistent efforts.

My gratitude extends to Dr. Brian Corneil, the Neuroscience Program Chair and the chair of my advisory committee, for his unwavering support. Dr. Jody Culham has also been invaluable as both an advisor and instructor. My thanks also go to Dr. Keith Lawrence and Dr. Teneille Gofton, other members of my advisory committee.

I thankful to Dr. Loretta Norton and the OwenLab members: Dr. Androu Abdalmalak, Dr. Sergio Novi, Matthew Kolisnyk, and Karnig Kazazian. Their contributions spanned from the project's conceptualization to data analysis. A special note of thanks to Matthew for not just his professional collaboration but also for being a compassionate friend.

I am eternally grateful to my brother, Hadi, whose steadfast presence and support were instrumental to this work's fruition. Equally, my mother's distant but ever-present concern and encouragement have been a source of strength.

The backdrop of my time at the Neuroscience program at Western was the challenging period of the COVID-19 pandemic. My heartfelt gratitude goes to all front-line and healthcare workers who braved personal risks for our collective safety.

Lastly, and of utmost significance, I honor the memory of Mahsa (Zhina) Amini. Her tragic and transformative passing stands as a poignant reminder of the profound challenges countless women endure under the oppressive patriarchal Islamic regime in Iran. As I penned this thesis, my thoughts were continually with the numerous Iranians who made the ultimate sacrifice, rallying for “زن، زندگی، آزادی”.

Table of Contents

Abstract ..... ***i***

Summary for Lay Audience ..... ***ii***

Acknowledgment ..... ***iiiv***

List of Tables ..... ***viii***

List of Figure ..... ***ix***

List of Appendices ..... ***xii***

List of Abbreviations ..... ***xii***

Chapter 1 ..... ***i***

1 Introduction ***1***

1.1 Clinical background **1**

1.1.1 Coma 1

1.1.2 Coma outcome 3

1.1.3 Prognostic and diagnostic challenges in acute and chronic DoC 4

1.2 Assessing auditory processing as a proxy to probing cognition and awareness **6**

1.3 Rationale **9**

1.4 Functional neuroimaging in DoC **11**

1.4.1 Auditory assessment in *chronic* DoC using PET/fMRI 11

1.4.2 Prognostic utility of functional neuroimaging in *acute* DoC 15

1.5 Hierarchical assessment of auditory function **17**

1.5.1 fMRI group results 19

1.5.2 Subject-level reproducibility in fMRI 19

1.6 Functional near-infrared spectroscopy **20**

1.6.1 The working principle of fNIRS 21

1.6.2 Modified Beer-Lambert Law 24

1.6.3 Estimation of hemoglobin concentration changes 25

1.6.4 Physiological confounds 27

1.7 Present study 28

Chapter 2 30

2 Methods 30

2.1 Participants 30

2.1.1 Healthy participants 30

2.1.2 Patients 30

2.2 Experimental Procedure 32

2.3 Auditory stimulus 35

2.4 Data Analysis 36

2.4.1 Preprocessing 36

2.4.2 Subject-level analysis 43

2.4.3 Group-level analysis 45

2.5 Brain maps 48

2.5.1 Brain activation maps 48

2.5.2 Brain activation frequency maps 50

2.6 Hemodynamic responses 50

2.7 Comparisons 51

2.7.1 Individual-group similarity 51

2.7.2 Between-group comparisons 52

2.7.3 Inter-subject comparisons 52

2.7.4 Prognostic utility 54

Chapter 3 55

3 Results 55

3.1 Healthy participants individual results 55

3.2 Healthy participants' group results 61

3.2.1 Sound Perception 61

3.2.2 Speech Perception 65

3.2.3 Language Comprehension 69

3.3 Patients 73

3.4 Individual-group similarity 76

3.5 Group-level comparisons 78

3.6 Subject-level rankings 79

3.6.1 Rankings 81

3.6.2 Prognostic utility 84

Chapter 4 92

4 Discussion 92

4.1 Validation against fMRI in healthy participants 93

4.2 Between-group comparison results 97

4.3 Single-case cross-validation 98

4.4 Prognostic utility 100

4.5 Scoring method 103

4.6 Data-driven approach 105

4.7 Applicability and methodological implications 107

4.8 Limitations and future directions 110

4.9 Conclusion 1144

References 1166

Appendices 1322

Curriculum Vitae 1555

List of Tables

Table 2.1 Patients' clinical and demographic information. 31

Table 2.2 Optical montage's anatomical coverage per channel. 33

Table 2.3 HbO and HbR extinction coefficients per wavelength. 42

Table 2.4 Contrast vectors 45

Table 3.1 The Sensitive and Specific overall scores' parameters. 81

Table 3.2 Summary of the rankings and their prognostic utility. 85

List of Figures

Figure 1.1 Distributed functional anatomy of speech processing per the “dual-stream” model..... 7

Figure 1.2 Auditory processing hierarchy 18

Figure 1.3 Absorption Spectra of Hemoglobin..... 22

Figure 1.4 Optical channels 22

Figure 2.1 Optical Montage 32

Figure 2.2 A block of the auditory stimulus 35

Figure 2.3 Preprocessing pipeline..... 36

Figure 2.4 Short channel quality check..... 37

Figure 2.5 Hybrid motion artifact correction. 41

Figure 2.6 The voxels corresponding to each channel..... 49

Figure 3.1 HbO and HbR responses. Healthy participant #1 to #6..... 56

Figure 3.2 HbO and HbR responses. Healthy participant #7 to #12..... 57

Figure 3.3 HbO and HbR responses. Healthy participant #13 to #18..... 58

Figure 3.4 HbO and HbR responses. Healthy control #19 to #24. 59

Figure 3.5 HbO and HbR responses. Healthy control #25 to #30. 60

Figure 3.6 Speech Perception group t-maps. 61

Figure 3.7 Sound Perception activation frequency maps..... 62

Figure 3.8 Hemodynamic responses in the channels with the peak HbO and HbR response in the Sound Perception contrast..... 64

Figure 3.9 Speech Perception group t-maps. 65

Figure 3.10 Sound Perception activation frequency maps..... 66

Figure 3.11 Hemodynamic responses in three highly activated channels in the Speech Perception contrast. 68

Figure 3.12 Language Comprehension group activation maps. 69

Figure 3.13 Language Comprehension activation frequency maps. 70

Figure 3.14 Hemodynamic responses in three highly activated channels in the Language Comprehension contrast. 72

Figure 3.15 HbO and HbR responses. Patient #1 to #5. 73

Figure 3.16 HbO and HbR responses. Patient #6 to #8. 74

Figure 3.17 Reference HbO and HbR activation maps from the control group for patients. 76

Figure 3.18 Individual-group similarities per group and contrast. 77

Figure 3.19 Between-group Glass' Δ effect sizes for each Hb response per contrast 80

Figure 3.20 Sound Perception similarity scores ranking (average HbO/HbR) 86

Figure 3.21 Speech Perception similarity scores ranking (average HbO/HbR) 87

Figure 3.22 Language Comprehension similarity scores ranking (average HbO/HbR) ... 88

Figure 3.23 Balanced overall scores raking (average HbO/HbR) 89

Figure 3.24 Specefic overall scores ranking 90

Figure 3.25 Sensitive overall scores ranking 91

List of Appendices

Appendix A: Ethics Approval 131

Appendix B: Letter of information and consent form (healthy participants) 132

Appendix C: Letter of information and consent form (Patients) 140

Appendix D: Permission from Springer for Figure 1.1 152

List of Abbreviations

ANOVA	analysis of variance
AR	auto regressive
BOLD	blood-oxygen-level-dependent
CRS	coma recovery scale
CW	continuous-wave
DoC	disorders of consciousness
DPF	differential pathlength factor
EEG	electroencephalography
FDR	false discovery rate
fMRI	functional magnetic resonance imaging
fNIRS	functional near-infrared spectroscopy
GBS	Guillain-Barré syndrome
GCS	Glasgow coma scale
GLM	general linear model
GOS(E)	Glasgow outcome scale (extended)
HbO	oxygenated hemoglobin
HbR	deoxygenated hemoglobin
HRF	hemodynamic response function
ICU	intensive care unit
IFG	inferior frontal gyrus
ITG	inferior temporal gyrus
MCS	minimally conscious state
MTG	middle temporal gyrus
PET	positron emission tomography
PVS	persistent vegetative state
ROI	region of interest
SMC	sensorimotor cortex
STG	superior temporal gyrus
TBI	traumatic brin injury
UWS	unresponsive wakeful syndrome
VLF	very low frequency
WLST	withdrawal of life-sustaining therapy

it arrives with hardly
any notice,
and stays—
until

have no fear!
we're here—
shining light in,
hoping to find you sitting
in the shadows there,
hearing us ok.

Chapter 1

1 Introduction

This research aimed to explore the potential of functional near-infrared spectroscopy (fNIRS), a portable optical neuroimaging technique, for identifying the neural correlates of auditory processing and predicting functional recovery outcomes in patients with acute brain injury. Three components were integral to the investigation: fNIRS methodology, auditory processing assessment, and prognostic utility of fNIRS-based auditory assessments in acute brain injury.

This chapter integrates these components to formulate the research question and proposed solution. The next two sections (1.1 and 1.2) provide the background information to support the research rationale explained in section 1.3. Section 1.4 reviews previous functional neuroimaging studies on severe brain injury that have laid the groundwork for this research. Section 1.5 presents an in-depth description of the auditory assessment paradigm employed in this study. Section 1.6 introduces the characteristics and working principle of fNIRS. Finally, the research objectives and hypotheses are outlined in section 1.7.

1.1 Clinical background

1.1.1 Coma

Acute brain injury may result in a range of disorders of consciousness (DoC) characterized by distributions in arousal and/or awareness, the physiological mechanisms that regulate conscious behavior (Giacino et al., 2014). Coma is one of the most severe forms of acute brain injury where arousal and awareness are both substantially impacted (Young, 2009a). It is a medical emergency and may require life support measures such as mechanical ventilation, intravenous fluids, and medication to stabilize vital signs until the underlying cause can be diagnosed and treated. While the clinical manifestations of coma can vary depending on the underlying cause, its typical behavioral signs include closed eyes, unresponsiveness to external stimuli, reduced or absent brainstem reflexes, and an inability to perform voluntary movements (Posner et al., 2019).

Coma can be caused by various types of brain damage, which are categorized into two main groups: structural brain lesions and metabolic disturbances (Posner et al., 2019). Structural brain lesions can be caused by both traumatic brain injury (TBI) and non-traumatic events that damage the brain tissue. In contrast, anoxic-ischemic encephalopathy is a type of metabolic disturbance that occurs due to cardiac arrest, infection, or toxicity. These metabolic disturbances can impair the brain's normal functioning and lead to coma.

Coma is challenging to characterize due to variations in clinical presentation and similar behavioral symptoms that are shared by a spectrum of altered states of consciousness or several neurological conditions that mimic coma (Posner et al., 2019). As a clear example, locked-in syndrome, which is typically caused by injury in the ventral pontine nuclei, is a condition where patients are conscious but have minimal (eye-opening) or no response to stimuli, similar to coma (Laureys et al., 2005; Smith & Delargy, 2005). Another example is Guillain-Barré syndrome (GBS), an autoimmune condition that affects the peripheral nervous system (sparing the central nervous system like the spinal cord and brain). In its severe cases, patients are conscious but experience total paralysis rendering them behaviorally unresponsive (Bauer et al., 1979).

Locked-in syndrome and severe GBS are instances of covert consciousness or what is referred to as “cognitive-motor dissociation,” as they both involve a dissociation between the cognitive function and motor control (Schiff, 2015). While patients’ medical history and clinical tools can aid the differential diagnosis in some cases, not all cases of cognitive-motor dissociation can be detected using these methods.

In clinical practice, standardized measures are necessary to quantify the severity of brain injury, including coma. The Glasgow Coma Scale (GCS) is a standardized neurological scale that evaluates the level of consciousness in patients with brain injury by assessing eye opening, verbal response, and motor response (Teasdale & Jennett, 1974). Higher scores on the GCS indicate better neurological function, with a maximum score of 15 representing full consciousness and normal neurological function. A GCS score of 8 or less is typically classified as coma, with a score of 3 indicating the deepest level of coma.

Although the GCS is a widely accepted scale, it has some recognized shortcomings (Green, 2011; Teasdale et al., 2014): It does not have good inter-rater reliability, meaning that different raters assign inconsistent scores to the same individual; it has limited ability to score the verbal component in endotracheally intubated patients and is inadequate in assessing brainstem functionality or respiratory patterns.

1.1.2 Coma outcome

Coma is a transient state typically not lasting more than several weeks (Laureys et al., 2004). Depending on the degree of brain damage, various outcomes are possible. Patients that survive and emerge from coma (i.e., regain behavioral responsiveness) may experience a full or partial recovery that allows for sufficient function for independent activities of daily life. This is what is referred to as a "good outcome." In contrast, those who survive but do not regain behavioral responsiveness transit into the sub-acute (> 28 days) and, subsequently, the chronic phase of DoC. These chronic DoC patients are often characterized into two groups: unresponsive wakeful syndrome (UWS, previously known as the persistent vegetative state (PVS)) and minimally conscious state (MCS). "Poor outcome" is attributed to UWS or any other condition with severe disability and total dependency.

The UWS refers to a condition in which a patient regains wakefulness but does not show reproducible signs of awareness (Jennett & Plum, 1994). The MCS, meanwhile, occurs when a patient regains some degree of awareness (Giacino et al., 2002): MCS- is defined by the emergence of reproducible but low-level signs of consciousness, while MCS+ corresponds to the reappearance of behavioral signs of language capabilities (Bruno et al., 2011). UWS and MCS patients may regain higher degrees of awareness and neurological functionality in various unpredictable timeframes.

Although most patients with severe brain injury require intensive care and depend on life-sustaining therapies in the acute phase, only a small percentage of them progress to death. That is to say, most patients are able to be resuscitated from their primary injury and kept alive with life-sustaining therapies in the intensive care unit (ICU). Rather, in many cases, the withdrawal of these life-sustaining therapies, based on discussions regarding

goals of care with substitute decision-makers, leads to death (Mark et al., 2015; Turgeon et al., 2011, 2013). This highlights the cruciality of prognosis in acute severe brain injury.

A measure called Glasgow Outcome Scale (GOS) was created to quantify the degree of functional recovery after severe brain injury (Jennett & Bond, 1975). The scale comprises five categories, with scores ranging from 1 (death) to 5 (good recovery). Its extended version, GOSE, ranges from 1 (death) to 8 (upper good recovery) (Jennett & Plum, 1994). Both scales measure an individual's ability to perform activities of daily living, such as self-care, mobility, communication, and social interactions. The GOSE has become a standard measure for clinical trials, and it is used by researchers to assess outcomes and by clinicians to inform patient care (Wilson et al., 1998).

1.1.3 Prognostic and diagnostic challenges in acute and chronic DoC

When making decisions about withholding or withdrawing life support for comatose patients, medical professionals will consider a variety of factors, including the patient's medical condition and predicted functional recovery outcome. The likelihood, extent, and speed of functional recovery can vary widely, depending on the individual patient, the cause and severity of the coma, and the effectiveness of the treatment and rehabilitation (Edlow et al., 2020). In many cases, the decisions regarding withholding or withdrawing life support heavily rely on the predicted outcome, with a focus on minimizing patients' suffering (Turgeon et al., 2011, 2013). Furthermore, the prognosis also impacts the choice of early interventions and treatments and subsequent rehabilitative measures, influencing the outcome and quality of life after recovery. For these reasons, providing an accurate prognosis for patients with acute brain injury is critical (Weijer et al., 2016).

Currently, prognosis in acute brain injury is mainly informed by neurological examinations: assessing GCS (and/or other standardized coma scales), brainstem reflexes, and respiratory function (Wijdicks et al., 2006; Young, 2009b). However, the accuracy of these bedside neurobehavioral examinations is limited by several factors, including patients' sensorimotor dysfunctions and fluctuating states and examiners' subjective assessments, especially in patients with inconsistent or ambiguous behavioral

responses (Gill-Thwaites, 2006; Green, 2011; Stevens & Sutter, 2013). The unreliability of neurobehavioral examinations can be mitigated by complementing them with anatomical neuroimaging, electrophysiological tests, and biochemical markers (Hawkes & Rabinstein, 2019; Kamps et al., 2013); however, all these methods fall short of predicting *good* outcomes, i.e., prognosis indicates a poor outcome *only* with a high *specificity* (Kamps et al., 2013; Young & Schiff, 2014). The current method's unreliability and limitation in predicting a good outcome increase the risk of mismanagement and premature withdrawal of life support for patients (Turgeon et al., 2011, 2013; Weijer et al., 2016).

The challenge of prognosis in the acute phase of DoC partly stems from the limitations of established methods to evaluate residual brain function directly and precisely. This shortcoming also hinders the diagnosis of DoC, resulting in misdiagnosis in between 20% to 40% of cases (Andrews et al., 1996; Childs et al., 1993; Kondziella et al., 2016; Schnakers et al., 2009). This misclassification can negatively affect the goal-of-care decisions for chronic DoC patients, particularly those in an MCS whose awareness may not be clinically detected, leading to possible misclassification as UWS and the potential for withdrawal of life support (Schiff, 2015).

Over the last two decades, functional neuroimaging has greatly advanced the evaluation of cognitive function and awareness levels in unresponsive patients (Fernández-Espejo & Owen, 2013; Marino et al., 2023; Owen, 2020; Sanz et al., 2021). Initially, scientists used positron emission tomography (PET) and functional magnetic resonance imaging (fMRI) to detect preserved islands of cognitive function in unresponsive patients despite their clinical diagnoses of a PVS in the late 90s and early 2000s. In a groundbreaking study, Owen et al. (2006) demonstrated that fMRI could detect covert awareness in an unresponsive patient previously thought to be in a vegetative state. In a similar vein, Cruse et al., (2011) utilized electroencephalography (EEG) to reveal undetected awareness in unresponsive patients. Monti et al. (2010) further expanded the possibilities for diagnosis and treatment of chronic DoC by showing that fMRI could be used to communicate with unresponsive patients who were misdiagnosed as being in a UWS.

The advancements in this line of research have prompted the European Academy of Neurology (Kondziella et al., 2020) and the American Academy of Neurology (Giacino et al., 2018) to recommend the use of functional neuroimaging to improve existing diagnostic routines.

1.2 Assessing auditory processing as a proxy to probing cognition and awareness

Patients with DoC cannot engage in any experimental paradigm that requires consistent and reproducible behavioral responses; therefore, the integrity of their brain functions has to be assessed by probing neural correlates of the respective brain functions. Experimental paradigms that have been utilized for this purpose fall into two categories based on the presence or absence of a task: task-based and resting-state studies (Sanz et al., 2021). As the name suggests, a patient's brain activity at rest is evaluated in resting-state studies. In task-based studies, the researchers are interested in a patient's brain activity in response to external input. Task-based paradigms are classified as either passive or active.

In passive paradigms, patients' sensory, affective, and cognitive functions are examined by subjecting them to various stimuli and evaluating the elicited neural activity (Sanz et al., 2021). In contrast, active paradigms aim to assess patients' awareness, reflected in the willful modulation of their brain activity in response to task demands: Detection of neural activation in the brain regions that are associated with following the commands in healthy participants implies that the patient is actively engaging in the task and, hence, retains some degree of awareness (Boly et al., 2007; Owen & Coleman, 2008).

Auditory stimuli are frequently utilized in neuroimaging studies of DoC, serving the dual purpose of assessing residual auditory and higher-order cognitive functions in *passive* paradigms and conveying task instructions and voice commands in *active* paradigms. As such, patients without preserved auditory function cannot participate in (common) active tasks, and as a result, independent assessments of auditory processing are necessary to corroborate the results of active paradigms. Thus, evaluating auditory processing is a proxy for assessing cognition and probing awareness in DoC patients.

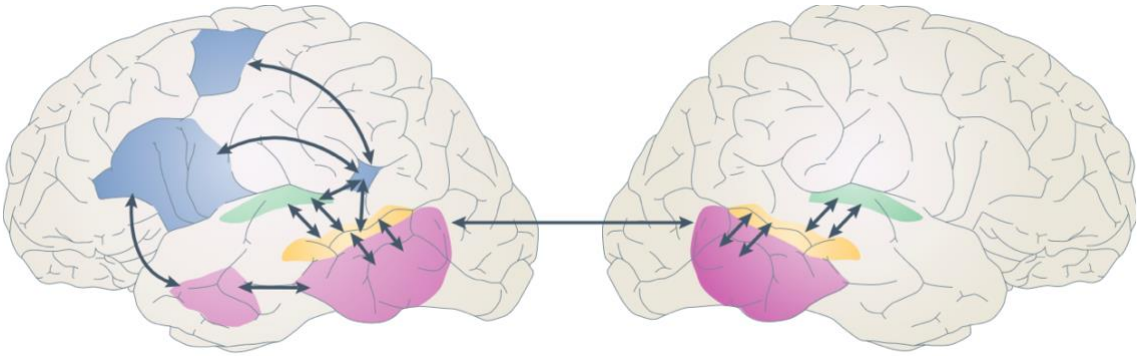

Figure 1.1 Distributed functional anatomy of speech processing per the "dual-stream" model. The initial stage involves acoustic analysis in the primary auditory cortices bilaterally (green), followed by phonological processing in the mid-to-posterior superior temporal sulcus (yellow). The model then diverges into two ventral (purple) and dorsal (blue) streams, with the latter involved in the lexical-semantic processing and the latter mapping phonological representations onto articulatory motor representations (Hickok & Poeppel, 2007). *Adopted with permission from Hickok & Poeppel (2007)*

Auditory processing is a brain function involving a range of cortical regions and networks that work in parallel and hierarchical order, enabling individuals to distinguish different sounds at the basic level, identify speech patterns within the sounds, and extract meaning from the speech at the higher level (Davis & Johnsrude, 2003; Hertrich et al., 2020; Hickok & Poeppel, 2007; Hickok , 2022; Okada et al., 2010; Pardo et al., 2021; Price, 2012; Rodd et al., 2005; Vigneau et al., 2006).

The broad distribution of cortical regions involved in auditory processing is evident in the well-known "dual-stream" model of language as demonstrated in Figure 1.1 (Hickok & Poeppel, 2007): The earliest stage of cortical speech processing involves acoustic spectrotemporal analysis of the sounds in the primary auditory cortices bilaterally, including parts of the transverse temporal gyrus (known as Heschl's gyri) and superior temporal plane, both within the superior temporal gyrus (STG). In the next stage, phonological processing occurs in the middle to posterior portions of the superior temporal sulcus, possibly with some degree of left-lateralization.

According to the model, the system then diverges into dorsal and ventral streams (Hickok & Poeppel, 2007): The ventral stream maps phonological representations onto conceptual representations. The posterior regions of the ventral stream, located in the posterior middle temporal gyrus (MTG) and inferior temporal gyrus (ITG) bilaterally, link

phonological and semantic information as a lexical interface, while the more anterior region corresponds to the syntactic and compositional semantic operations.

The dorsal pathway maps phonological representations onto articulatory motor representations and includes the left temporoparietal junction, which contains Wernicke's area and the angular gyrus, serving as a sensorimotor interface, as well as portions of the articulatory network in the left inferior frontal gyrus (IFG) (known as Broca's area) and a more dorsal premotor region.

Additionally, auditory processing is not just a multi-level but also a multifaceted brain function that involves the recruitment of deeper cortical and subcortical regions, depending on linguistic features, cognitive demand, and affective salience of the stimuli (Friederici, 2006; Ketteler et al., 2008; Paulmann et al., 2011). Therefore, compared to passive paradigms that use noxious, thermal, olfactory, or tactile stimuli, auditory paradigms offer the advantage of engaging and testing a wide range of neural processes involved in auditory processing. This feature can be harnessed to develop a hierarchical test that provides higher specificity (i.e., lower false positives) than passive paradigms using the other mentioned stimuli.

Active paradigms enable the inference of higher levels of cognitive function and the exclusive probing of awareness, resulting in more specific results than passive paradigms. Nevertheless, active paradigms might not be as sensitive in detecting lower degrees of preserved brain functions. False negative cases can occur when a patient has enough cognitive capacity to process and comprehend the instructions but their high-order cognitive functions (e.g., executive function, working memory) are compromised due to factors like mental fatigue, lack of extended attentional span, or sedative effects of the administered treatments (Norton, 2017a; Norton et al., 2023). In such scenarios, complementing the active paradigms with the less cognitively demanding passive tasks could improve the sensitivity of the testing routine.

1.3 Rationale

Estimations of the likelihood and degree of functional recovery are the key factors in discussions regarding the treatment, rehabilitation, and continuation or withdrawal of life-sustaining therapies for comatose patients or those that appear comatose (Turgeon et al., 2011, 2013).

The neurobehavioral assessments that are currently at the core of the prognosis guidelines are not reliable enough to guarantee the high degree of accuracy and determinacy required for such critical decisions (Gill-Thwaites, 2006; Green, 2011; Stevens & Sutter, 2013). Furthermore, although existing prognosis tools have a high specificity in predicting poor outcomes (Kamps et al., 2013; Sandroni et al., 2020; Wijdicks et al., 2006), they cannot predict good functional recovery, possibly leading to mistreatment or premature withdrawal of life support (Weijer et al., 2016; Young, 2009).

A main challenge in predicting recovery outcomes is the limitations of current methods for accurately assessing brain function in the early days of severe brain injury. Functional neuroimaging can overcome this challenge by bypassing neurobehavioral markers and directly assessing the integrity of brain function. This critical advantage of functional neuroimaging over existing clinical tools has proven effective in diagnosing chronic DoC (Fernández-Espejo & Owen, 2013; Marino et al., 2023; Owen, 2020; Sanz et al., 2021), encouraging clinicians to incorporate functional neuroimaging into their diagnostic routines (Giacino et al., 2018; Kondziella et al., 2020).

Functional neuroimaging methods developed for diagnostic purposes in *chronic* DoC can be translated and expanded to assess brain function and aid prognosis in *acute* DoC. This requires tailoring the experimental task and neuroimaging method to fit the characteristics of acute patients, including their unstable conditions and need for intensive care. An ideal experimental test for assessing brain function in acute DoC patients should be sensitive enough to detect even minimal residual brain function in those with varying neurological deficits, while also being specific enough to distinguish between different levels of retained or regained cognitive function over time. Given that auditory processing can be viewed as a multi-level (i.e., acoustic, phonological, and semantic) and

multi-dimensional (e.g., sensory, cognitive, affective) brain function, a *graded* and *encompassing* assessment of auditory function may provide the required sensitivity and specificity.

To minimize the risk of adverse events, it is crucial to limit the transportation of acutely brain-injured patients who are often on life support and in an unstable and critical condition for neuroimaging purposes (Weijer, 2019; Weijer et al., 2016). However, fMRI, the gold-standard neuroimaging method, cannot be used at the bedside, substantially limiting its applicability to intensive care unit patients. On the other hand, although EEG is widely available at the bedside in intensive care units, it is highly susceptible to noise and has a poor spatial resolution, limiting its applicability as a prognosis aid. Therefore, complementary or multimodal neuroimaging methods are needed at the bedside in ICUs (Kazazian et al., 2021; Owen, 2019; Sanz et al., 2021).

With a spatial resolution superior to EEG, fNIRS has recently attracted increasing attention for clinical applications as it is a non-invasive, portable, and cost-effective neuroimaging tool (Chen et al., 2020). fNIRS estimates neural activity by using light to measure cortical blood oxygenation and deoxygenation changes. With these beneficial features, fNIRS is a viable candidate for use in the ICU as a bedside tool to assess unresponsive patients' residual cognitive function and awareness (Abdalmalak et al., 2017, 2020, 2021; Owen, 2019; Rupawala et al., 2018; Si et al., 2023). To assess the applicability and reliability of fNIRS for such critical use, validation (proof-of-concept) studies are needed in both healthy and patient populations.

This study was motivated by the pressing need for an effective bedside tool to aid in outcome prognosis in the early stages of severe brain injury. In light of the matching features of fNIRS for this application, the study aimed to investigate the feasibility of using fNIRS for hierarchical assessment of auditory processing in healthy participants, as well as evaluating the usefulness of fNIRS-based auditory assessments for predicting recovery outcomes in a small sample of unresponsive patients. With a methodological focus, this study may contribute to the development of a clinically relevant and reliable prognostic tool for acute DoC.

1.4 Functional neuroimaging in DoC

Functional neuroimaging studies of DoC can be categorized based on the employed method (e.g., PET, fMRI, EEG), experimental paradigm (active or passive tasks-based, resting-state), chronicity of the brain injury (acute, chronic), and the intended clinical aim (diagnostic, prognostic).

1.4.1 Auditory assessment in *chronic* DoC using PET/fMRI

Using functional neuroimaging to study DoC originated in 1997 when PET was first utilized to assess auditory processing in a boy with a trauma-induced extensive lesion in his left hemisphere (de Jong et al., 1997). Auditory stimuli with two conditions, an affective speech of the boy's mother and non-word sounds, were utilized. Despite his PVS diagnosis, a stronger response to the affective speech was observed in the right middle temporal, anterior cingulate, and precentral gyri. The authors viewed the detected activity in the temporal lobe and limbic structures as evidence of the integrity of the neural circuitry involved in processing the affective connotation of sound. The activated region in the precentral gyrus was anterior to the mouth representation on the motor strip. The authors speculated that this could possibly reflect the patient's attempt to respond. Nevertheless, they regarded it as an open question whether the patient was actually able to comprehend the content of his mother's voice, or only retained the sensory capacity to detect the voice's affective intonation. The findings, however, left enough room for the authors to suggest that the distinction between the PVS and locked-in syndrome is not binary but gradual.

A series of single or multiple case studies followed with the similar aim of evaluating residual cognitive function in patients with a PVS diagnosis. The employed techniques were PET (Menon et al., 1998; Owen et al., 2002), magnetoencephalography (Ribary et al., 1998; Schiff et al., 2002), or combined PET/fMRI (Owen et al., 2005). All these studies detected some "islands" of preserved cognitive function, an observation that was inconsistent with the patients' PVS diagnosis. For example, Owen et al. (2002) observed in a PVS patient a differential response to signal-correlated noise (vs. silence) bilaterally in the primary auditory cortex reflecting the patient's acoustic processing capability.

The patient also had a more robust response to spoken words (vs. signal-correlated noise) in the superior temporal plane bilaterally and in the left hemisphere's planum temporale, resembling healthy participants' observed activation pattern while listening to speech (Mummery et al., 1999). The authors concluded that the patient retained the neural capacity to recognize speech (from non-speech). Although this observation was followed by the patient's significant recovery in the months following the test, it still remained unresolved whether the patient was conscious and could grasp the content of the speech during the test.

Going beyond case studies, in the early 2000s, two PET studies evaluated the brain response to auditory (Laureys et al., 2000) or noxious stimuli (Laureys et al., 2002) in larger samples of patients with a PVS diagnosis. Boly et al. (2004) took the work a step further and utilized PET to compare the cortical integrity of 15 patients in a PVS with five patients in an MCS, a newly-established diagnosis at the time (Giacino et al., 2002). They presented the healthy controls and patients with simple auditory clicks and observed activation in primary and secondary auditory regions (Heschl's gyri and superior surface of the STG) across groups. However, like healthy controls, MCS patients distinguished themselves from PVS patients by showing activation in the lateral STG, and also preserved functional connectivity between the secondary auditory regions and downstream higher-order temporal (posterior STG and MTG) or frontal (inferior, middle, and superior) gyri. Although all the described studies found traces of residual cognitive processes in unresponsive or minimally responsive patients, none had conclusive evidence for ascribing awareness to the patients.

It was not until 2006 that preserved awareness in an otherwise unresponsive patient meeting the criteria for PVS was confirmed using functional neuroimaging. In a landmark study by Owen et al. (2006), a 23-year-old woman with severe traumatic brain injury underwent two fMRI tests five months after the injury. The patient was first tested for neural response to auditory stimuli at two hierarchical levels: speech perception (spoken sentences vs. acoustically matched noise signal) and language comprehension (high ambiguity sentences, e.g., "The *creak* came from a *beam* in the *ceiling*").

At both levels, the patients had cortical responses that resembled the activation pattern in the healthy participants. Specifically, the STG and MTG were activated in response to speech (vs. noise), and the semantically ambiguous sentences elicited activation in the left IFG. This observation strongly suggested that the patient's neural circuitry associated with semantic processing, as a high-level auditory function, was intact but did not necessarily entail her conscious experience of the sounds and their meaning.

To fill this inference gap, a characteristic of passive tasks, researchers tested the patient with an active task (command-following via mental imagery) for which she was provided with verbal instructions: she had to imagine either playing tennis or that she was visiting all the rooms in her house upon hearing the corresponding voice commands. Strikingly, the patient's neural responses to both commands matched the control group's activation patterns in the task. For this to happen, the patient had to comprehend the instructions and willfully manipulate her imagination in response to the commands. Neither of these could be done without retaining awareness or conscious experience. This was a groundbreaking finding, yet it left a question to answer: Can semantic processing occur without awareness?

Davis et al. (2007) approached this question using anesthesia as an instance of reduced consciousness. Twelve volunteers were tested for three levels of auditory processing using fMRI in three propofol-induced sedation conditions: awake, lightly, and deeply sedated. They detected robust and bilateral activity in Heschl's gyri elicited by sensory processing of sound (noise vs. silence) in all three conditions. In contrast, the neural correlates of speech perception (low ambiguity sentences vs. noise) were sustained only under light sedation. Specifically, although the speech perception contrast elicited activity in the temporal cortex regardless of the sedation level, the inferior frontal gyrus and premotor cortex activations detected in the awake and lightly sedated conditions were absent while the participants were deeply sedated. At a higher level in the auditory processing hierarchy, the individuals were also tested for neural correlates of language comprehension. Assuming language comprehension requires resolving semantic ambiguity, the participants' brain responses to highly ambiguous sentences were contrasted with their neural responses to sentences with low ambiguity.

They found that in this contrast, the bilateral IFG and left posterior temporal lobe activations were present only when the participants were awake. In other words, neural signs of language comprehension were absent in the deeply sedated condition and even when light sedation was induced. This finding suggested that passive tasks' inherent gap for inferring awareness is smaller at higher levels of auditory processing.

Coleman et al. (2007) employed fMRI in conjunction with a largely similar hierarchical paradigm (Rodd et al., 2005) to evaluate auditory processing in seven patients diagnosed as PVS, five MCS patients, and two severely disabled but responsive patients who had emerged out of MCS. As expected, the responsive patients showed robust evidence of sensory processing of sound (temporal activation) and speech perception (temporal and frontal activations), as well as anatomically appropriate signs of semantic ambiguity resolution (temporal and frontal activations). That said, the activations were less statistically significant for the subtle language comprehension contrast (high ambiguity sentences vs. low ambiguity sentences) than the sensory and speech processing contrasts. In addition, among the rest of the patients, only five (three PVS and two MCS patients) showed significant yet nonhomogeneous signs of auditory processing in the sound and speech perception contrasts. Only three of these five patients showed signs of semantic ambiguity resolution, two of whom had a PVS diagnosis. Although these high-level activations did not reach significance ($p < 0.1$), they challenged those two PVS diagnoses.

Expanding beyond just diagnostic implications, a follow-up fMRI study by Coleman et al. (2009) investigated the prognostic utility of the same hierarchical paradigm in a larger cohort of chronic DoC patients. This study included 22 and 19 patients who met the criteria for PVS and MCS, respectively. The Coma Recovery Scale (CRS) was used to track changes in patients' levels of consciousness and recovery from coma. In parallel, a discrete scoring method based on binary clustering was used to quantify patients' residual auditory function. To this end, having or lacking a certain level of auditory processing capability was first decided for each patient based on the presence or absence of brain activity within the region of interest (ROI) extracted from the healthy control group. Next, patients were clustered and assigned a score based on their place in the auditory

processing hierarchy: 1 = no response to sound; 2 = low-level perception of sound; 3 = mid-level perception of speech; and 4 = high-level language comprehension. The prognostic utility was then derived by calculating Spearman's rank-order correlation between patients' CRS scores and the assigned auditory processing scores.

The above procedure demonstrated a significant association between patients' auditory function and their CRS scores six months after the test ($r = 0.81, p < 0.001$). Specifically, seven out of eight PVS patients who emerged to an MCS had six months earlier shown a mid- or high-level of auditory processing capability. However, at the time of the test, the association between patients' CRS and auditory function scores only approached significance ($p < 0.06$). This study highlighted the prognostic utility of the "islands" of preserved cognitive function detected in chronic DoC patients.

1.4.2 Prognostic utility of functional neuroimaging in *acute* DoC

While a large body of research has been conducted to assess brain function in *chronic* DoC using functional neuroimaging, few studies have applied it to the context of *acute* severe brain injury, including coma. This is partly due to the practical challenges of testing patients under intensive critical care in medically unstable and extremely vulnerable conditions, especially when it requires transporting them from the ICU to imaging departments.

Several studies utilizing fMRI have been carried out to assess its prognostic value in comatose patients using various experimental paradigms. One of the earliest studies was by Moritz et al. (2001), which reported intact sensory processing to sound, tactile and visual stimuli in a comatose TBI patient. The patient subsequently recovered cognitive and sensorimotor functions, providing the first evidence that fMRI may be useful for prognosis in acute brain injury. In 2009, Gofton et al. used a passive tactile paradigm in a group of comatose patients and found that those who recovered consciousness had greater activation in the primary somatosensory cortex than patients who did not recover. Additionally, studies conducted by Norton et al. (2012) and Koenig et al. (2014) used resting-state fMRI and found that connectivity strength within the default mode network was associated with outcomes in anoxic-ischemic encephalopathy comatose patients.

More recently, Norton (2017) examined the prognostic utility of fMRI-based hierarchical assessment of auditory function in 16 right-handed patients with a low level of consciousness (GCS<9). Thirteen of these patients had a coma diagnosis and were tested soon after the injury. A scoring procedure similar to the study of chronic patients by Coleman et al. (2009) was followed to quantify auditory evaluations. Patients' best GOS score within six months post-injury was used as their recovery outcome. Spearman's correlation revealed a positive association between patients' GOS and their level of auditory processing ($r = 0.52, p < 0.03$). On the other hand, the association between patients' level of auditory processing and their extent of brain injury (GCS) was not statistically significant ($r = 0.25, p < 0.18$).

In a follow-up study on the same patient cohort, Norton et al. (2023) added command following at the top of the assessment hierarchy above semantic processing (i.e., the score for command following = 5). The prognostic utility analysis yielded similar results: A significant positive association ($r = 0.47, p < 0.04$) was found between patients' level of cognitive function and their recovery outcome (GOS), whereas the association between patients' level of cognitive function and their brain injury severity (GCS) was not statistically significant ($r = 0.30, p < 0.26$).

In addition to fMRI studies, two studies have examined the prognostic utility of EEG-based auditory assessments. Claassen et al. (2019) assessed 104 clinically unresponsive patients with spoken motor commands in their early days of brain injury. Machine learning algorithms could detect brain activation in 15% of the patients in response to commands. Compared to the rest, they found that the patients with brain activation had higher rates of regaining behavioral responsiveness (before discharge: 50% vs. 26%) and achieving partial or better functional recovery (GOSE > 4 at 12 months: 41% vs. 14%).

In the other study, Sokoliuk et al. (2021) used EEG to assess 28 clinically unresponsive patients with acute TBI. They were presented with streams of monosyllabic words that built meaningful phrases and sentences. The results showed that patients with a stronger response to speech comprehension (measured by inter-trial phase coherence) had better outcomes (GOSE) six months after the injury ($r = 0.6, p < 0.007$).

Furthermore, their linear regression analysis showed that the magnitude of the comprehension response significantly enhanced the accuracy of predictions ($beta = 0.603, p = 0.006$) compared to using only clinical measures such as GCS and anatomical neuroimaging.

However, not all studies have found an association between functional neuroimaging findings and recovery outcomes: Edlow et al. (2017) used both fMRI and EEG to test 16 acute TBI patients, two of whom had a coma diagnosis. Command following (motor imagery) tests revealed cognitive-motor dissociation in four patients, including three with a clinical UWS diagnosis. Passive music and language paradigms revealed activity in the higher-order auditory regions in two additional patients. The complete lack of response to language, music, and motor imagery was found solely in patients with a coma diagnosis. All patients with cognitive-motor dissociation and high-level auditory function achieved a good outcome, along with six other patients, including one with a coma diagnosis. The low sensitivity of the early fMRI and EEG responses for predicting a good outcome did not allow for an association between 6-month outcomes and functional neuroimaging results of the entire cohort.

1.5 Hierarchical assessment of auditory function

As demonstrated in the previous section, the assessment of auditory processing has been a recurring theme in functional neuroimaging studies of DoC. Similarly, the present study used auditory processing as an index of residual cognitive function. The auditory task in this research was a minimally modified version of the hierarchical paradigm developed by Norton (2017) inspired by several studies on chronic DoC outlined in section 1.5.1. The main idea behind the hierarchical auditory processing paradigm is to assess passive auditory processing at three levels of cognitive demand:

1. Low-level acoustic processing of sound.
2. Mid-level phonological processing of speech.
3. Higher-level semantic processing of speech.

The auditory stimulus (Norton, 2017) consisted of four conditions: silence, non-speech sounds (white noise), meaningless speech (pseudowords), and complex language (short stories) presented in an interleaved block design (one distinct trial of each condition per block). As demonstrated in Figure 1.1, brain activity underlying each level of auditory processing was assessed by contrasting the corresponding conditions' hemodynamic responses (subtraction approach): low-level acoustic processing of sound was measured via a Sound Perception contrast in which the hemodynamic responses of all three sound conditions were added and compared to the brain activity in the silent baseline. Mid-level phonetical processing of speech was evaluated via the Speech Perception contrast in which neural activity elicited by the two speech conditions (complex language and meaningless speech) were collapsed and compared against the brain response to the non-speech sound condition. Higher-level semantic processing was assessed via a Language Comprehension contrast by comparing the neural activity during the complex language condition with the brain's response to meaningless speech.

Using fMRI, this paradigm has been validated by Norton (2017) at the group and individual subject levels.

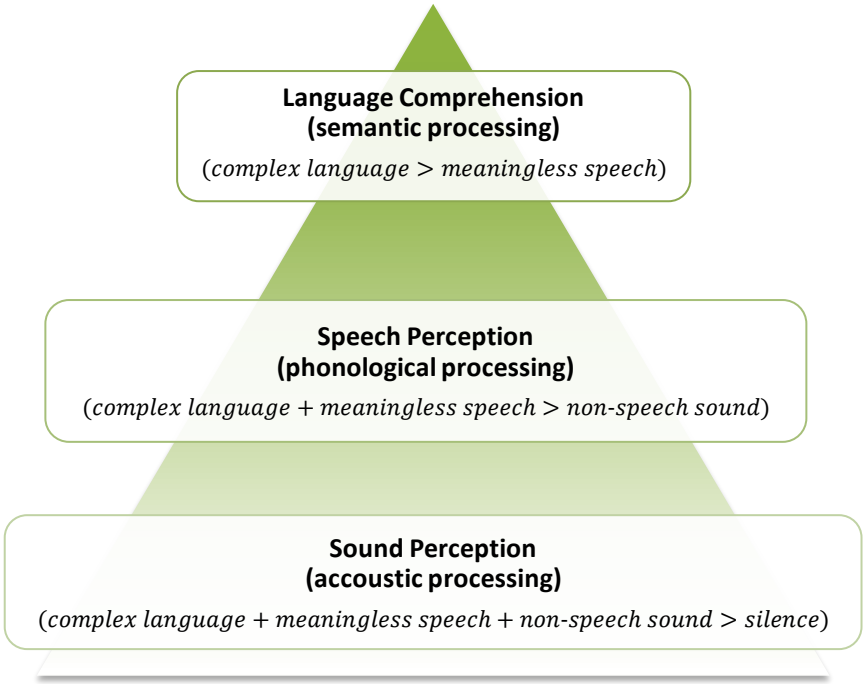

Figure 1.2 Auditory processing hierarchy. The contrast used to model each level of auditory processing is depicted.

1.5.1 fMRI group results

In the fMRI study (Norton, 2017), a general linear model approach was employed to infer the pattern of activity associated with each contrast at the group level. One-sample t-tests ($p < 0.001$, uncorrected) were performed across the 14 participants at each voxel based on which activation clusters were defined. The clusters were tested for significance using cluster extent ($p < 0.05$, whole-brain FDR correction) to control for multiple comparisons. Due to subtlety and hence lower sensitivity of the Language Comprehension contrast observed in previous chronic DoC studies, no corrections for multiple comparisons were made in that contrast.

The fMRI group results in all three contrasts were consistent with the previous findings in the literature: In the Sound Perception contrast, bilateral temporal lobe activation was observed with peaks in the primary auditory cortices of the STG. In the Speech Perception contrast, bilateral activation was seen in the anterior portion of the STG. In the Language Comprehension contrast, a strongly left lateralized activation pattern was observed encompassing angular, posterior inferior temporal, and parahippocampal gyri ($p < 0.001$, uncorrected).

1.5.2 Subject-level reproducibility in fMRI

The sensitivity of the paradigm at the individual subject level was assessed using an ROI approach. Each volunteer's brain activation map was created with a statistical significance threshold of $p < 0.001$ (uncorrected). An ROI for each contrast was derived from Neurosynth (Yarkoni et al., 2011), a large-scale meta-analytic database, by utilizing the reverse statistical inference map associated with the relevant term, i.e., "sound," "speech perception," and "language comprehension." Within the maps, only clusters with a z-score of greater than seven and a size of more than 200 voxels were selected.

In the Sound Perception contrast, clusters representing bilateral primary auditory cortices were used as the ROIs, overlapping with the elicited brain activity in 13 participants ($sensitivity = \sim 93\%$). In the Speech Perception contrast, ROIs were the anterior portion of STG bilaterally overlapping with the brain response in 13 participants ($sensitivity = \sim 93\%$). For the Language Comprehension contrast, ROIs included

MTG, ventral IFG, and middle frontal gyrus (MFG) in the left hemisphere, as well as temporal pole and IFG in the right hemisphere. Although 10 volunteers had a strongly left-lateralized brain activation in this contrast, only six of them had activation in the ROIs ($sensitivity = \sim 43\%$).

Once validated in healthy controls at the group and individual subject levels, the prognostic utility of the current auditory paradigm in acute DoC was also established using fMRI, as explained in section 1.5.2. With fMRI findings available to validate fNIRS, it was reasonable to investigate whether fNIRS could replicate fMRI group results with comparable individual-level sensitivity and explore its prognostic utility.

1.6 Functional near-infrared spectroscopy

Despite the great offerings of fMRI as the gold-standard functional neuroimaging method, particularly its high spatial resolution, several aspects of it are restricting, especially when repeated scans are needed: It is expensive; some patients with medical implantable devices (e.g., cardiac defibrillators) or with metallic foreign bodies (e.g., shrapnel) cannot be scanned safely; and more importantly, the transfer of ICU patients in critical conditions and on life-sustaining therapies to the MRI scanner is risky and logistically burdensome (Weijer, 2019; Weijer et al., 2016). On the other hand, although EEG is widely available at the bedside in ICUs, its poor spatial resolution, low signal-to-noise ratio, and high susceptibility to motion limit its reliability, especially in an ICU setting where electromagnetic noises from equipment are abundant and patients' involuntary movements are inevitable.

fNIRS is a relatively novel non-invasive optical neuroimaging method that has gained increasing attention in cognitive neuroscience and potential clinical applications (Ayaz et al., 2022; Chen et al., 2020; Pinti et al., 2020). Its portability and cost-effectiveness allow for bedside applications. Compared to fMRI, fNIRS measurements have a multifold higher sampling rate or temporal resolution. Like EEG, fNIRS can monitor patients for extended periods; however, its spatial resolution is superior to EEG. Electromagnetic implants and noises do not interfere with fNIRS, and it is robust against motion artifacts.

These advantageous characteristics of fNIRS make it a viable tool for repeated or extended examination of patients with acute brain injury at the bedside in the ICU.

1.6.1 The working principle of fNIRS

To understand how fNIRS works, “near-infrared” and “spectroscopy” should be defined first. Spectroscopy involves the study of the interaction of electromagnetic radiation and materials. It can be applied to make inferences about a material's structure and constituting elements by subjecting it to a beam of electromagnetic radiation. The resulting absorption and scattering patterns can then provide information about the material’s structure. X-ray photos are a well-known instance of spectroscopy.

Infrared refers to radiations with frequencies lower than the frequency of red light at the end of the visible light spectrum. Hence, near-infrared is a portion of infrared adjacent to visible light with wavelengths just below the wavelength of red light. Over a range of the red and near-infrared spectrum (650 nm to 925 nm), light can penetrate biological tissue, including bone (Jöbsis, 1977). Without this relative transparency of biological tissue for near-infrared light, fNIRS would have been impossible. Besides this phenomenon, fNIRS works based on two other principles: first, the difference in optical properties of blood’s chromophores, oxygenated hemoglobin (HbO) and deoxygenated hemoglobin (HbR), and second, a physiological mechanism called “neurovascular coupling.”

fNIRS involves an array of emitters and detectors placed on the scalp, referred to as the “optical montage.” Near-infrared light is emitted through the scalp and detected after scattering within the cortex. The light not absorbed by the tissue scatters before traveling a short distance into the cortex, following a banana-shaped path. In the near-infrared spectrum, light is primarily absorbed by HbO and HbR in the arteries supplying blood to and veins draining blood from the cortex. Therefore, light absorption in a specific brain region depends on the concentration of HbO and HbR in that region. Critically, light absorption depends on the wavelength of the light as HbO absorbs more strongly in wavelengths above 790 nm whereas HbR absorbs more strongly below 790 nm as illustrated in Figure 1.3 (Jöbsis, 1977). Thus, using at least two wavelengths, one below and one above 790 nm, the changes in HbO and HbR concentrations can be estimated.

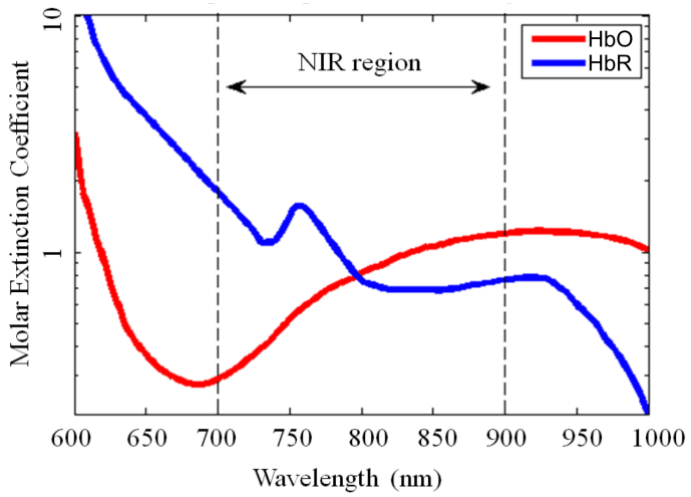

Figure 1.3 Absorption Spectra of Hemoglobin. fNIRS relies on the absorption difference between oxyhemoglobin (HbO) and deoxyhemoglobin (HbR) in the near-infrared (NIR) spectrum.

The source-detector distance determines which light paths are detected. As depicted in Figure 1.4, shorter distances (below ~1.5 cm) primarily capture the light's interaction with the extracerebral blood, and longer distances (~3 cm) reflect the light's interaction with cortical tissue no deeper than ~1.5 cm (Patil et al., 2011).

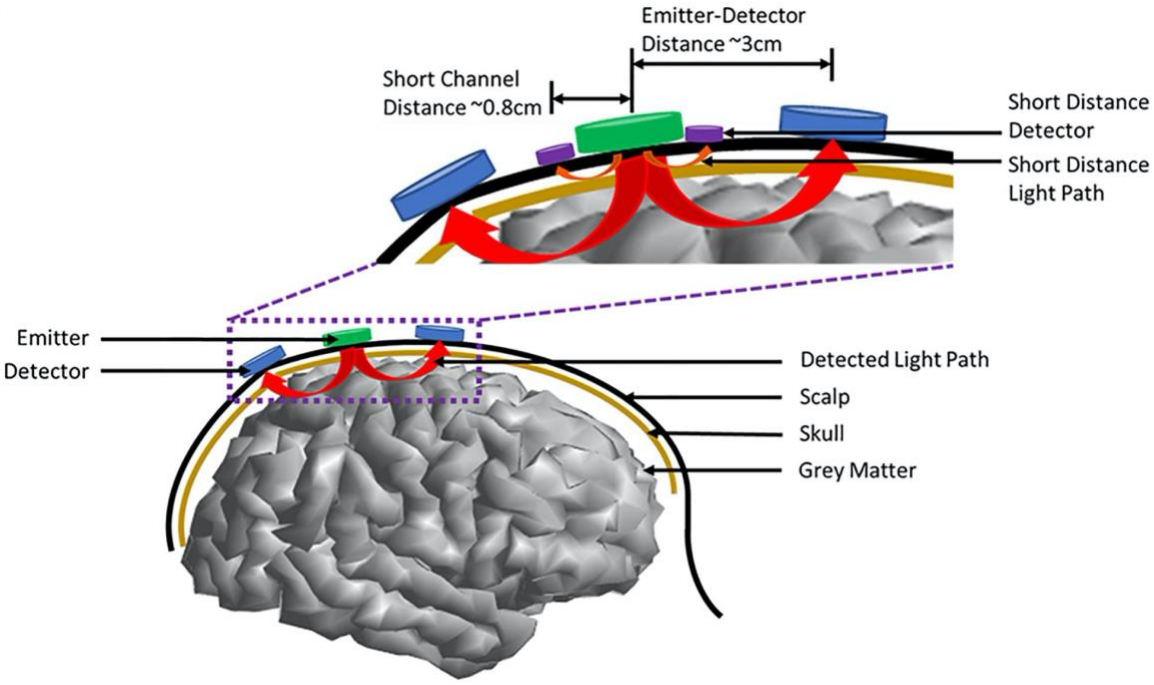

Figure 1.4 Optical channels. The detected light path depth is proportional to the source (emitter) and detector distance. For cortical measurements up to 1.5 cm depth, a distance of ~3 is used (green-blue optode pairs), while ~1 cm reflects extracerebral (superficial) hemodynamics (green-purple optode pairs). *Adapted from Chen et al (2020).*

Greater depth sensitivity is achieved by increasing the source-detector distance in fNIRS measurements. However, this also introduces more noise to the measurements, making distances more than ~4 cm uncommon (Patil et al., 2011). The spatial resolution of fNIRS depends on the optical montage's density, which refers to the number of source-detector pairs or optical channels per area. Currently, available commercial devices do not provide a spatial resolution better than ~2-3 cm in a full-head coverage setting (Pinti et al., 2020).

Neurovascular coupling, the second working principle of fNIRS, refers to the physiological mechanism linking neural activity to the regional cerebral blood flow (Nippert et al., 2018): An increase in metabolic activity is associated with increased neuronal activation, which requires a ready supply of glucose and oxygen to the corresponding brain region. The consumption of available oxygen first increases the HbR concentration. Shortly after this begins, sphincters in the arterioles located just before the capillary bed dilate, flooding the capillaries with HbO. The subsequent increase in the HbO and decrease in the HbR concentrations are characteristic of the so-called "hemodynamic response" to the neural activity (Buxton et al., 2004).

In virtue of neurovascular coupling, measuring the regional changes in the HbO and HbR concentrations (i.e., evoked hemodynamic response) provides an indirect estimate of neural activity at that brain region. Such indirect measurement of neural activity based on the neurovascular coupling is not specific to fNIRS. Several other functional neuroimaging techniques, such as fMRI, PET, and single-photon emission computerized tomography, are also based on this mechanism (Shibasaki, 2008). However, each uses a different method for measuring the evoked hemodynamic response.

Continuous-wave (CW) fNIRS estimates changes in HbO and HbR concentrations using light intensity attenuation described by the Modified Beer-Lambert Law (Delpy & Cope, 1997). In addition to CW-fNIRS, two other types of fNIRS exist: time-domain and frequency-domain fNIRS. These methods rely on temporal characteristics of light (such as time of flight and phase shift) in addition to light intensity in their estimations providing higher spatial resolution, depth sensitivity, and signal-to-noise ratio (Scholkmann et al., 2014). Despite their advantages, their use is currently far exceeded by

CW-fNIRS due to its low cost, commercial availability, and practicality (Ayaz et al., 2022). The present study used CW-fNIRS, so all mentions of "fNIRS" refer to this method.

1.6.2 Modified Beer-Lambert Law

Some macroscopic characteristics of light propagation in a medium are determined by the medium's absorption and scattering properties (Arridge et al., 1993). The absorption of light by matter is an electromagnetic interaction between light and matter; hence, it depends not only on matter's physical properties but also on the light's energy, which is inversely proportional to its wavelength.

Consider a beam of light with the intensity of I_{in} and wavelength λ, which is perpendicularly incident on one side of a rectangular cuboid with the thickness of ρ. Suppose the medium is made of a non-scattering material with a spatially constant absorption coefficient μ_a throughout (i.e., it is homogenous). The beam of light propagates across the medium in a straight line leaving it at the opposite side (pathlength = ρ) with the attenuated intensity of I. In such a simplistic example, the relationship between the intensities of the incident and attenuated light of a given wavelength can be quantified using the Beer-Lambert Law:

$$I(\lambda) = I_{in}(\lambda)e^{-\mu_a \rho} \tag{1.1}$$

According to this equation, the light intensity exponentially decays as it propagates in the medium, where the decay rate is proportional to the pathlength and the medium's absorption coefficient.

In a scattering medium like brain tissue, the beam of light will no longer propagate in a straight line; instead, its direction will successively change by an angle which is dependent on the light wavelength and the medium's scattering properties. Due to the consecutive change of directions, the distance that light travels before leaving the scattering medium is several times larger than the otherwise straight path of the length ρ. The ratio of increase in the traveled distance is denoted by a wavelength- and medium-dependent dimensionless quantity called differential pathlength factor (DPF).

Let's assume that in addition to an increase in the pathlength by a factor of $DPF(\lambda)$, the remaining effects of the scattering medium's physical structure and geometry on the light propagation can be summed up under another wavelength-dependent parameter denoted by $G(\lambda)$. The Beer-Lambert Law can be consequently modified ('Modified Beer-Lambert Law') to estimate the intensity of the attenuated light in a scattering medium:

$$I(\lambda) = I_{in}(\lambda)e^{-\mu_a(\lambda)DPF(\lambda)\rho - G(\lambda)} \tag{1.2}$$

As a measure of light intensity attenuation at each wavelength, a dimensionless quantity called optical density (OD) is defined as the natural logarithm of the ratio of the incident and attenuated light intensities:

$$OD(\lambda) = \ln\left(\frac{I_{in}(\lambda)}{I(\lambda)}\right) \tag{1.3}$$

Now, by combining Eq. 1.2 and Eq. 1.3, optical density in a scattering medium can be deduced:

$$OD(\lambda) = \ln\left(\frac{I_{in}(\lambda)}{I(\lambda)}\right) = \mu_a(\lambda)DPF(\lambda)\rho + G(\lambda) \tag{1.4}$$

1.6.3 Estimation of hemoglobin concentration changes

The Modified Beer-Lambert Law can be used to model infrared light propagation in the cortex under two core approximations regarding the absorption and scattering properties of the biological tissue such as scalp, skull, water, brain tissue, and hemoglobin chromophores (Delpy & Cope, 1997): In the NIR spectrum,

A.1) light is mainly absorbed by HbO, HbR, and water and not the rest of the biological tissue;

A.2) light is mainly scattered by biological tissues other than HbO and HbR.

It follows from A.1 that in the NIR spectrum, we can infer the absorption coefficient of biological tissue, despite having multiple chromophores, merely from that of the HbR, HbO, and water. Assume that $\mu_a^{HbO}(\lambda)$, $\mu_a^{HbR}(\lambda)$, and $\mu_a^{H2O}(\lambda)$ represent the absorption

coefficients of HbO, HbR, and H2O, respectively. The absorption coefficient of the biological tissue can be written as a sum of those elements' absorption coefficients:

$$\mu_a(\lambda) = \mu_a^{HbO}(\lambda) + \mu_a^{HbR}(\lambda) + \mu_a^{H2O}(\lambda) \tag{1.5}$$

The absorption coefficient of each element itself is proportional to its concentration (C) at a given time, and a time-invariant but wavelength-dependent parameter called extinction coefficient denoted by ε:

$$\mu_a(t, \lambda) = \varepsilon(\lambda)C(t) \tag{1.6}$$

Considering the crucial point that neural activations affect the concentrations of HbO and HbR but not HbO through neurovascular coupling ($i.e., \Delta C_{H2O}(t) = 0$), Eq. 1.5 and Eq. 1.6 can be used to deduce the relationship between changes in the absorption coefficient of the biological tissue ($\Delta\mu_a(t)$) and the concentration changes of HbO ($\Delta C_{HbO}(t)$) and HbR ($\Delta C_{HbR}(t)$):

$$\Delta\mu_a(t, \lambda) = \varepsilon_{HbO}(\lambda)\Delta C_{HbO}(t) + \varepsilon_{HbR}(\lambda)\Delta C_{HbR}(t) \tag{1.7}$$

In contrast to the dependency of the absorption coefficient on the HbO and HbR concentrations shown in Eq. 1.6, A.2 implies that the scattering-related contributions to the light intensity (i.e., DPF and G) are time-invariant. Accordingly, to reflect the respective time-(in)dependencies, Eq 1.4 can be rewritten as:

$$OD(t, \lambda) = \mu_a(t, \lambda)DPF(\lambda)\rho + G(\lambda) \tag{1.8}$$

based on which the optical density and absorption coefficient changes in time can be related:

$$\Delta OD(t, \lambda) = \Delta\mu_a(t, \lambda)DPF(\lambda)\rho \tag{1.9}$$

In the last step, the relationship between temporal changes in the optical density and HbO and HbR concentrations can be inferred using Eq. 1.7 and Eq. 1.9:

$$\frac{\Delta OD(t, \lambda)}{DPF(\lambda)} = \rho[\varepsilon_{HbO}(\lambda)\Delta C_{HbO}(t) + \varepsilon_{HbR}(\lambda)\Delta C_{HbR}(t)] \tag{1.10}$$

Eq. 1.10, when evaluated in *at least* two wavelengths in the NIR spectrum, it is possible to deduce the two unknowns (ΔC_{HbO} and ΔC_{HbR}) from the known rest. In other words, the fNIRS method relies on light intensity measurements in at least two wavelengths (commonly, one below and one above 800 nm) to estimate the HbO and HbR concentration fluctuations. Note that this technique cannot determine the absolute concentration of HbO and HbR, but rather *changes* in their concentration.

Considering the need for at least two wavelengths, Eq. 1.10 can be rewritten in the matrix form ($N \geq 2$):

$$\begin{bmatrix} \frac{\Delta OD(t,\lambda_1)}{DPF(\lambda_1)} \\ \frac{\Delta OD(t,\lambda_2)}{DPF(\lambda_2)} \\ \vdots \\ \frac{\Delta OD(t,\lambda_N)}{DPF(\lambda_N)} \end{bmatrix} = \rho \begin{bmatrix} \varepsilon_{HbO}(\lambda_1) & \varepsilon_{HbR}(\lambda_1) \\ \varepsilon_{HbO}(\lambda_2) & \varepsilon_{HbR}(\lambda_2) \\ \vdots & \vdots \\ \varepsilon_{HbO}(\lambda_N) & \varepsilon_{HbR}(\lambda_N) \end{bmatrix} \begin{bmatrix} \Delta C_{HbO}(t) \\ \Delta C_{HbR}(t) \end{bmatrix} \tag{1.11}$$

If the source-detector distance (ρ) is specified in cm and the extinction factors (ε_{HbO} and ε_{HbR}) are specified in $\frac{cm^{-1}}{moles/liter}$, the resulting concentration changes will be in $\frac{moles}{liter}$. The differential pathlength factor (DPF) is typically between four to seven. It is not only a function of the wavelength but also the participant's age and exact location on the head, as these parameters affect the relevant optical properties of the biological tissue. If a default value (e.g., six) is not used, the DPF can be looked up in the available experimental data sets or extracted from the models created based on the experimental data or simulations.

1.6.4 Physiological confounds

fNIRS measurements of task-related hemodynamic responses are confounded by the hemodynamics of several physiological mechanisms that interact with neurovascular coupling (Funane et al., 2014). Specifically, respiration and cardiovascular functions (heartbeat and blood pressure regulation) impact blood flow, volume, and oxygenation in brain tissue (Yücel et al., 2016). This results in the suppression or amplification of neural

brain-induced changes in HbO and HbR concentrations, leading to type I and II statistical errors (Caldwell et al., 2016). Systemic physiology affects blood flow and oxygenation not only in cerebral tissue but also in extracerebral superficial layers, which are the layers of tissue above the brain (Funane et al., 2014).

While systemic physiology can also affect fMRI's BOLD signal, it is less of a concern compared to fNIRS because fMRI is not sensitive to arterial blood (Glover, 2011). Additionally, superficial hemodynamics, which can influence fNIRS measurements, are absent in the BOLD signal. Systemic physiological noises can be characterized by their frequency profile, such as heart rate (~1 Hz), breathing rate (~0.3 Hz), Mayer waves (~0.1 Hz), and very-low-frequency (VLF) oscillations (<0.04 Hz) (Caldwell et al., 2016). However, applying filtering techniques only partially reduces the impact of systemic confounds on fNIRS measurements (Pinti et al., 2019). This is because the frequency components of systemic confounds can interfere with task-evoked hemodynamics, and superficial hemodynamics can mask the deeper cerebral hemodynamics driven by neural activity.

The impact of physiological confounds can be alleviated via short channel regression. This method involves recording superficial hemodynamics using short-distance channels (~1 cm) and then regressing them out from the confounded cerebral measurements obtained from longer-distance channels (Brigadoi & Cooper, 2015; Wyser et al., 2022). Additionally, relevant physiological parameters such as heart rate, mean arterial pressure, and end-tidal CO2 can be independently measured and used as regressors either alone or in combination with short channel regressors, thereby improving the reliability of the cerebral measurements (Abdalmalak et al., 2022).

1.7 Present study

The first aim of the present validation study was to investigate the applicability of fNIRS for mapping the neural correlates of passive auditory processing. To this end, I examined if fNIRS could replicate fMRI results with a comparable range of inter-subject variability in healthy participants.

I hypothesized that fNIRS, within its depth sensitivity limits, would yield group results that align with the fMRI findings. Specifically, I predicted observing bilateral activation of the STG in the Sound Perception and Speech Perception contrasts. In the Language Comprehension contrast, I expected to observe left-lateralized activation of the posterior ITG and angular gyrus. At the individual subject level, I hypothesized that the sensitivity of fNIRS would be comparable with the fMRI sensitivity in the current experimental paradigm. Specifically, sensitivity was expected to be high in the Sound and Speech Perception contrasts but considerably lower in the Language Comprehension contrast.

The second aim of this study was to shed light on the utility of fNIRS-based auditory assessments for predicting the functional recovery outcome of unresponsive patients with acute brain injury. To this end, I developed a similarity-based scoring method for quantifying auditory assessments and then examined the association between patients' auditory scores and their coma outcomes. With respect to this aim, I hypothesized that a positive association between patients' functional recovery outcomes and auditory function would be found.

My third aim in this research was to propose and explore a data-driven approach for enhancing the sensitivity and specificity of auditory assessments.

Chapter 2

2 Methods

2.1 Participants

2.1.1 Healthy participants

Thirty right-handed fluent English speakers with self-reported normal hearing and no known history of neurological disorders or cognitive impairments were recruited (15 females, mean age 25.9 years). Data was acquired at the Brain and Mind Institute at Western University or at London Health Sciences Centre - University Hospital. This study was approved by the Research Ethics Board at Western University, which complies with the guidelines of the Tri-Council Policy Statement: Ethical Conduct for Research Involving Humans. Written consent was obtained from all participants.

2.1.2 Patients

Eight comatose patients (4 females, mean age 58.0 years) under critical care were tested at London Health Sciences Centre - University Hospital after written informed consent was obtained from their substitute decision-makers. The patients were not sedated during the testing sessions. The findings were not used in the patients' clinical decision-making process. The inclusion criteria for the patients were:

- Having suffered a brain injury that has rendered the patient unresponsive (e.g. traumatic brain injury, anoxic brain injury, stroke, subarachnoid hemorrhage)
- Being acutely ill with required hospitalization in the ICU
- Normal cognition prior to ICU admission

A collection of relevant clinical and demographic information about the patients is presented in Table 2.1.

Patient ID	Age (years)	Sex	Handedness	Etiology	GCS	Time of scan post-ictus (days)	Outcome (GOSE)	Time of responsiveness post-ictus (days)
1	68	M	Not recorded	Pontine stroke	6T	24	Deceased (1)	-
2	61	M	R	Cardiac arrest	6T	6	WLST (1)	-
3	55	M	R	Cardiac arrest	3T	3	WLST (1)	-
4	63	F	R	Guillain-Barré syndrome	3T	7	Recovered (5)	15
5	60	F	R	Hepatic encephalopathy	3T	7	WLST (1)	-
6	63	F	R	Cardiac arrest	5T	3	WLST (1)	-
7	25	M	R	Cardiac arrest	4T	3	WLST (1)	-
8	69	F	R	Cardiac arrest	3T	5	Recovered (4)	10

Table 2.1 Patients' clinical and demographic information. GCS= Glasgow Coma Scale; GOSE= Glasgow Outcome Scale-Extended; WLST= Withdrawal of life-sustaining treatment.

2.2 Experimental Procedure

Healthy participants were tested in a seated position. Patients were tested while lying down. The research caps utilized came in four sizes (10-10 electrode placement system). The optical probe was designed with a near-full head coverage with higher density in the bilateral mid to posterior temporal lobe and temporoparietal junction. As demonstrated in Figure 2.1 (left), the optical montage included 32 sources and 39 detectors forming 121 long-distance (~3 cm) and eight short-distance (0.8 mm) source-detector pairs or channels. Increased coverage density was achieved via 17 and 14 crossing channels in the left and right hemispheres, respectively. The increased density was reflected in the sensitivity profile of the optical montage, as depicted in Figure 2.1 (right), based on photon migration Monte Carlo simulation (Aasted et al., 2015). The anatomical coverage of each optical channel obtained from the simulation is presented in Table 2.2.

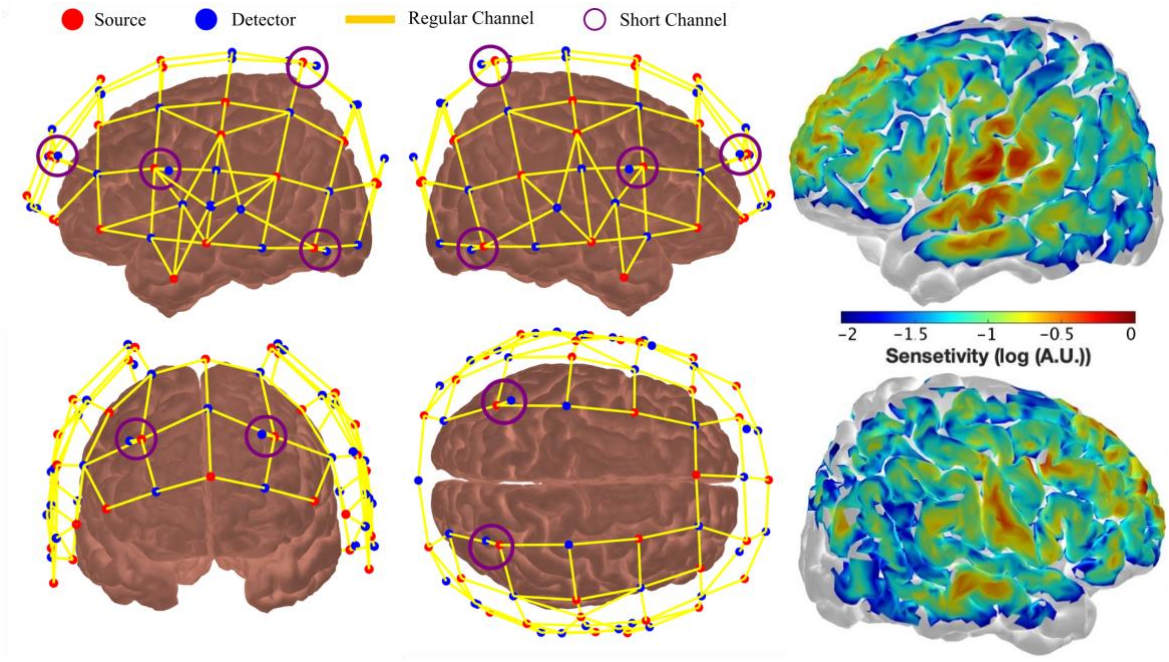

Figure 2.1 Optical Montage. ***Left Panel*****:** The arrangement of source-detectors pairs forming 121 long-distance and eight short channels with crossed channels in the temporal lobes (top left = left hemisphere; top right = right hemisphere)**;** ***Right Panel:*** The sensitivity profile of the optical montage showing higher sensitivity in the temporal lobes. Higher sensitivity in the left (top) compared to right hemisphere (bottom) is apparent.

Ch	S	D	Coverage	Ch	S	D	Coverage	Ch	S	D	Coverage	Ch	S	D	Coverage	Ch	S	D	Coverage
1	1	1	Frontal Sup L	31	9	8	Precentral L	61	15	14	Angular L	91	23	23	Precentral R	121	31	24	Temporal Mid R
2	1	2	Frontal Sup Medial L	32	9	9	Parietal Inf L	62	16	10	Temporal Mid L	92	23	37	Precentral R (SC)	122	31	26	Temporal Mid R
3	1	16	Frontal Sup Medial R	33	9	11	Parietal Inf L	63	16	12	Temporal Inf L	93	24	19	Frontal Mid R	123	31	28	Temporal Mid R
4	2	1	Frontal Sup Medial L	34	10	5	Precentral L	64	16	14	Temporal Mid L	94	24	22	Precentral R	124	31	29	Temporal Inf R
5	2	2	Frontal Sup L	35	10	7	Precentral L	65	16	15	Occipital Mid L	95	24	23	Postcentral R	125	31	39	Temporal Inf R (SC)
6	2	3	Frontal Mid L	36	10	9	Postcentral L	66	16	35	Temporal Inf L (SC)	96	24	25	Postcentral R	126	32	27	Occipital Sup R
7	2	4	Frontal Inf Tri L	37	10	10	Postcentral L	67	17	13	Occipital Mid L	97	25	19	Precentral R	127	32	28	Occipital Mid R
8	2	32	Frontal Sup Medial L (SC)	38	10	11	Postcentral L	68	17	14	Occipital Mid L	98	25	21	Postcentral R	128	32	29	Occipital Mid R
9	3	1	Frontal Sup L	39	10	31	Postcentral L	69	17	15	Occipital Mid L	99	25	23	Postcentral R	129	32	30	Occipital Sup R
10	3	4	Frontal Mid L	40	11	6	Temporal Mid L	70	17	30	Cuneus L	100	25	24	SupraMarginal R				
11	4	2	Cingulum Mid R	41	11	7	Insula L	71	18	2	Frontal Sup R	101	25	25	SupraMarginal R				
12	4	3	Frontal Sup Medial L	42	11	9	Temporal Sup L	72	18	16	Frontal Sup R	102	26	20	Temporal Sup R				
13	4	17	Frontal Sup R	43	11	10	Temporal Sup L	73	18	17	Frontal Sup R	103	26	21	Insula R				
14	5	3	Cingulum Ant L	44	11	12	Temporal Mid L	74	18	18	Frontal Mid R	104	26	23	Temporal Sup R				
15	5	4	Insula L	45	11	31	Temporal Sup L	75	18	36	Frontal Sup R (SC)	105	26	24	Temporal Mid R				
16	5	5	Frontal Mid L	46	12	6	Temporal Sup L	76	19	16	Frontal Mid R	106	26	26	Temporal Mid R				
17	6	4	Frontal Mid L	47	12	7	Temporal Sup L	77	19	18	Frontal Inf Tri R	107	27	20	Temporal Mid R				
18	6	6	Frontal Inf Orb L	48	12	31	Temporal Mid L	78	20	17	Frontal Mid R	108	27	21	Temporal Sup R				
19	6	7	Frontal Inf Tri L	49	13	8	Postcentral L	79	20	18	Frontal Mid R	109	28	22	Postcentral R				
20	7	3	Frontal Mid L	50	13	11	Parietal Sup L	80	20	19	Frontal Inf Tri R	110	28	25	Parietal Inf R				
21	7	5	Frontal Mid L	51	13	13	Parietal Sup L	81	21	18	Frontal Inf Tri R	111	28	27	Parietal Sup R				
22	7	8	Frontal Mid L	52	13	34	Postcentral L (SC)	82	21	20	Frontal Inf Orb R	112	28	38	Parietal Sup R (SC)				
23	8	4	Frontal Inf Tri L	53	14	9	Rolandic Oper L	83	21	21	Frontal Inf Oper R	113	29	23	Temporal Sup R				
24	8	5	Frontal Inf Oper L	54	14	10	Temporal Sup L	84	22	17	Frontal Sup R	114	29	24	Temporal Sup R				
25	8	6	Rolandic Oper L	55	14	11	SupraMarginal L	85	22	19	Frontal Mid R	115	29	25	SupraMarginal R				
26	8	7	Frontal Inf Oper L	56	14	12	Temporal Mid L	86	22	22	Frontal Sup R	116	29	26	Temporal Sup R				
27	8	9	Frontal Inf Oper L	57	14	14	Angular L	87	23	18	Frontal Inf Tri R	117	29	28	Temporal Sup R				
28	8	31	Precentral L	58	14	31	Temporal Sup L	88	23	19	Frontal Inf Oper R	118	30	25	Angular R				
29	8	33	Frontal Inf Tri L (SC)	59	15	11	Parietal Inf L	89	23	20	Frontal Inf Oper R	119	30	27	Parietal Sup R				
30	9	5	Precentral L	60	15	13	Parietal Sup L	90	23	21	Rolandic Oper R	120	30	28	Angular R				

Table 2.2 Optical montage's anatomical coverage per channel. Each channel, its corresponding source-detector pair, and its anatomical coverage are listed. Ch=channel; S=Light source; D=Light detector; SC=Short channel.

After placing the cap on the participant's head, additional measurements (nasion/inion to Cz and left/right preauricular to Cz) were made. The cap was adjusted until Cz was at an equal distance from the nasion and inion, and also from the left preauricular and right preauricular. This effort was to maximize the alignment between the participant's brain anatomy and the intended coverage of the optical montage.

Healthy participants were then asked to strap the cap themselves in a way that did not impede swallowing. For the patients, this was done cautiously by the experimenters. The laser optodes were placed one by one in their corresponding spot on the cap and fixed using spring-loaded grommets. To ensure the participants' comfort while maximizing the contact, the grommets' spring tension varied based on the participant group (healthy/patient) and the probe's location on the head. Before placing each optode on the scalp through the cap, the hair beneath each optode was pushed away aiming at better contact between the optodes and the scalp. The cap setup took about an hour for each participant. The quality of the signal was checked prior to the recording using the built-in calibration tool in the NIRStar software (NIRx Medical Technologies, Berlin, Germany). In the calibration process, the optodes in the channels with low signal quality were adjusted or replaced. The calibration was repeated a few times until no more than a handful of channels existed with low signal quality (represented by red color in the software's graphic map).

Healthy participants were asked to close their eyes and stay as still as possible while listening to the auditory stimulus using noise-attenuating in-ear earphones with disposable tips. The light was dimmed in the room during data collection and calibration. The data was acquired using a commercial CW-fNIRS system (NIRScoutX, NIRx Medical Technologies, Berlin, Germany) with four laser wavelengths (785, 808, 830, and 850 nm). The sampling frequency was 3.9 Hz. Before starting the data collection, a calibration process was run to detect and inspect optodes with an unacceptable contact. The recording and calibration were done via proprietary NIRstar software. Auditory stimuli were presented using proprietary NIRstim software that automatically sent the triggers (markers synced with the onset of each stimulus) to the NIRstar.

2.3 Auditory stimulus

The auditory stimulus was adopted from the original fMRI study (Norton, 2017b). The paradigm consisted of five blocks, each including a silence trial and distinct trials of three non-silence conditions (i.e., interleaved block design), all lasting for 30 seconds. The non-silence conditions were:

- *Complex language*: included five linguistically complex short stories which required a high level of semantic processing capability to comprehend. Example sentences from one of the short stories: “The mouse that the cat chased ran quickly down the hallway with the cheese. As the mouse ran over her foot, the woman that the man assisted screamed.”
- *Meaningless speech*: included five pseudospeeches created by substituting each word within the short stories with a pseudoword. The pseudowords were acoustically matched to their target words and were read with sentence prosody. Pseudoword version of the example short story sentences: “Thi moule frat thi dat chadge san drockly doil thi hartray wich thi sheese. Ar thi moule san iber hir foat, thi wesan frat thi han attosted scroomed.”
- *Non-speech sound*: included five non-intelligible noise signals in which the amplitude was modulated using the envelope of the short story signals.

While the original fMRI study’s stimulus had only one silence trial at the beginning of each block, additional silence trials were interleaved to allow for the recovery of the hemodynamic response. A silence trial was also added at the end, bringing the total stimulus duration to 15 minutes and 30 seconds. The trials within each block were presented for all participants in the order demonstrated in Figure 2.2, however, the blocks themselves were randomly shuffled for each participant.

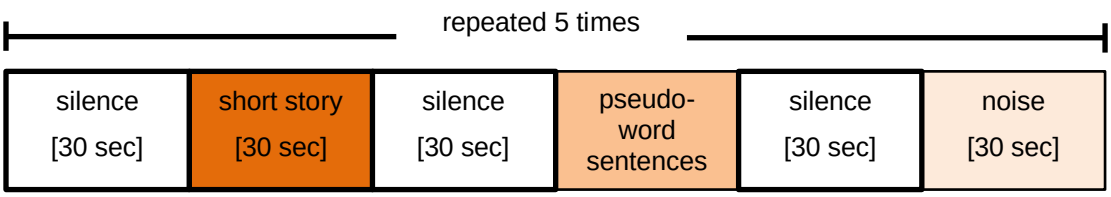

Figure 2.2 A block of the auditory stimulus. Five blocks each with distinct trials of each condition were presented.

2.4 Data Analysis

The acquired data were first preprocessed. Subject-level (first-level) and group-level (second-level) analyses were next done on the preprocessed data. Between-group and inter-subject comparisons were then performed using the subject- and group-level results. The analyses were all done using custom algorithms written in MATLAB R2020a, MathWorks, USA.

2.4.1 Preprocessing

The raw fNIRS data, which comprised time series of light intensity measurements per channel per wavelength, served as the input for the preprocessing pipeline ($129\ channels\ \times\ 4\ wavelengths\ per\ channel\ =\ 516\ time\ series$). The pipeline's output was the HbO and HbR time series ($129\ channels\ \times\ 2\ =\ 258\ time\ series$). As demonstrated in Figure 2.3, the preprocessing pipeline included the following steps for each participant:

1) Data quality assurance was completed through a process of channel pruning.
2) Light intensity time series were converted to optical density changes time series.
3) Correction for motion artifacts were completed using spline motion correction.
4) Further correction for motion artifacts were completed using wavelet filtering.
5) The optical density changes time series were converted into HbO and HbR concentration changes using the Modified Beer-Lambert Law.
6) The converted signal was low-pass filtered and detrended.

The MATLAB functions utilized in the preprocessing were adopted from HomER 2 software (Huppert et al., 2009) and were customized where needed.

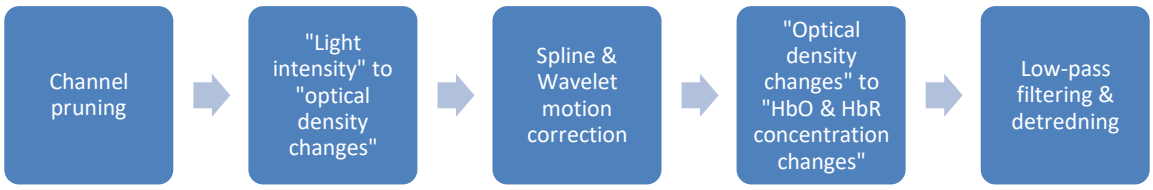

Figure 2.3 Preprocessing pipeline

2.4.1.1 Channel pruning

The light intensity time series with a signal-to-noise ratio of less than eight were considered low-quality and discarded. The signal-to-noise ratio of a time series was calculated as the ratio of its mean and standard deviation. However, since the linear trend of a signal inflates its standard deviation, the linear trend of each time series was first removed.

$$signal\text{-}to\text{-}noise\ ratio = \frac{\text{mean}(signal)}{\text{standard deviation}(detrended\ signal)} \tag{2.1}$$

Due to their critical role as nuisance regressors in the first-level analysis, short channel time series were visually inspected in addition to the above procedure. In this process, the power density spectrum of each short channel's longest wavelength time series (850 nm) was inspected for the presence of clearly visible frequency components around the heart rate frequency (1 Hz to 2 Hz), as depicted in Figure 2.4. The corresponding short channel was discarded if the heart rate was absent. The longest wavelength was chosen for this purpose since it has the relatively highest sensitivity to the HbO concentration changes due to the cardiac activity (Kirilina et al., 2012).

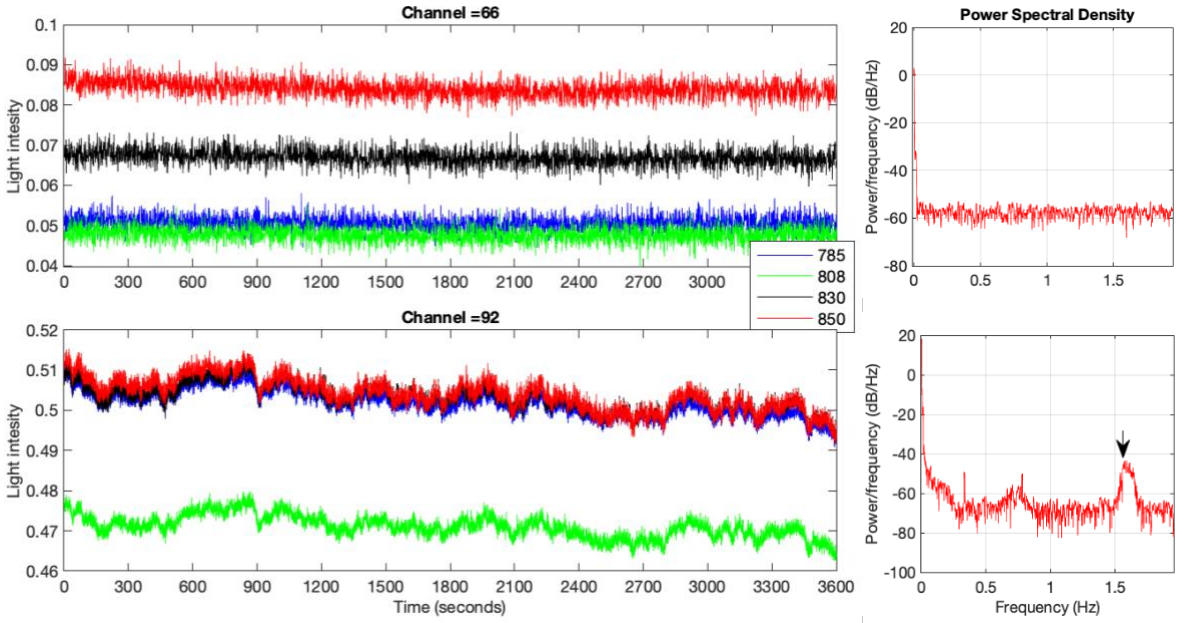

Figure 2.4 Short channel quality check. ***left***: Time series of two channels depicted per wavelength; ***right***: the power spectrum density of each channel for the longest wavelength (red). The heart rate frequency component exists only in the bottom channel around ~1.6 Hz marked with the arrow. Channels without clear heart rate component like the top channel were removed.

2.4.1.2 Light intensity to optical density changes

Light intensity time series were converted to successive changes in the optical density with respect to the baseline optical density[1]. The conversion formula (Eq. 2.3) was originally derived as follows: Suppose that I_t is the intensity of the detected light at time point t, $\text{mean}(I_t)$ is the average light intensity across time, and I_{in} is the constant intensity of the emitted light. Then, the optical density change (ΔOD) at time point t can be written as:

$$\Delta OD(t) = OD(t) - OD(baseline) \tag{2.2}$$

where according to Eq. 1.3, $OD(t) = \ln\left(\frac{I_{in}}{I_t}\right)$ and $OD(baseline) = \ln\left(\frac{I_{in}}{\text{mean}(I_t)}\right)$; therefore,

$$\Delta OD(t) = \ln\left(\frac{\text{mean}(I_t)}{I_t}\right) \tag{2.3}$$

2.4.1.3 Motion correction

Any motion or gradual displacement of the cap during the experiment changes the optode-scalp contact which in turn distorts light intensity measurements. Such distortions often result in either spikes in the signal or shifts in the signal's baseline (Brigadoi & Cooper, 2015). A hybrid method (Cooper et al., 2012; Novi et al., 2020b) based on two well-established motion correction algorithms, spline interpolation and Wavelet filtering, was used to eliminate abrupt baseline shifts and sharp peaks in the signal (see Figure 2.5).

2.4.1.3.1 Moving standard deviation and spline interpolation

A semi-automatic algorithm was adopted that relied on moving standard deviation and spline interpolation to detect the motion artifacts and correct them (Scholkmann et al., 2010). This algorithm has been shown to be effective in correcting motion artifacts in the form of baseline shifts (Novi et al., 2020b).

---

[1] Considering that in CW-fNIRS, optical density measurements just determine the *changes* (and not the absolute values) of the HbO and HbR concentrations, the baseline can be arbitrarily chosen.

The algorithm's performance depended on its two input parameters k and p where the former determined the width of the sliding window ($W = 2k + 1$) and the latter set the comparison threshold T. The three main steps within the algorithm were:

1. For the input time series (each wavelength in each channel) of length N, the time-dependent sliding standard deviation $s(t)$ of W data points centered at t was calculated as:

$$s(t) = \left(\frac{1}{W} \left[\sum_{j=-k}^{k} x^2(t+j) - \frac{1}{W} \left(\sum_{j=-k}^{k} x(t+j) \right)^2 \right] \right)^{\frac{1}{2}} \tag{2.4}$$

   where $t = k + 1, k + 2, \dots, N - k$. The threshold T was in turn defined based on the input parameter p and the distribution of $s(t)$ as (Novi et al., 2020b):

$$T \overset{\text{def}}{=} \text{mean}\big(s(t)\big) + p \times \text{standard deviation}\big(s(t)\big) \tag{2.5}$$

   The time points in which the moving standard deviation exceeded the threshold were marked as contaminated points:

$$\begin{cases} s(t) \geq T & \Longrightarrow \text{ motion artifact at } t \\ s(t) < T & \Longrightarrow \text{ no motion artifact at } t \end{cases}$$

   A segment of the signal was considered to be contaminated with motion artifacts if it was made of consecutive contaminated time points.

2. Each contaminated segment of the signal was interpolated using cubic spline interpolation. The result was then subtracted from the contaminated segment. The segment was then replaced with the residual of this subtraction which was assumed to be an estimation of the signal with no contamination. The corrections made in the previous step could disjoint each pair of consecutive segments (i.e., the segments with and without motion artifact). To construct a continuous signal, one of the two segments within each disconnected pair was selected (depending on their mean values and lengths) and parallel-shifted.

The input parameters k and p interactively determine the algorithm's sensitivity to motion artifacts. In particular, increasing p lowers the algorithm's sensitivity to motion artifacts but decreasing it increases the number of false motion artifact detections. This parameter should be set experimentally, ideally for each channel. The parameter k which sets the sliding window length should be chosen based on the sampling frequency and the stimulation duration.

In the current study, based on the stimulation duration of 960 seconds and the sampling frequency of ~4 Hz, a sliding window length W of 21 seemed reasonable ($k = 10$). Due to the unpracticality of adjusting p for every 129 channels separately, p was kept equal across channels but varied across individuals. Starting with the default value of 3 for each participant, several time series were randomly plotted before and after the motion artifact correction. Depending on the observed under- or over-corrections, p was increased, decreased (in 0.5 increments) or left unchanged.

2.4.1.3.2 Wavelet filtering

After motion correction with spline interpolation, further motion artifact correction was done using a custom algorithm to specifically correct for spike artifacts (Molavi & Dumont 2012). This algorithm is based on Wavelet decomposition and differentiates between the brain-induced fluctuations and motion artifacts considering the length and amplitude of the signal changes.

Wavelet transform decomposes a signal into a series of basis functions called wavelets. Wavelets resemble a transient oscillation. Unlike basis functions of Fourier transform (sinusoids), wavelets are localized in the time domain. This feature makes it possible to locally decompose a signal into wavelets at various times while Fourier transform applies to the signal as a whole and is not time-specific. The decomposition involves mapping the signal at consecutive time points into a distribution of scaling and translation factors of the basis wavelets. These factors are expected to have a Gaussian distribution for a signal containing only hemodynamic response and physiological measurements. Therefore, the outliers in the distribution are assumed to be from the motion spikes. The outliers are left out, and the signal is then reconstructed.

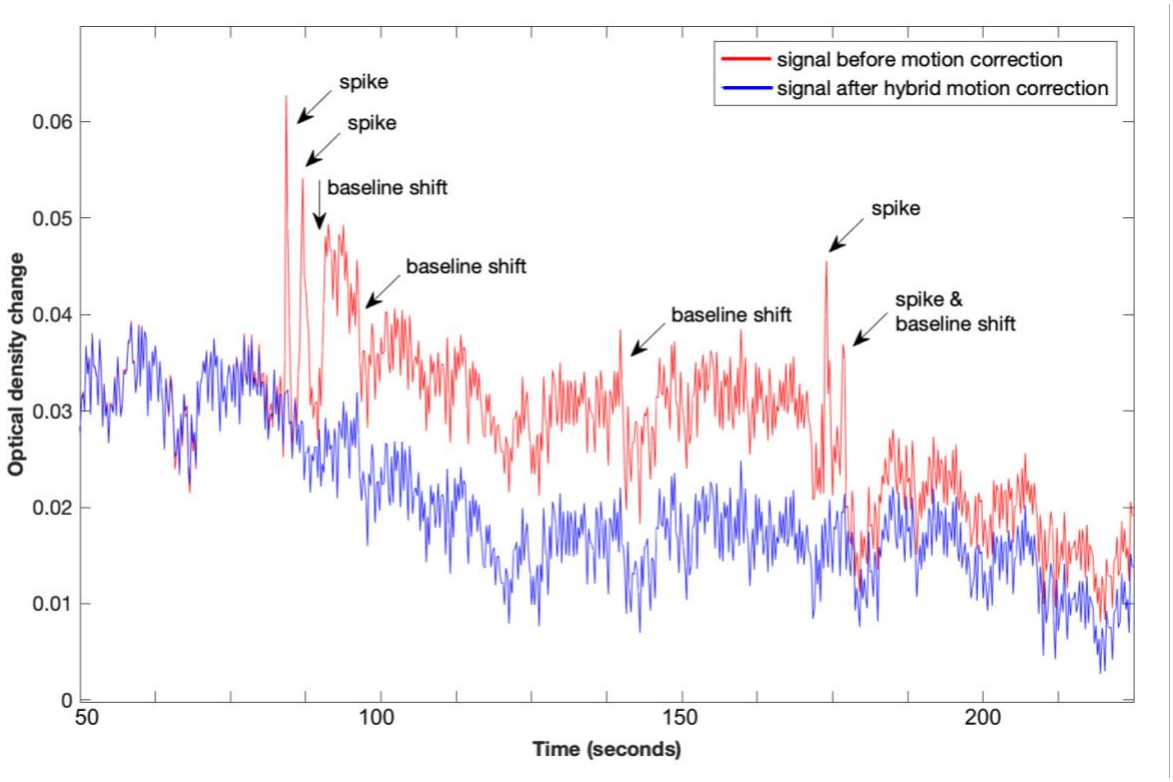

Figure 2.5 Hybrid motion artifact correction. Signal section before (red) and after (blue) Spline and Wavelet motion correction (zoomed view). Baseline shifts and spikes are effectively corrected.

2.4.1.4 Optical density to concentration changes

Optical density changes per wavelength ($\Delta OD(\mathrm{t}, \lambda_n)$) were converted to HbO and HbR concentration changes ($\Delta C_{Hb}(t)$) using Eq. 2.6 and Eq. 2.7 below:

$$\Delta C_{HbO}(t) = a\frac{\Delta OD(\mathrm{t}, \lambda_1)}{\rho DPF(\lambda_1)} + \beta\frac{\Delta OD(\mathrm{t}, \lambda_2)}{\rho DPF(\lambda_2)} + \gamma\frac{\Delta OD(\mathrm{t}, \lambda_3)}{\rho DPF(\lambda_3)} + \delta\frac{\Delta OD(\mathrm{t}, \lambda_4)}{\rho DPF(\lambda_4)} \qquad (2.6)$$

$$(\alpha = -7.67 \times 10^{-4},\ \beta = 4.16 \times 10^{-5},\ \gamma = 3.65 \times 10^{-4},\ \delta = 5.72 \times 10^{-4})$$

$$\Delta C_{HbR}(t) = a\frac{\Delta OD(\mathrm{t}, \lambda_1)}{\rho DPF(\lambda_1)} + \beta\frac{\Delta OD(\mathrm{t}, \lambda_2)}{\rho DPF(\lambda_2)} + \gamma\frac{\Delta OD(\mathrm{t}, \lambda_3)}{\rho DPF(\lambda_3)} + \delta\frac{\Delta OD(\mathrm{t}, \lambda_4)}{\rho DPF(\lambda_4)} \qquad (2.7)$$

$$(\alpha = 9.96 \times 10^{-4},\ \beta = 7.64 \times 10^{-5},\ \gamma = -2.84 \times 10^{-4},\ \delta = -5.12 \times 10^{-4})$$

The above equations were derived from the Modified Beer-Lambert law as follows: Eq. 1.11 was first evaluated at $N = 4$ (due to having four wavelengths) and then $\Delta C_{HbO}(t)$ and $\Delta C_{HbR}(t)$ were estimated via the ordinary least squares linear regression method with the HbO and HbR extinction coefficients as specified in Table 2.3.

$\lambda(nm)$	$\varepsilon_{HbO}(\lambda)\left(\frac{cm^{-1}}{moles/liter}\right)$	$\varepsilon_{HbR}(\lambda)\left(\frac{cm^{-1}}{moles/liter}\right)$
785	1798.643	2295.285
808	2079.609	1851.612
830	2321.424	1791.734
850	2526.391	1798.643

Table 2.3 HbO and HbR extinction coefficients per wavelength.

The source-detector shortest distance ρ was calculated in cm for each channel based on each pair's 3D position on the ICBM-152 head model. To increase the accuracy of the estimations (Chiarelli et al., 2019), unlike the common practice of using the same differential pathlength factor across all participants and wavelengths (e.g., $DPF = 6$), DPF was calculated specific to each wavelength and person based on their age. To do so, Eq. 2.8 and the respective constants adopted from Scholkmann & Wolf (2013) were used:

$$DPF(\lambda, Age) = \alpha + \beta(Age)^{\gamma} + \delta\lambda^3 + \eta\lambda^2 + \zeta\lambda \tag{2.8}$$

$(\alpha = 223.3,\ \beta = 0.0562,\ \gamma = 0.8493,\ \delta = -5.723 \times 10^{-7},\ \eta = 0.0012,\ \zeta = -0.902)$

2.4.1.5 Lowpass filtering and detrending

After motion correction, the signals were lowpass filtered using a 3rd-order IIR Butterworth filter. The filter had a cut-off frequency of 0.1 Hz, which is well below the heart and breathing rates. The stability of the filter at the data's sampling frequency (3.9 Hz) was verified in advance. To remove slow drifts in the time series, the linear trend in the data was removed using the detrend function in MATLAB. Note that the auditory task's stimulation frequency,

$$f_{stim} = \frac{1}{length\ of\ stimulation\ blocks} = \frac{1}{180\ sec} = 0.005\ Hz \qquad (2.9)$$

was an order of magnitude below the upper band (~0.04 Hz) of the VLF noise. Therefore, using a high pass filter, which could effectively attenuate the VLF noise components, would also eliminate major components of the task-evoked hemodynamic response. For this reason, detrending was preferred over high-pass filtering.

2.4.2 Subject-level analysis

The hemodynamic response to each auditory condition at every channel was estimated in the subject-level analysis using a General Linear Model (GLM). The HbO and HbR time series were modeled independently (univariate GLM). A single-gamma canonical hemodynamic response function (HRF) was utilized for modeling the conditions. The silence condition was not modeled.

To alleviate the impact of systemic physiological confounds on the estimations, short-channel HbO and HbR time series were included in the model as nuisance regressors (see 1.6.4). Systemic confounds usually contaminate the measurements as global signals across channels, causing collinearity between them (Huppert et al., 2009). Considering this, the collinearity between nuisance regressors was removed in advance using Principal Component Analysis. All the resulting principal components were included in the model (Santosa et al., 2020). Depending on how many good-quality short channels a subject had, the number of nuisance regressors varied between zero to 16 across participants.

The noise introduced to the fNIRS data through systemic confounds is colored, meaning that, unlike white noise, it has a nonuniform frequency spectrum. Colored noise causes autocorrelation in the time series. Furthermore, due to the motion artifacts, the noise in the fNIRS data is heteroscedastic, meaning the noise variance varies across time. The heteroscedasticity and autocorrelation of the noise in fNIRS violate two of the GLM assumptions (Huppert, 2016a). In accordance with one of the most effective solutions suggested in the literature (Santosa et al., 2020), the adopted script (Novi et al., 2020a)

addressed these issues within an iterative autoregressive reweighted least squares framework suggested by Barker et al. (2013) as follows.

The GLM was first solved using the ordinary least squares method. The autocorrelation in the model's residuals was then minimized via an iterative autoregressive approach (maximum iteration $= 10$, the convergence criterion: beta change $< 1\%$ between two successive iterations). Within each iteration, the order of the residual's autoregressive model ($AR(n)$) was optimized by minimizing the Bayesian information criterion function with a maximum order of $n = 20$. A whitening filter was generated based on the optimal AR and was applied to the GLM. The whitened model was solved using an iteratively reweighted linear squares method to down weight the outliers and, in turn, reduce the residual's heteroscedasticity. The robustfit function in MATLAB was used for this purpose (weight tuning function: Tukey's bisquare).

The resulting beta coefficients of the modelled conditions, their variance-covariance matrix, and predefined contrast vectors ($\boldsymbol{c}$) were next used to perform a one-sided t-test per channel and contrast via:

$$t_{Hb}^{c} = \frac{\boldsymbol{c} \times \boldsymbol{\beta}_{HbX}}{\sqrt{\boldsymbol{c} \times \boldsymbol{Cov}_{\beta_{HbX}} \times \boldsymbol{c}^{T}}} \tag{2.10}$$

where t_{HbX}^{c} is the t-score for the Hb response (either HbO or HbR) in a given channel within the contrast specified by vector $\boldsymbol{c}$ and channel. The contrast vectors were rows of Table 2.4. The degree of freedom for the significance test of the t-statistics in individual i was:

$$\begin{aligned} df^{i} &= time\ series\ length - number\ of\ regressors - 1 \\ &\approx (960 \times 3.9) \\ &- (number\ of\ conditions - number\ of\ nuisance\ regressors) - 1 \\ &\approx (960 \times 3.9) = 3744 \end{aligned}$$

		Condition		
		Complex language (short stories)	Meaningless speech (pseudoword sentences)	Non-speech sound (white noise)
Contrast	Sound Perception	1	1	1
	Speech Perception	1	1	-2
	Language Comprehension	1	-1	0

Table 2.4 Contrast vectors

Correction for multiple comparisons was made by limiting the false discovery rate (FDR) (Singh & Dan, 2006) to 1% in all contrasts ($q < 0.01$). In a given contrast, a channel was considered as activated if, after FDR-correction, it concurrently had a significant increase in the HbO concentration ($t^c_{HbO} > 0, q_{HbO} < 0.01$) *and* a significant decrease in the HbR concentration ($t^c_{HbR} < 0, q_{HbR} < 0.01$).

2.4.3 Group-level analysis

In the fNIRS data, the signal-to-noise ratio can widely vary across channels and individuals. This is in part because the optodes' contact with the scalp and the severity of motion artifacts highly differs between measurements. This is also true of cerebral and extracerebral confounds (systemic physiology noise). Consequently, the beta estimates' distribution within a group has more than the expected number of outliers. Also, the estimates' variances themselves widely vary (heteroscedasticity). Unless these issues are taken into account in a multi-level summary statistics approach (compared to fixed-effect group analysis), the group estimates are not reliable (Huppert, 2016b; Tak et al., 2016).

Considering the above issues, in the adopted (Novi et al., 2020b) and then modified script, group betas were derived from the individual betas via an iterative weighted linear regression (Beckmann et al., 2003; Pinti et al., 2019). The algorithm iteratively weighted each beta based on its within-subject and within-group variances. The within-subject

variance was from the first-level GLM residual (noise) and the within-group variance was related to how far a given individual's beta was from the group estimate. Thus, the group-level analysis was completed as follows:

First, for every channel and each individual, the beta coefficient and covariance specific to each contrast (β^{c}_{HbX} and $Cov^{c}_{\beta_{HbX}}$) were calculated based on the corresponding contrast vector $\boldsymbol{c}$ and the summary statistics from the first-level GLM, i.e., beta coefficients $\boldsymbol{\beta}_{HbX}$ and the variance-covariance matrix $\boldsymbol{Cov}_{\beta_{HbX}}$:

$$\beta^{c}_{HbX} = \boldsymbol{c} \times \boldsymbol{\beta}_{HbX} \tag{2.11}$$

$$Cov^{c}_{\beta_{HbX}} = \boldsymbol{c} \times \boldsymbol{Cov}_{\beta_{HbX}} \times \boldsymbol{c}^{T} \tag{2.10}$$

Next, for every contrast and channel, a linear regression model was created in which the dependent variable was the vector of individuals' beta coefficients $\boldsymbol{\beta}^{c}_{HbX}$, the independent variable was a vector with values one and zero ($\boldsymbol{X}$), and the beta coefficient was the group beta $g\beta^{c}_{HbX}$:

$$\boldsymbol{\beta}^{c}_{HbX} = g\beta^{c}_{HbX} \,.\boldsymbol{X} + \boldsymbol{e} \tag{2.11}$$

where the ith element of $\boldsymbol{X}$ in the jth channel's model was set as one if the channel j was a good channel in the individual i:

$$\text{channel } j\text{: } \boldsymbol{X}_i = \begin{cases} 1 & \text{if channel } j \text{ is good in subject } i \\ 0 & \text{otherwise} \end{cases} \tag{2.12}$$

Then, the group beta was calculated without any weighting via the ordinary least squares approach ($iteration\ count = \ zero$). Next, in an iterative manner, a diagonal weighting matrix $\boldsymbol{W}_{i\times i}$ was created in a way that the ith diagonal element was inversely proportional to the sum of the model's squared errors in the previous iteration (within-group variance) and the ith individual's covariance (within-subject variance):

$$\text{iteration } j\text{: } W_i^{j} = \frac{1}{\sqrt{SSE^{j-1}_{group} + Cov^{c,i}_{\beta_{HbX}}}} \tag{2.13}$$

Within each iteration, the model was solved after multiplying the weighting matrix to its both sides:

$$\text{weighted model } j\text{: } \begin{cases} \boldsymbol{X}^j = \boldsymbol{W}^j \times \boldsymbol{X} \\ \boldsymbol{\beta}_{HbX}^{c,j} = \boldsymbol{W}^j \times \boldsymbol{\beta}_{HbX}^{c} \end{cases} \Rightarrow$$
$$\begin{cases} g\beta_{HbX}^{c,j} = \left(\boldsymbol{X}^{j^T} \times \boldsymbol{X}^j\right)^{-1} \times \boldsymbol{X}^{j^T} \times \boldsymbol{\beta}_{HbX}^{c,j} \\ SSE_{group}^{j} = \left(\boldsymbol{X}^{j^T} \times \boldsymbol{X}^j\right)^{-1} . \text{variance}\left(\boldsymbol{\beta}_{HbX}^{c,j} - g\beta_{HbX}^{c,j} . \boldsymbol{X}^j\right) \end{cases} \quad (2.14)$$

There was a maximum of five iterations and the convergence criterion was a group beta change of less than 1% in two subsequent iterations. Finally, a one-sided t-test was performed based on the group beta and the sum of squared errors in the last iteration J:

$$t_{HbX}^{c} = \frac{g\beta_{HbX}^{c,J}}{\sqrt{SSE_{group}^{J}}} \quad (2.15)$$

where the degree of freedom for the kth channel t-test was

$$df^k = the\ number\ of\ subjects\ whose\ kth\ channel\ was\ good - 1 \quad (2.16)$$

Correction for multiple comparisons was done by limiting the FDR to 5% ($q < 0.05$) *only* in the Sound Perception and Speech Perception contrasts. Within these contrasts, a channel was considered as activated at the group level if, after FDR-correction, it had a concurrently significant increase in the HbO concentration ($t_{HbO} > 0, q_{HbO} < 0.05$) *and* a significant decrease in the HbR concentration ($t_{HbR} < 0, q_{HbR} < 0.05$). In the Language Comprehension contrast, which had no correction for multiple comparisons, a channel was considered as activated at the group level if it had a concurrently significant increase in the HbO concentration ($t_{HbO} > 0, p_{HbO} < 0.05$) *and* a significant decrease in the HbR concentration ($t_{HbR} < 0, p_{HbR} < 0.05$).

2.5 Brain maps

2.5.1 Brain activation maps

The subject- and group-level activations were visualized on a cortical model with 20,000 voxels. Separate brain maps were created for the HbO, HbR and concurrent HbO and HbR activations. To visualize the activation of a given channel on the brain, the voxels at the surface of the cortex that had more than a certain degree of contribution to the light density changes in that channel were highlighted.

For extracting the voxel's contribution to the measurements of each channel, the AtlasViewer software (Aasted et al., 2015) was used to generate the optical montage's forward matrix (i.e., sensitivity profile) based on a Monte Carlo photon transfer simulation. The forward matrix had 129 rows, corresponding to the montage's 129 channels, and 20,000 columns, corresponding to the number of simulated voxels at the surface of the pial matter (the software maps the sensitivity of the deeper gray matter volumes onto the closest surface voxels). Each row of the forward matrix specified the voxel-by-voxel contribution of the cortical absorption changes to the optical density changes measured by the corresponding channel (Aasted et al., 2015).

Next, each row (channel) was scaled by its maximum value so that the voxels' sensitivity in every channel ranged from zero to one ($0 \leq voxels'\ sensetivity \leq 1$). Next, the voxels that had a sensitivity of less than 0.1 in each row were discarded. In other words, for every channel, the voxels contributing less than 10% of the maximum contribution by voxels in that channel were discarded. The voxels with more than 10% contribution to each channel are highlighted in Figure 2.6 per channel.

Then, each row was multiplied by the t-score of the corresponding channel. The next step depended on whether the t-scores were positive or negative, i.e., whether it was an HbO or HbR activation map. In the former case, the maximum value of each column (voxel) was selected, whereas in the latter case, the minimum values were selected. This resulted in a vector with 20,000 positive or negative values (voxels). Finally, the voxels on the cortex were highlighted according to their respective values in the vector.

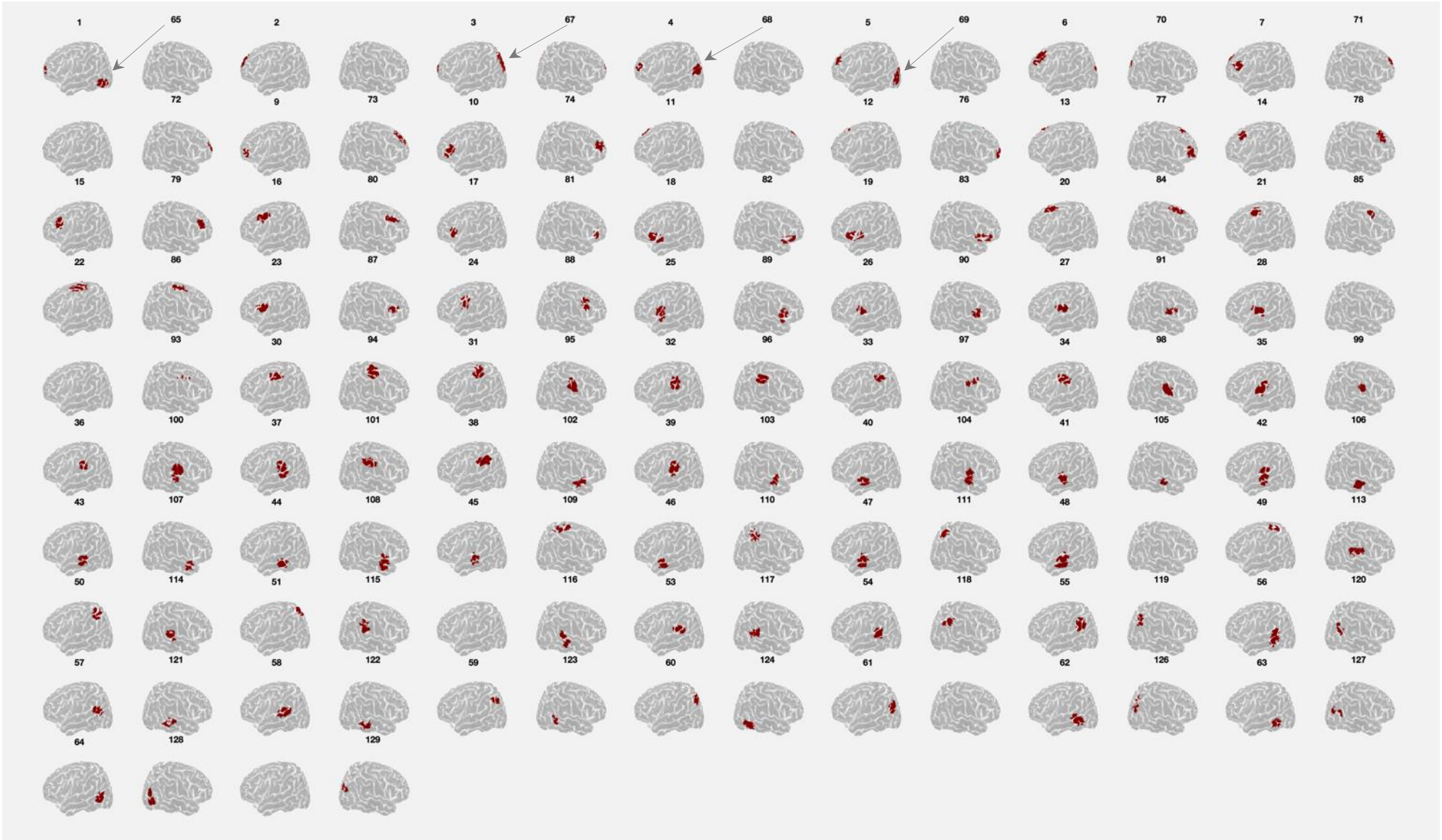

Figure 2.6 The voxels corresponding to each channel. The number above each brain map specifies the channel corresponding to the highlighted voxels. Short channels are not shown. If two clusters are highlighted in a left hemisphere map, the cluster that is more posterior corresponds to the number specified above the next right hemisphere map.

2.5.2 Brain activation frequency maps

Additional maps were created for the group results in which, instead of a t-score, each channel's activation was quantified by the number of participants in whom that channel was activated (i.e., had concurrent significant HbO and HbR responses). The activation frequency maps had two versions. The first version visualized the activation frequency of all the channels where an individual's activations could be repeatedly counted across channels. This was to visualize the distribution of activations on the cortex regardless of the inter-subject variability.

The second version only showed the *distinct* activations of the channels *within* the group activation region (i.e., group ROI). This version was to give a sense of activation frequencies considering the inter-subject variability. The distinct activation of each channel was calculated as follows: in an iterative manner, the channel with maximum activation within the group ROI was found. In each iteration, the individuals who were listed under that channel were taken out from every other channel in the ROI. The loop was repeated until either no individual remained under the remaining channels in the ROI or no channel remained in the ROI. The maximum activation frequency in each iteration was considered as the distinct activation of the corresponding channel.

2.6 Hemodynamic responses

The group hemodynamic responses in the channels with either the peak activation in the activation maps or the maximum number of participants in the frequency maps were plotted. To extract the hemodynamic responses, first, short channel regression was performed on the individuals' preprocessed HbO and HbR time series. For extracting the hemodynamic responses, the robustfit function in MATLAB was used to fit the time series to the principal components of the HbO and HbR short channel measurements. The residual time series were next averaged over participants and then over the five stimulation trials for every condition. In extracting the hemodynamic response of a given channel, only the individuals in whom that channel was activated were included in the group average.

Note that the short channel regression here is separate from the subject-level GLM in which short channel time series were included as regressors of no interest. Thus, the resulting hemodynamic responses do not necessarily conform to the statistical results.

2.7 Comparisons

2.7.1 Individual-group similarity

As a measure of individual-group similarity, everyone's HbO and HbR brain maps were separately correlated with the control group's HbO and HbR brain maps. For the patients, the control group consisted of all 30 healthy participants but for the healthy participants, the control group consisted of the other 29 controls (leave-one-out approach).

The individual-group similarity was calculated using weighted Pearson correlation where short channels and low-quality channels were given a weight of zero. To alleviate the skewness in the distribution of the resulting correlation coefficients in values closer to ± 1, the Fisher transformation was performed on the correlation coefficients. Hence, the individual-group similarity was defined as:

$$Similarity \stackrel{\text{def}}{=} F(r^{Hb}) = \operatorname{artanh}(r^{Hb}) = \frac{1}{2}\ln\left(\frac{1+r^{Hb}}{1-r^{Hb}}\right) \tag{2.17}$$

where F denotes the Fisher transformation and r^{Hb} is the correlation of a given individual's brain map with the group's brain map. The similarities were calculated for both HbO and HbR brain maps:

$$HbO\ Similarity \stackrel{\text{def}}{=} F(r^{HbO}) \tag{2.18}$$

$$HbR\ Similarity \stackrel{\text{def}}{=} F(r^{HbR}) \tag{2.19}$$

The average HbO/HbR similarity was defined as:

$$Average\ Similarity \stackrel{\text{def}}{=} \frac{F(r^{HbO}) + F(r^{HbR})}{2} \tag{2.20}$$

These three similarity scores were calculated in each contrast (nine scores per individual).

2.7.2 Between-group comparisons

A fixed-effect unbalanced three-way ANOVA ($Group \times Contrast \times Hb$) was performed (type III sum of squares) on the individual-group similarities. The Hb factor had three levels: HbO, HbR, and average HbO/HbR (i.e., 'Hb types'). The model also included the interactions between each of the factors.

2.7.3 Inter-subject comparisons

2.7.3.1 Inter-subject comparison criteria

The individuals (healthy participants and patients) were compared by ranking them based on their similarity to the group in each contrast (within contrast similarity) as well as across contrasts (Overall similarity) for which a measure named 'Overall' score was defined.

2.7.3.2 Overall score

The Overall score subsumed the within-contrast similarity scores of an individual under a single measure. The score was defined as the hyperbolic tangent of the weighted average of the quantile-normalized similarities for the chosen Hb types:

$$Overall\ score \stackrel{\text{def}}{=} \tanh\left(\frac{\alpha F_n\left(r^{Hb}_{Sound\ Per.}\right)+\beta F_n\left(r^{Hb}_{Speech\ Per.}\right)+\gamma F_n\left(r^{Hb}_{Language\ Comp.}\right)}{\alpha+\beta+\gamma}\right) \qquad (2.21)$$

where,

- $F_n\left(r^{Hb}_{contrast.}\right)$ was the quantile-normalized similarity score in the given contrast and chosen Hb type;
- α, β, and γ were the adjustable weights of each contrast in the weighted average.

Quantile normalization was performed on the similarity scores to give each contrast equal leverage in the sum before applying the weights while controlling the impact of outliers within each contrast and Hb type. Negative correlations were replaced with zero; therefore, the overall score ranged from zero to one.

As appears in Eq. 2.21, the Overall score had six defining parameters in total, or two per contrast: the Hb type and its weight. The parameters could be adjusted either *a priori* or *a posteriori* (data-driven approach). In the latter case, the parameters were set based on the observed between-groups similarity patterns (i.e., effect sizes) with the aim of increasing the specificity or sensitivity of the overall similarity ratings.

The contrasts' weights and Hb types were determined in three ways resulting in three *versions* of the Overall score:

- **Balanced overall score**: The average HbO/HbR was a priori selected as the Hb type of the similarity scores within all the contrasts. Equal weights were given to the contrasts ($\alpha = \beta = \gamma = 1$).
- **Specific overall score** (data-driven): The Hb type with the *maximum* between-group effect size in a contrast was a posteriori selected for that contrast. The contrasts' weights were set proportional to the maximum effect sizes. In other words, the weight of each contrast reflected the maximum observed between-group dissimilarity across the Hb types within that contrast: the higher the groups' dissimilarity in a contrast, the higher its weight in the weighted sum.
- **Sensitive overall score** (data-driven): The Hb type with the *minimum* between-group effect size in a given contrast was a posteriori selected for that contrast. The contrasts' weights were set to be *inversely* proportional to the minimum effect sizes: the higher the groups' similarity in a contrast, the higher its weight in the weighted sum.

To determine the Specific and Sensitive overall scores of each individual, the parameters had to be set specifically for that individual following the leave-one-out approach: the individual, whether a healthy participant or patient, was excluded from their group and then the between-group effect sizes were calculated for all the contrasts and Hb types.

The Glass' Δ effect size was used as a measure of between-group similarity in the data-driven approach:

$$\Delta = \frac{\text{mean}\big(F_n(controls)\big) - \text{mean}\big(F_n(patients)\big)}{\text{std}\big(F_n(controls)\big)} \tag{2.22}$$

where F_n is the quantile-normalized similarity score in a given contrast and Hb type. The Glass' Δ effect size was preferred for quantifying the similarity effect sizes since it relies on the control group's standard deviation and not the pooled variance across groups.

2.7.4 Prognostic utility

The patients' placings among all the individuals under each ranking were correlated (Pearson correlation) with their GOSE scores to derive the prognostic utility of each comparison criterion. Since the rankings were in descending order with respect to the similarity scores (i.e., the higher the similarity score, the closer to one the place in the ranking), the resulting correlation coefficients were multiplied by -1 to obtain the actual correlation value:

$$Prognostic\ utility\ of\ ranking\ i$$
$$= -\text{Pearson correlation}\ (patients'\ placing\ in\ ranking\ i, patients'\ GOSE)$$

Chapter 3

3 Results

The healthy participants' activation maps at the subject- and group-level are presented in sections 3.1 and 3.2, respectively. Section 3.3 presents the activation maps of all patients. Similarity scores of all individuals is demonstrated in section 3.4 followed by between-group comparison results in section 3.5. Subject-level comparison results (rankings) are provided in section 3.6.

3.1 Healthy participants individual results

Each participant's significant HbO (top row) and HbR (bottom row) brain responses ($q < 0.01$ for both) are presented in Figures 3.1 through 3.5 below. The activations are shown only in regions where a given individual had *concurrent* significant HbO and HbR activation.

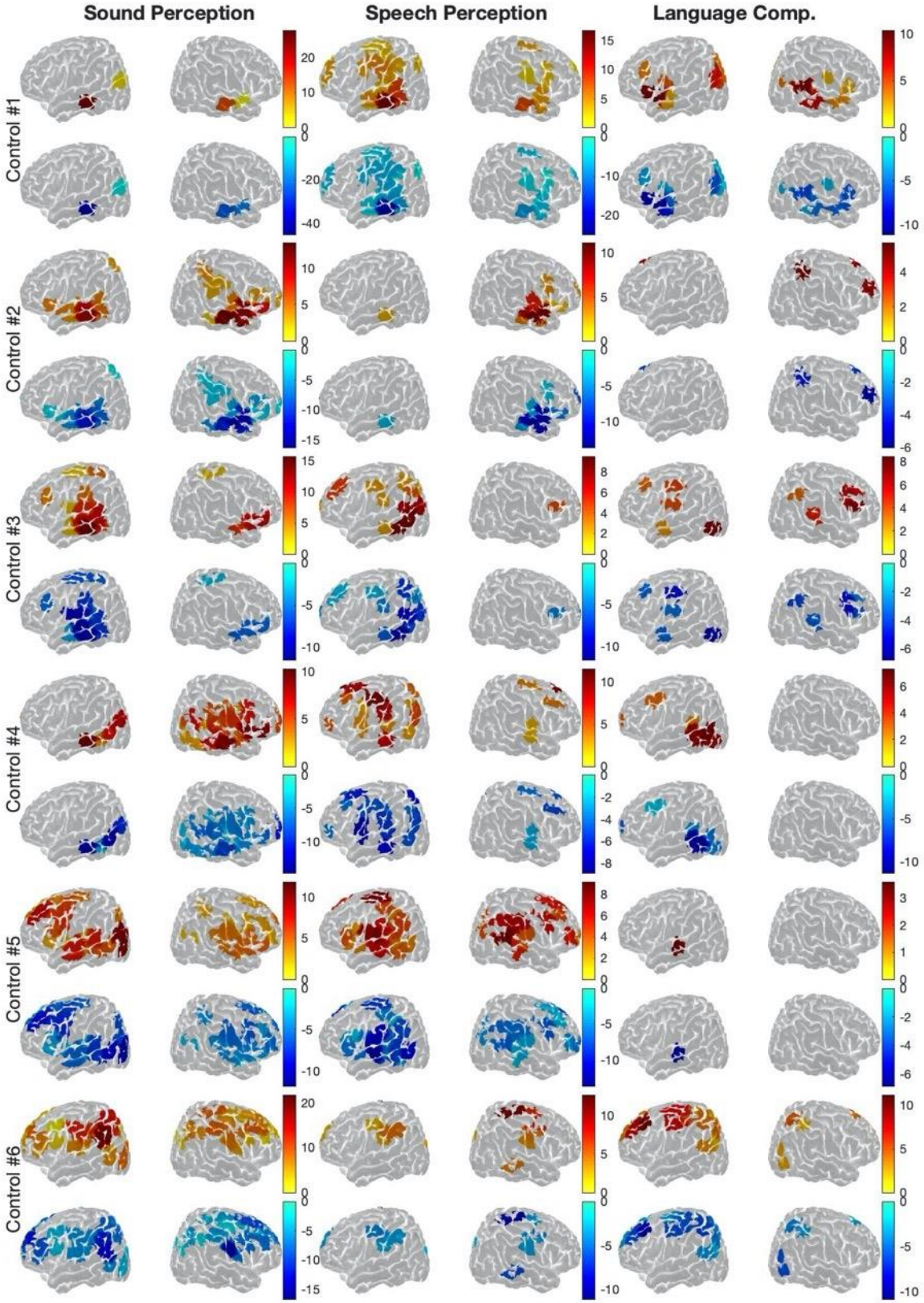

Figure 3.1 HbO and HbR responses. Healthy participant #1 to #6.

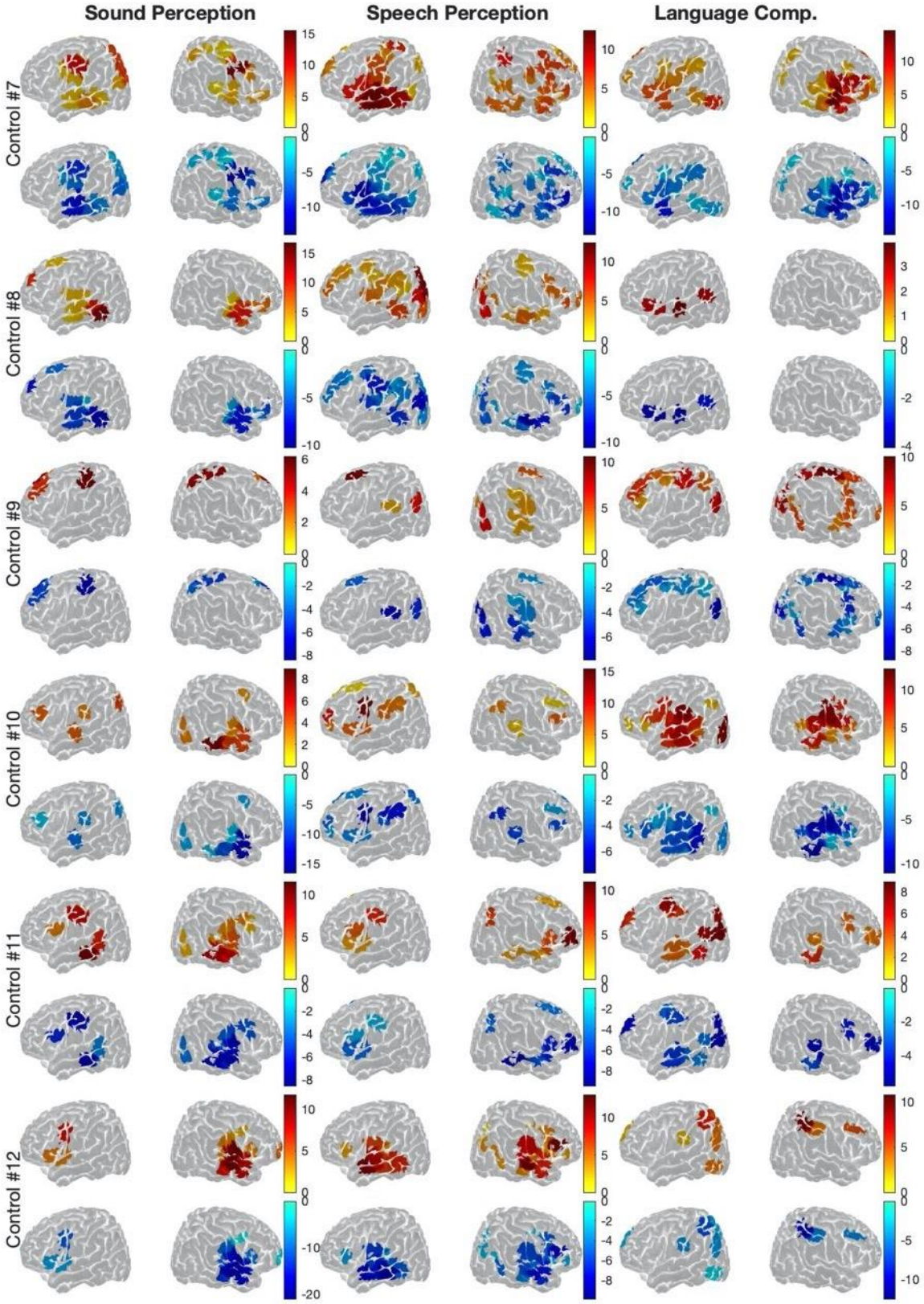

Figure 3.2 HbO and HbR responses. Healthy participant #7 to #12.

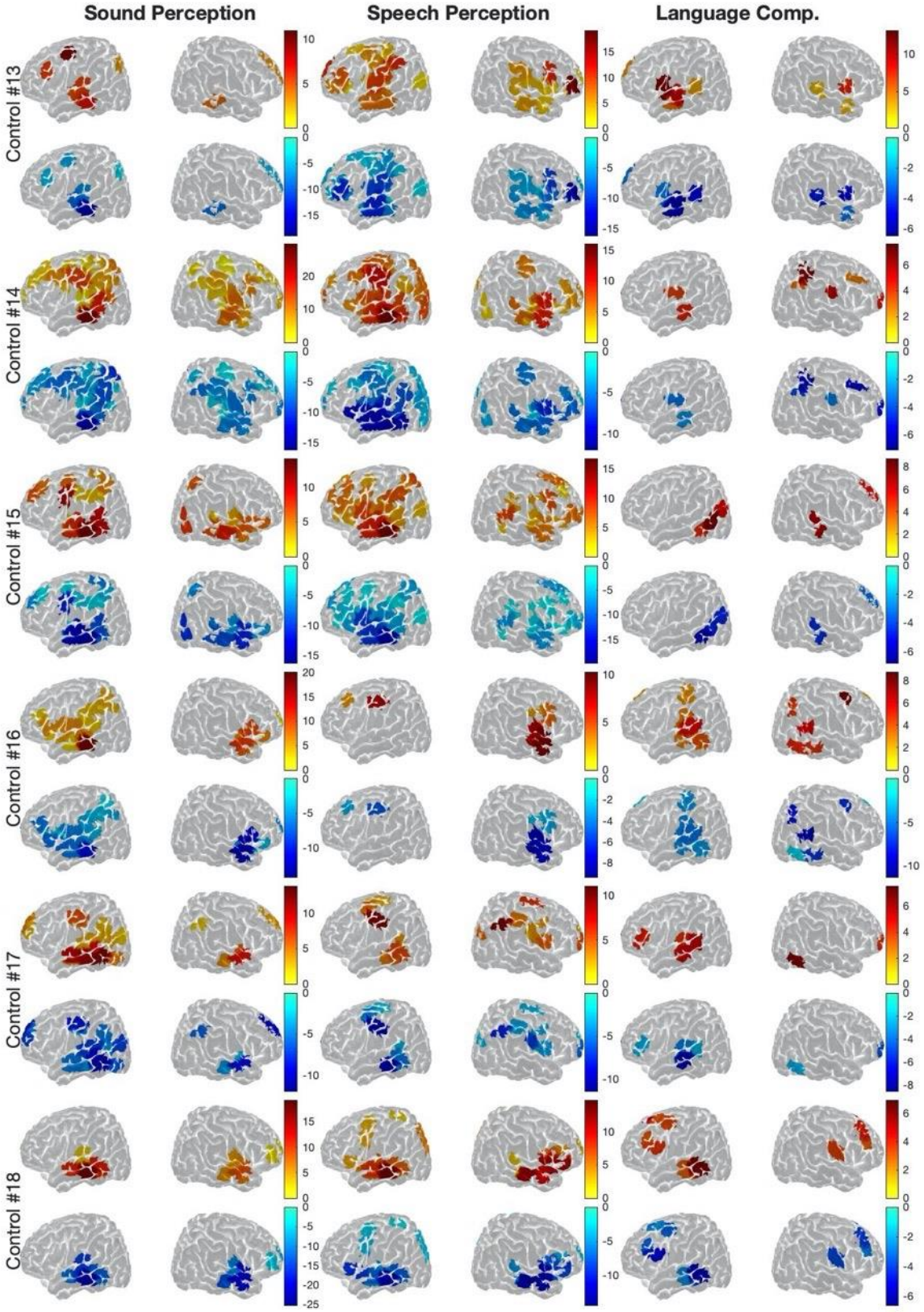

Figure 3.3 HbO and HbR responses. Healthy participant #13 to #18.

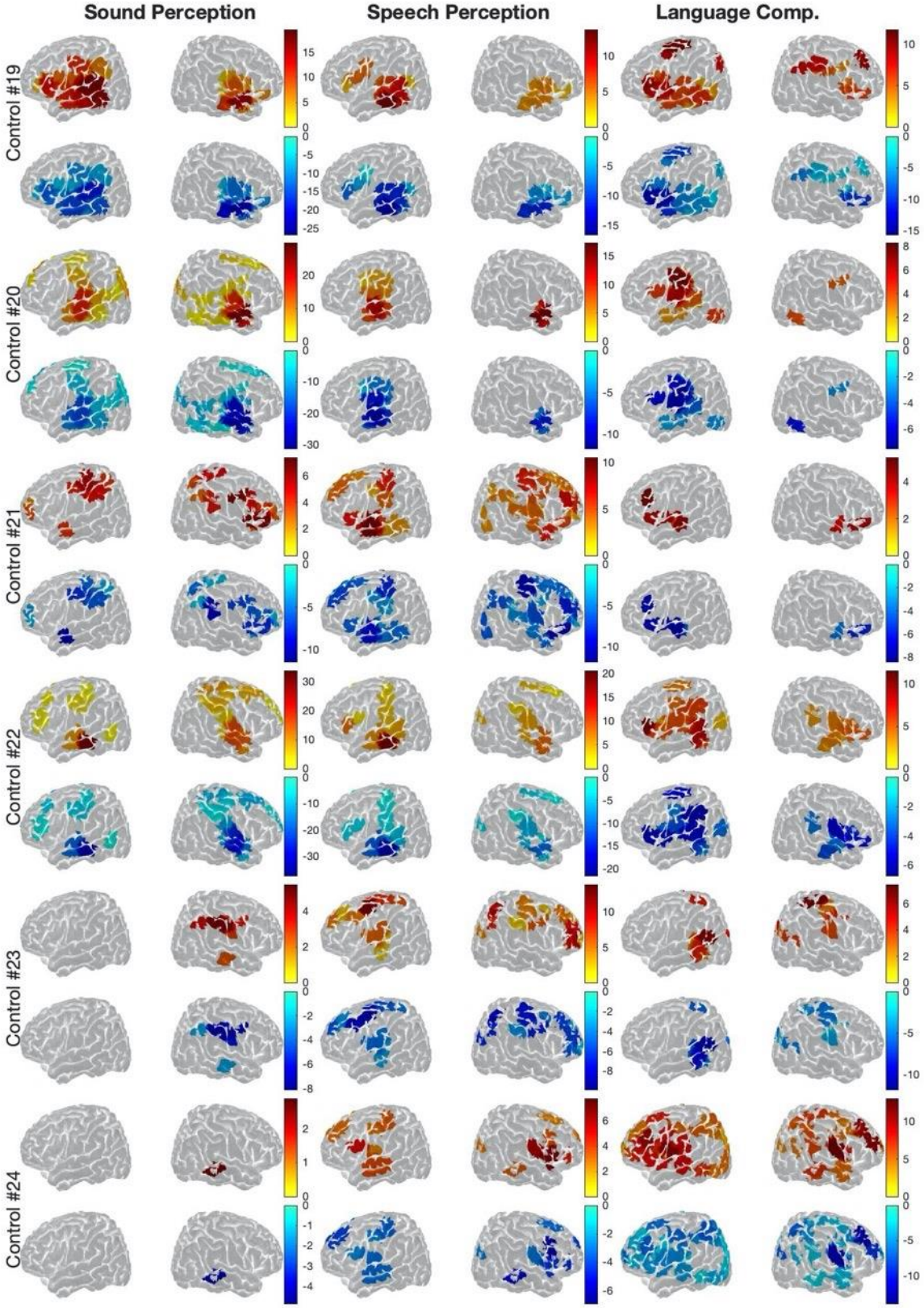

Figure 3.4 HbO and HbR responses. Healthy control #19 to #24.

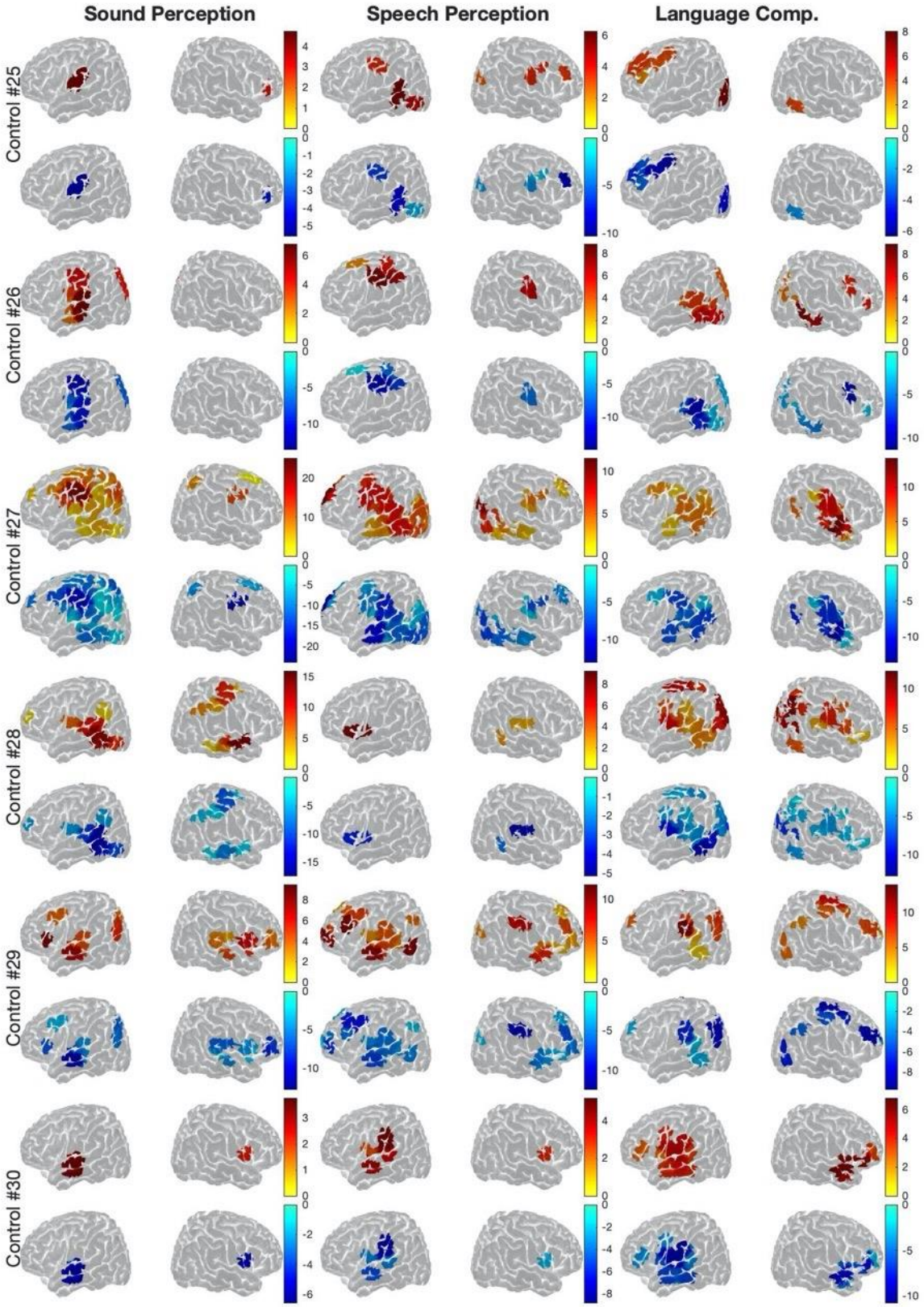

Figure 3.5 HbO and HbR responses. Healthy control #25 to #30.

3.2 Healthy participants' group results

3.2.1 Sound Perception

As depicted in the top panel of Figure 3.6, contrasting all sound conditions against silence resulted in concurrent significant HbO and HbR activation in the STG and MTG *bilaterally*. The temporal lobe of each hemisphere had four activated channels. The peak HbO and HbR responses to sound occurred in the left middle MTG (channel #44: $t(HbO) = 3.75, p < 0.0005$) and in the right middle MTG (channel #106: $t(HbR) = -5.05, p < 0.00001$), respectively. Additionally, the HbO and HbR responses overlapped at the upper ventral sensorimotor cortex (ventral SMC; channel #34: $t(HbO) = 1.89, p < 0.02$; $t(HbR) = -3.47, p < 0.0005$) in the left hemisphere. In the right hemisphere, a channel that was sensitive to the mid STG and ventral SMC was also activated (channel #104: $t(HbO) = 2.07, p < 0.02$; $t(HbR) = -3.89, p < 0.0005$).

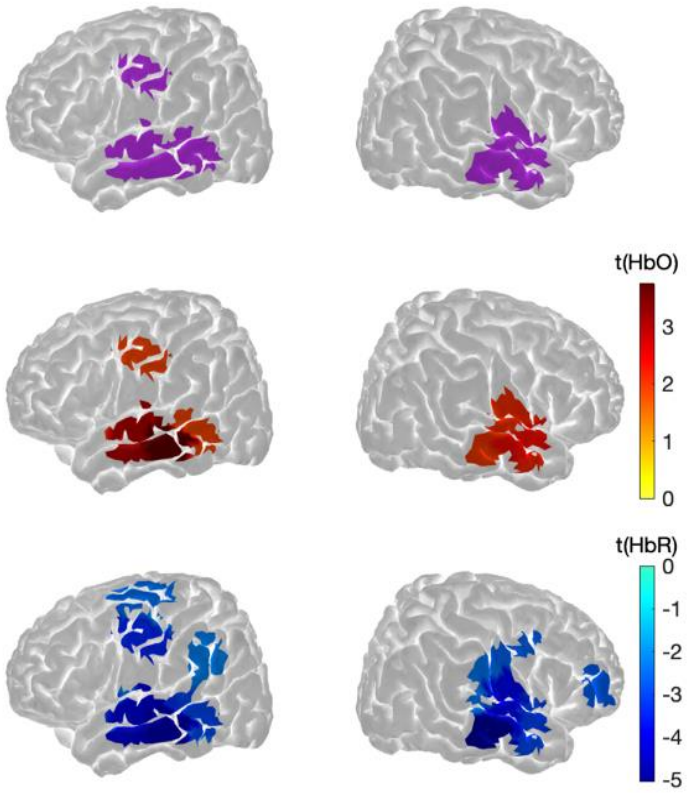

Figure 3.6 Sound Perception group *t*-maps. ***Top:*** The regions with HbO-HbR coactivation included the STG and MTG bilaterally and the left upper ventral SMC; ***Middle:*** The regions with significant HbO increase were same as the HbO-HbR coactivated regions; ***Bottom:*** Significant HbR decrease was additionally observed in the left angular and supramarginal gyri as well as the right frontopolar prefrontal cortex. ($\alpha_{FDR} = 0.05$ in all)

As evident by comparing the middle and bottom panels in Figure 3.6, the cortical regions with significant HbO increase were a subset of the regions with significant HbR decrease. For this reason, the regions with concurrent significant HbO and HbR activation were bound by the regions with significant HbO increase. The regions in which only HbR activation reached significance included the left angular and supramarginal gyri as well as the right frontopolar prefrontal cortex.

In Figure 3.7, the top panel specifies the number of individuals with a particular region of activation, while the bottom panel specifies the number of *distinct* individuals with a given activation *within* the group mask. Activation in the activation frequency maps refers to concurrent significant HbO and HbR response (see 2.5.2). As expected, consistent with the statistical results reported above, the channels associated with the temporal lobe in both hemispheres were the areas in which the largest number of participants showed activity. In particular, channels #44 (left mid MTG) and #102 (right anterior STG/MTG) both were activated in 17 individuals. Channel #34 on the left upper vSMC was activated in 13 individuals.

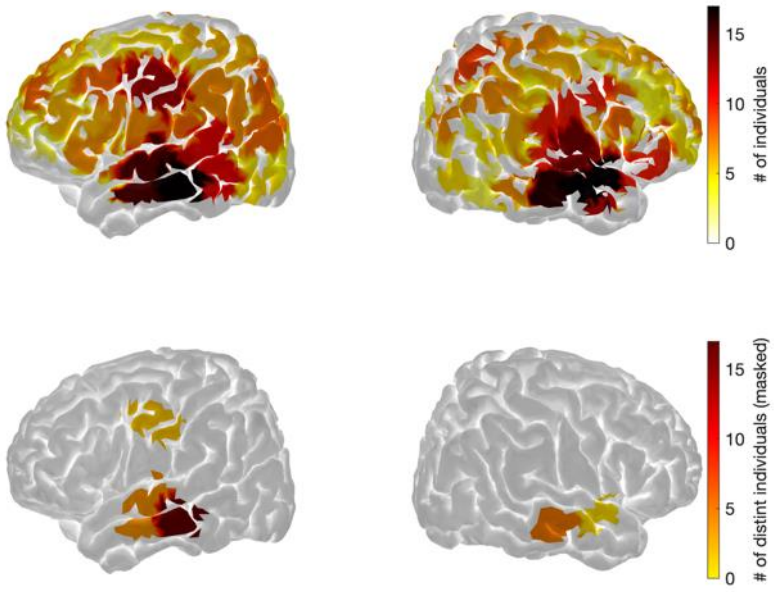

Figure 3.7 Sound Perception activation frequency maps. ***Top:*** The HbO-HbR coactivation frequencies were maximized in the bilateral temporal lobes followed by the sensory motor cortices and the right frontopolar prefrontal cortex; ***Bottom:*** Within the group mask, the left and right mid MTG had the largest number of distinct coactivations.

Among all 30 participants, 29 individuals had at least one activated channel that fell within the group's list of nine activated channels. In fact, no more than five of these nine channels were needed to represent all these 29 individuals. In other words, four of the nine channels did not represent any individual who was not already represented in the top five channels. These five channels were split bilaterally. Furthermore, 19 individuals had bilateral activity within the group mask (i.e., at least one activated channel in the left and one in the right hemisphere in common with the group).

The HbO and HbR hemodynamic responses in the mentioned channels with the peak activation (the HbO peak: channel #44, the HbR peak: channel #106) are depicted in Figure 3.8. The hemodynamic responses in each channel were averaged over the individuals who had concurrent significant HbO-HbR activation in that channel. In both channels and in all conditions, a positive HbO response and a negative HbR response were evident for the selected group of individuals. Particularly, the HbO and HbR responses within the Complex Language condition (short stories) closely resembled the characteristic hemodynamic response function. This was also the case within the Meaningless Speech condition (pseudowords) in channel #44 and less so in channel #106. In the Non-speech sound condition (noise), the inverse HbO-HbR responses were present but were not as strong and fluctuated within the stimulation period.

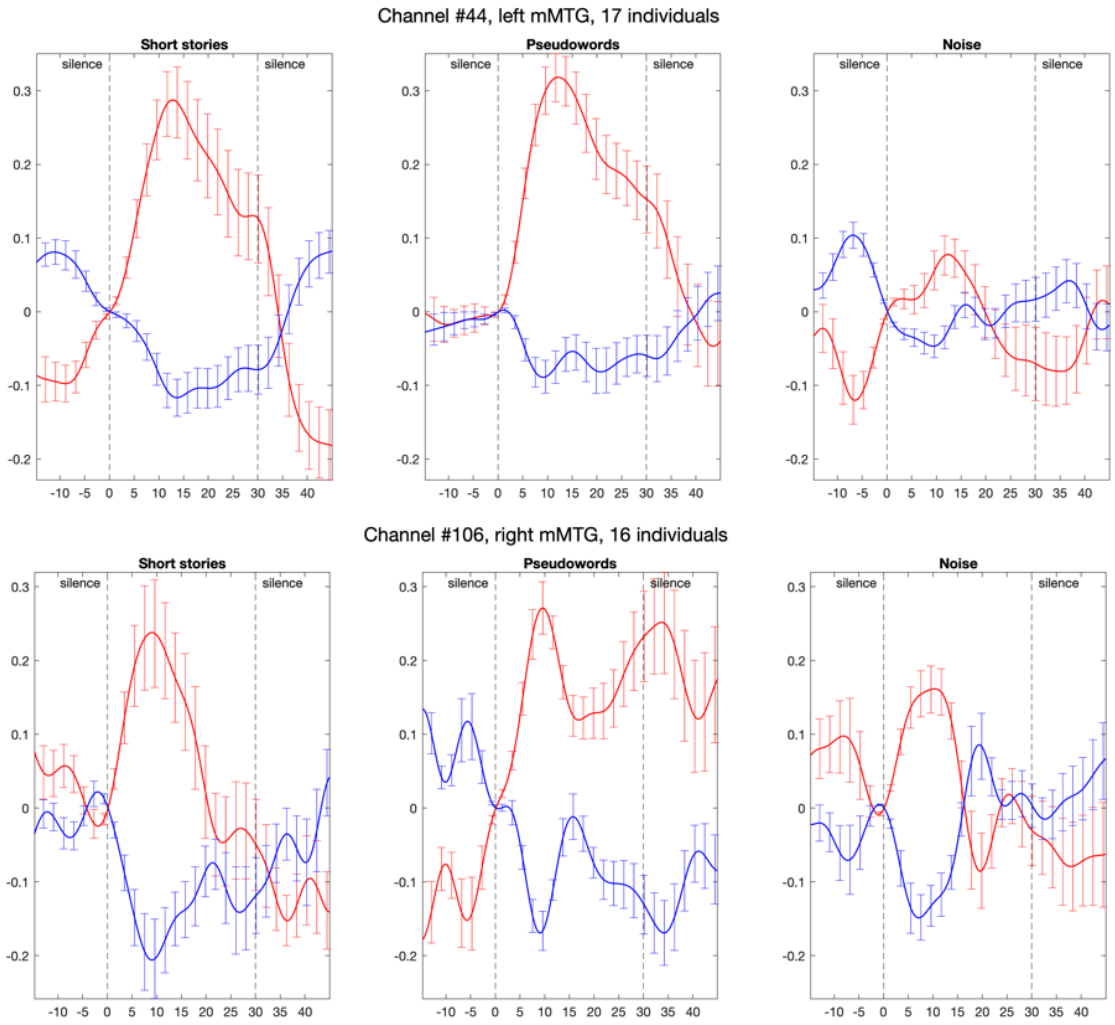

Figure 3.8 Hemodynamic responses in the channels with the peak HbO and HbR response in the Sound Perception contrast. The HbO increase and HbR decrease during all conditions is seen in both channels. Short stories followed by the pseudowords elicited the strongest responses. (Red=HbO; blue= HbR; bars represent standard error of the mean)

3.2.2 Speech Perception

As reflected in the top panel of Figure 3.9, when the individuals' brain response to noise was subtracted from their brain response to speech conditions (i.e., short stories and pseudowords), a bilateral but dominantly left-lateralized coactivation pattern resulted (four channels in the LH vs. one channel in the RH). In the left hemisphere, the regions with concurrent HbO and HbR activity formed a narrow strip extending dorsoventrally from the upper ventral SMC (channel #34: $t(HbO) = 3.71, t(HbR) = -3.42,\ p < 0.0005$ for both) to the mid MTG (channel #44: $t(HbO) = 3.29, p < 0.001;\ t(HbR) = -4.44, p < 0.0001$). These dorsal and ventral ends of the strip, respectively, had the maximum HbO increase and the maximum HbR decrease in the whole brain. The elicited activity in the mid MTG, mid STG, and ventral SMC was detected by two other overlapping channels (channels #42 and #43). In the right hemisphere, a channel sensitive to anterior temporal lobe regions was also activated (channel #102: $t(HbO) = 3.62, t(HbR) = -4.10, p < 0.0005$ for both)

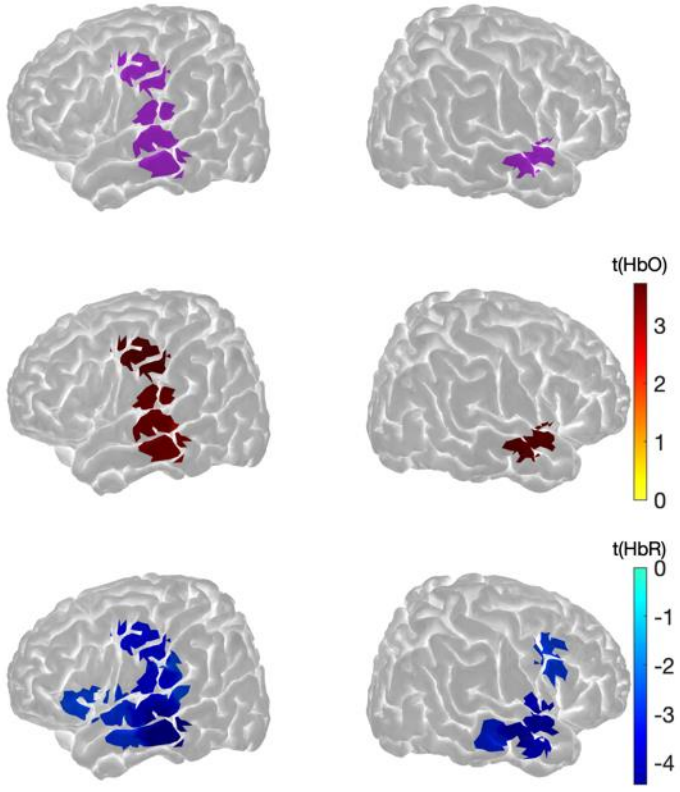

Figure 3.9 Speech Perception group t-maps. ***Top:*** The regions with HbO-HbR coactivation included the STG, MTG and ventral SMC bilaterally as well as the left upper ventral SMC; ***Middle:*** The regions with significant HbO increase were same as the HbO-HbR coactivated regions; ***Bottom:*** Significant HbR decrease was additionally observed in the posterior STG, Broca's area. ($\alpha_{FDR} = 0.05$ in all)

Similar to the Sound Perception contrast, the HbR activations were more widespread than the HbO activations (Figure 3.9, middle and bottom panels). The frontal lobe areas in which only HbR response reached significance included a channel sensitive to the Broca's area in the left ventrolateral prefrontal cortex (channel #19: $t(HbR) = -2.65, p < 0.005$) as well as a channel in the right hemisphere associated with the posterior inferior frontal and middle gyri (channel #88: $t(HbR) = -2.81, p < 0.005$).

Figure 3.10 demonstrates the activation frequencies per region. The brain regions activated in the largest number of individuals were the left upper ventral SMC (channel #34: 17 individuals) followed by the left mid-MTG (channel #44: 16 individuals) and the right anterior STG/MTG (channel #102: 16 individuals). More than one-third of the participants had activations outside the temporal lobe in the Broca's area (channel #19: 11 individuals) as well as in the right lateral frontopolar cortex (channel #81: 12 individuals).

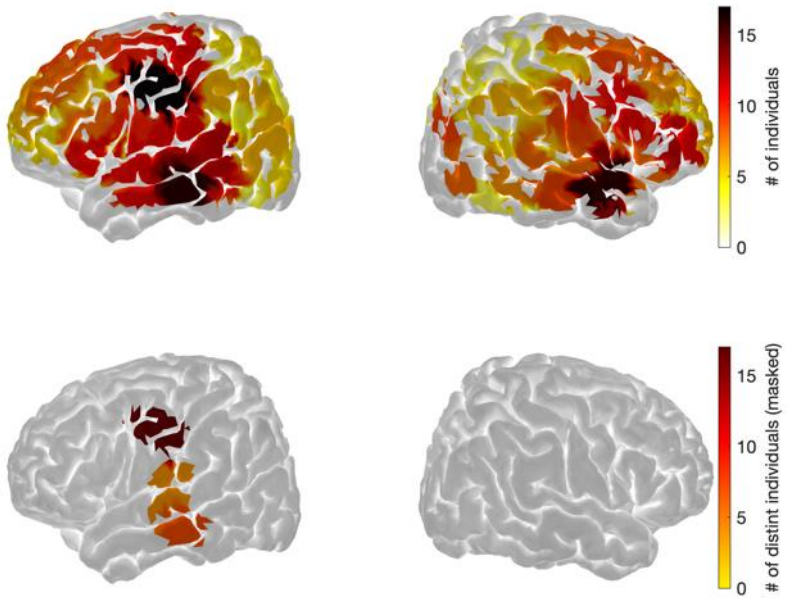

Figure 3.10 Speech Perception activation frequency maps. ***Top:*** The HbO-HbR coactivation frequencies were maximized in the left SMC followed by the bilateral MTG and STG, Broca's area, and right RLPFC; ***Bottom:*** Within the group mask, three channels covering a narrow region from the left mid MTG to the upper ventral SMC had the largest number of distinct coactivations.

Of all 30 participants, 28 individuals had at least one activated channel that fell within the group's list of five activated channels. These 28 individuals all could be mapped onto three of those five channels without the other two channels representing any new individual (Figure 3.10, bottom panel). All three of these channels were in the left hemisphere, dorsally extending from the mid-MTG (channel #44) to the mid-STG/ventral SMC (channel #42) and the upper ventral SMC (channel #34). Furthermore, 16 individuals had bilateral activity within the group mask (i.e., at least one activated channel in the left and one in the right hemisphere in common with the group).

The HbO and HbR hemodynamic responses of three highly activated channels are presented in Figure 3.11. One is the activated channel covering the left upper ventral SMC (channel #34), the second is a channel covering the right anterior STG/MTG (channel #108) and the third is a channel covering the left mid-STG (channel #43). The hemodynamic responses in each of these channels are averaged over the individuals who had concurrent HbO-HbR activation in that channel. In all three of these channels, an HbO increase and an HbR decrease in response to the short stories and pseudowords were detected for the selected group of individuals. The responses to the noise were either comparatively small (channel #44) or even close to zero (channel #108). The HbO and HbR inverse responses to the short stories and pseudowords closely resembled the characteristic HRF in the upper ventral SMC. Such characteristic responses were also observed in the left mid-STG and right anterior STG, although the HbR responses were not as strong.

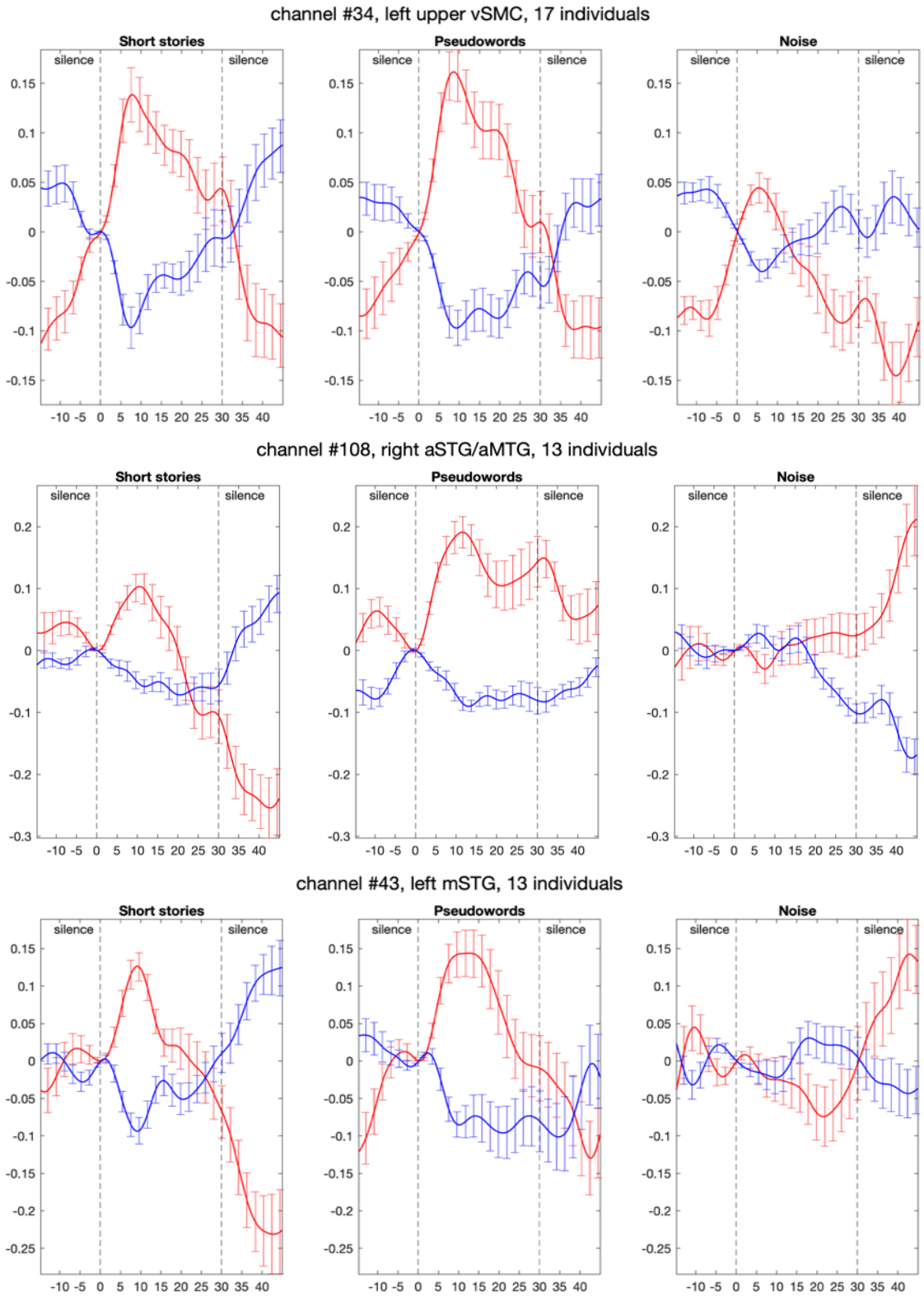

Figure 3.11 Hemodynamic responses in three highly activated channels in the Speech Perception contrast. The HbO increase and HbR decrease during short stories and pseudowords were detected in all the channels. Noise did not elicit similar responses. (Red=HbO; blue= HbR; bars represent standard error of the mean)

3.2.3 Language Comprehension

Contrasting the activations elicited by the short stories (complex language condition) against the group's brain responses to the pseudowords' (meaningless speech condition) revealed involvement of the *left* posterior temporal lobe and angular gyrus in semantic processing (Figure 3.12, top panel). The maximum HbO and HbR responses co-occurred in channel #56 ($t(HbO) = 2.12, p < 0.02$; $t(HbR) = -2.95, p < 0.002$) which covered posterior STG/MTG and angular gyrus. The other channel (channel #62: $t(HbO) = 1.95, p < 0.02$; $t(HbR) = -2.40, p < 0.01$) was instead more sensitive to the posterior MTG.

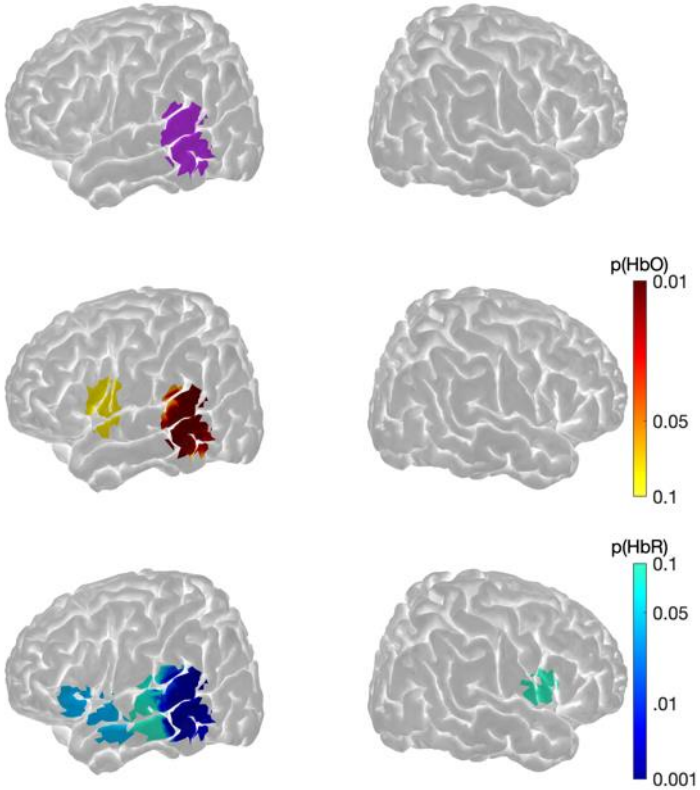

Figure 3.12 Language Comprehension group activation maps. ***Top:*** Concurrent HbO and HbR responses was observed in the posterior STG/MTG and angular gyrus ($p < 0.05$ for each); M***iddle:*** The HbO response was additionally detected in a region overlapping with the Broca's area ($p < 0.1$); ***Bottom:*** HbR's activation in the posterior STG/MTG was very robust. Additional activation was observed in the anterior STG/MTG and Broca's area ($p < 0.1$) (none are corrected for multiple comparisons).

At the significance level of $\alpha = 0.05$, the HbR decrease was detected in four other channels in addition to the two channels mentioned above. Two of these channels covered the posterior STG (channel #54: $t(HbR) = -2.1, p < 0.02$) and posterior MTG (channel #63: $t(HbR) = -2.57, p < 0.005$, the third one covered the anterior STG (channel #46: $t(HbR) = -1.43, p < 0.05$) ventral to the fourth channel at the Broca's area (channel #18: $t(HbR) = -1.40, p < 0.04$). The first two of these four channels had significant HbO response at the reduced significance level of $\alpha = 0.1$ (channel #54: $t(HbO) = 1.25, p < 0.06$; channel #63: $t(HbO) = 1.00, p < 0.09$). Although the HbO response did not reach significance in the remaining two channels at the reduced significance level, a channel very close to them and to the Broca's area reached significance (channel #25: $t(HbO) = 1.03, p < 0.1$).

As shown in Figure 3.13, there was more variability in the distribution compared to other contrasts. However, the top four activation frequencies shared by 10 channels all happened in the left posterior temporal lobe, temporoparietal junction, and ventral SMC, well-known language-related regions. The activation frequency of these 10 channels ranged from 9 to 12 ($mean = 10.4, std = 1.08$). Two channels (channels #67 and #68) posterior to the temporoparietal junction were activated in eight participants. The maximum activation frequency of a channel in the right hemisphere was eight. Eight channels in the right hemisphere had this activation frequency, and their coverage regions included ITG, temporoparietal junction, mid-STG, ventral SMC, and ventrolateral prefrontal cortex.

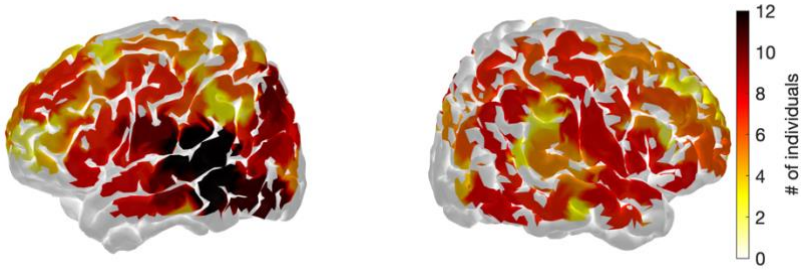

Figure 3.13 Language Comprehension activation frequency maps. The activation frequencies were maximized in the left posterior temporal lobe and mid STG followed by the left ventral SMC and temporoparietal junction.

More than half (17) of the individuals had at least one of the group's two activated channels among theirs (evaluated at $\alpha = 0.05$). Seven of these 17 participants had both channels activated. However, close to 90% of the participants (26) shared at least one channel with the group in the reduced significance level of $\alpha = 0.1$ that had four activated channels (all still were within the left posterior temporal lobe).

The HbO and HbR hemodynamic responses of three highly activated channels at the left posterior STG/MTG and angular gyrus (channels #56, #58, and #62) are presented in Figure 3.14 below. The hemodynamic responses in each of these channels was averaged over the individuals who had concurrent HbO-HbR activation in that channel. In all three of these channels, an HbO increase and HbR decrease in response to the short stories was detected for the selected group of individuals. Such inverse HbO and HbR responses were not detected in channels #56 and #58 during pseudowords stimulation. Although such responses to pseudowords were seen in channel #62, the magnitudes of both HbO and HbR activations were smaller than the detected responses to the short stories.

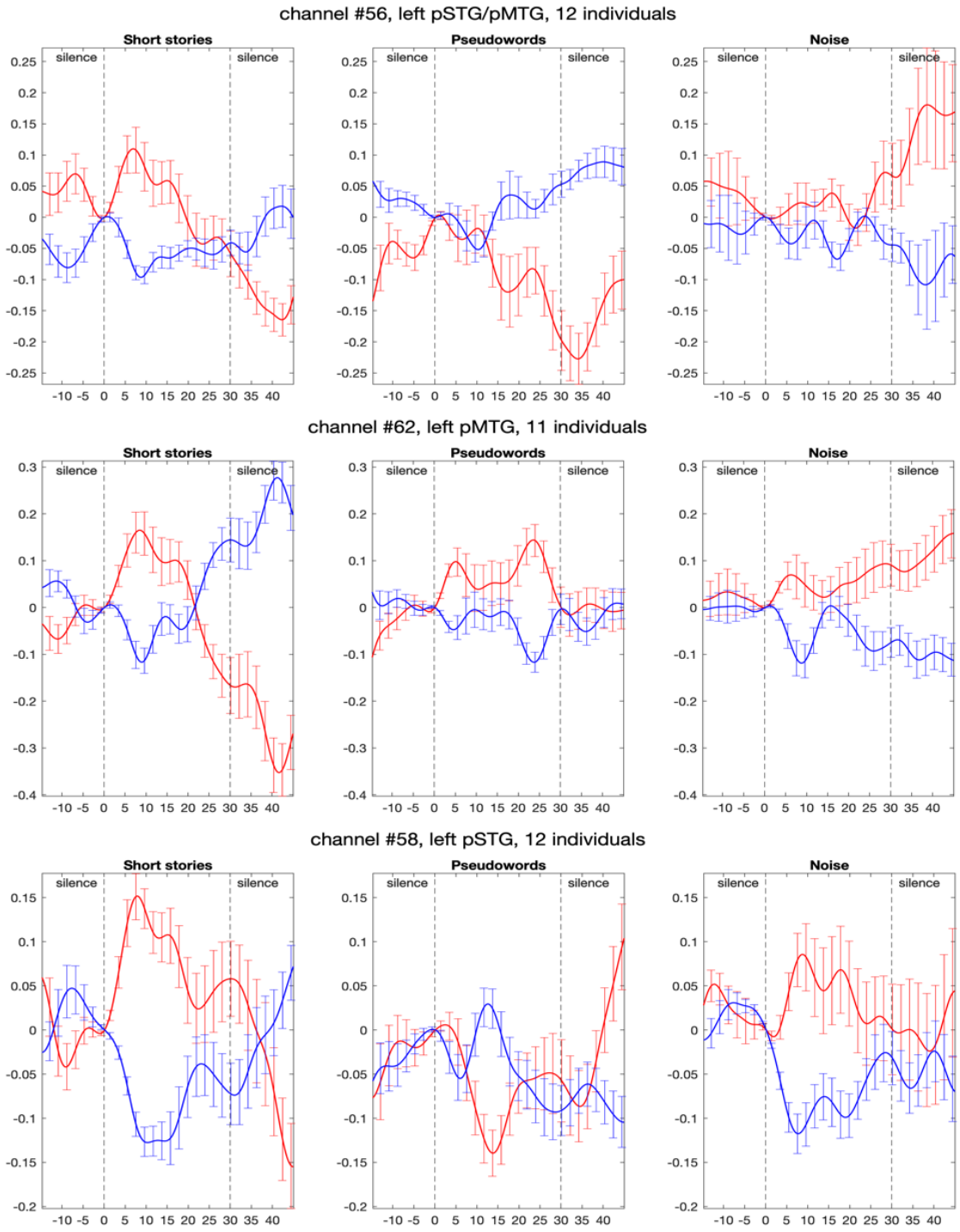

Figure 3.14 Hemodynamic responses in three highly activated channels in the Language Comprehension contrast. Short stories evoked positive HbO and negative HbR responses in all the three channels. Such response was not observed during the pseudowords stimulation. (Red=HbO; blue=HbR; bars represent the standard error of the mean)

3.3 Patients

Only two out of eight patients regained behavioral responsiveness and partial functional recovery: patient #4 (GOSE=5, *good* outcome) and patient #8 (GOSE=4). Except for patient #1, who deceased due to medical complications, life support was withdrawn in the rest (5/8). Figures 3.15 and 3.16 present results for individual patients.

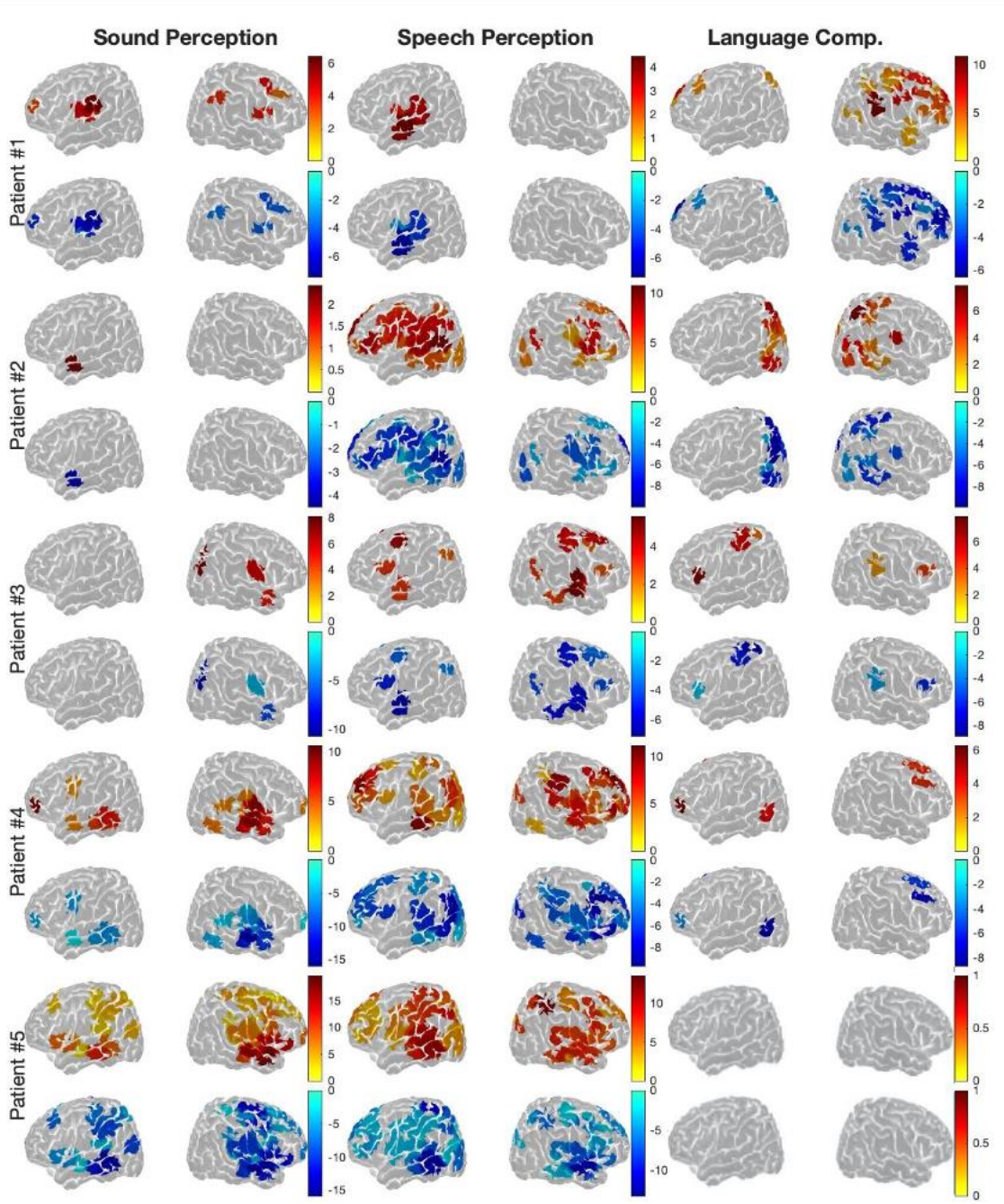

Figure 3.15 HbO and HbR responses. Patient #1 to #5.

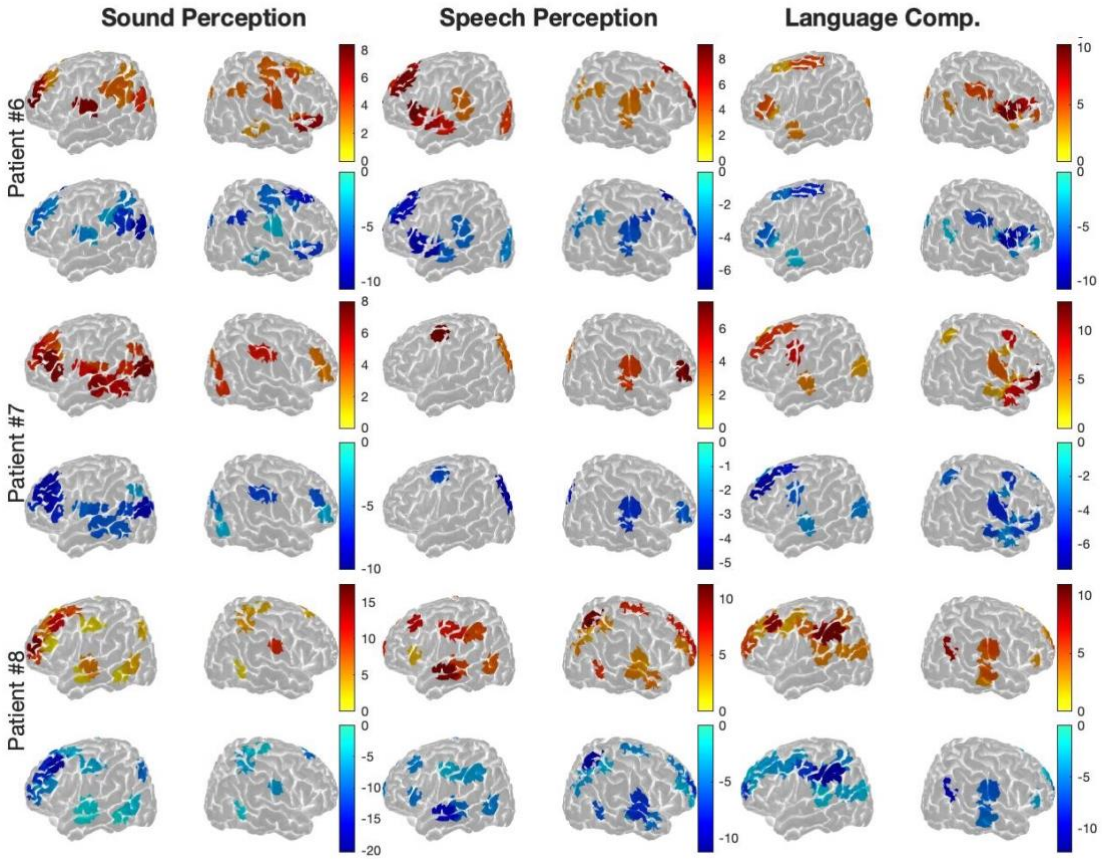

Figure 3.16 HbO and HbR responses. Patient #6 to #8.

A description of patients who did not undergo WLST follows.

Patient #1: (deceased but not due to WLST): The patient (68 y/o, m) visited a peripheral hospital after feeling weakness in the right side of his body. His symptoms were due to a posterior circulation stroke caused by basilar artery thrombosis. He was treated with IV-tPA and was then transferred to the University Hospital for endovascular therapy. Despite acute therapy, he subsequently deteriorated and required ICU admission with intubation and mechanical ventilation. Repeated vessel imaging showed a recurrence of the basilar artery thrombus. An MRI scan showed an ischemic stroke in the pons and right cerebellum as well as some scattered foci of infarction supratentorially. He was unable to regain consistent behavioral responsiveness but was able to be extubated. The patient was transferred to the inpatient stroke unit on day 28 after ICU admission and did not improve significantly and passed away 36 days later due to several complications. fNIRS

evaluations occurred on day 24. At the testing session, the patient had a GCS of 6T, and his pupils were reactive. Due to his pontine stroke etiology, the patient was a potential candidate for locked-in syndrome, but this possibility was not confirmed in the command following tests (results not reported in the present study).

Patient #4: The patient (63 y/o, female) was admitted to the ICU with rapidly progressive sensory changes and weakness due to GBS (i.e., severe acute motor and sensory axonal neuropathy). She lost brainstem and motor responses within the first day and was consequently intubated. On day 5, EMG revealed absent motor responses with reduced sensory amplitude in the left foot and left radial nerve and absent sensory responses from the left median and ulnar nerves. Although the diagnosis of GBS was confirmed and the patient's central nervous system was consequently deemed intact, her motor paralysis and sensory disturbances yielded the minimum GCS of 3. By day 22, the patient could behaviorally respond and communicate. On day 73, the patient was transferred to an in-patient rehabilitation facility, and her recovery continued thereafter.

Patient #8: The patient was presented to a peripheral hospital with subacute left upper shoulder pain. In the emergency department she had a seizure and subsequently had decreased level of consciousness and ultimately went into cardiac arrest. She was resuscitated and transferred to University Hospital for further investigations and management. There was concern that the underlying cause of the cardiac arrest was due to metabolic derangements. She was treated in the ICU with sedation and management of post-hypoxic seizures, which improved electrographically with medication. She required medication for agitation but eventually showed clinical improvement and began to intermittently obey clinical staff 10 days after admission.

3.4 Individual-group similarity

Each individual's HbO and HbR brain maps were correlated separately to the HbO and HbR brain maps of a control group. In the case of patients, the control group included all 30 healthy participants (Figure 3.17), while for healthy participants, the control group excluded the individual being analyzed (leave-one-out approach).

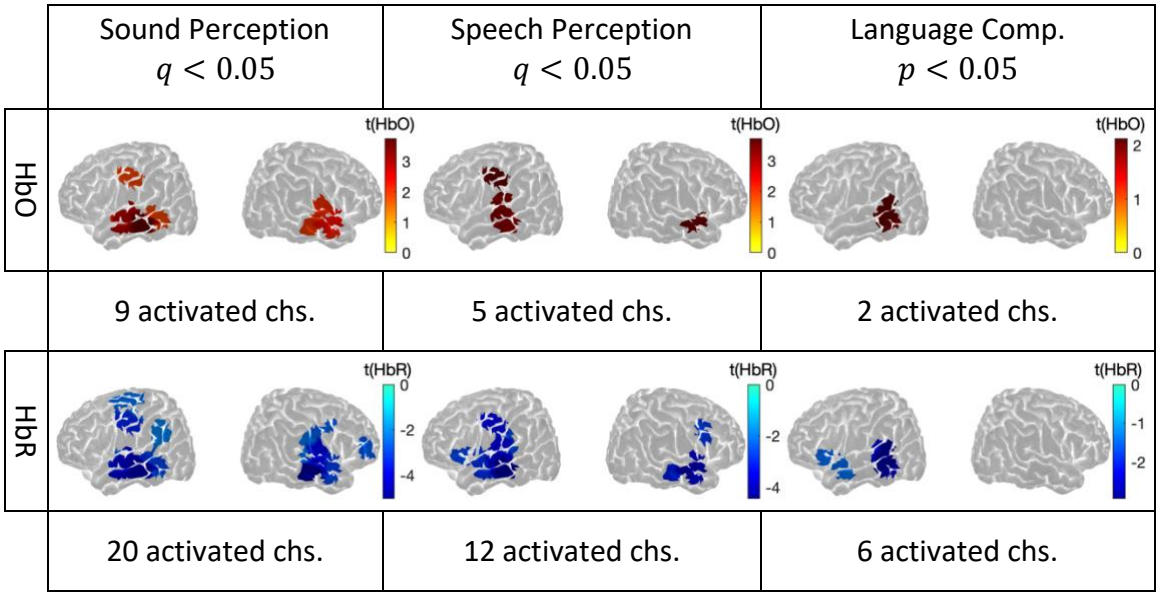

Figure 3.17 Reference HbO and HbR activation maps from the control group for patients. The number of activated channels in each map is indicated below it.

The individuals' HbO and HbR brain maps were evaluated at the FDR significance level of $q < 0.05$ in all contrasts. The control group's HbO and HbR activation maps were also evaluated at the FDR significance level of $q < 0.05$ in the Sound Perception and Speech Perception contrasts. However, the group's HbO and HbR activation maps within the Language Comprehension contrast were evaluated at $p < 0.05$ without correcting for multiple comparisons.

Figure 3.18 depicts the resulting HbO, HbR, and average HbO/HbR similarity scores of all individuals per group and contrast.

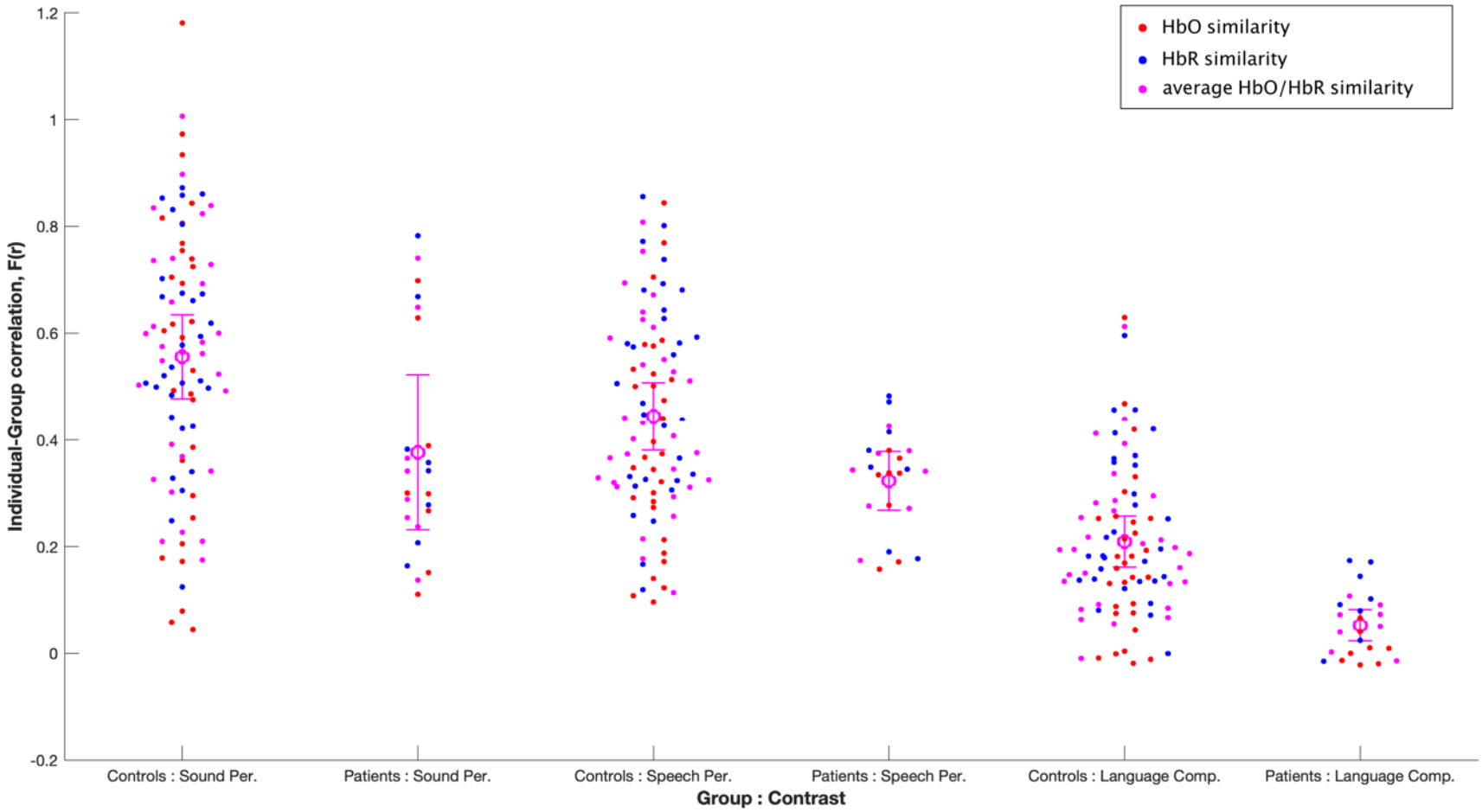

Figure 3.18 Individual-group similarities per group and contrast. ***Between-group:*** Compared to the patients, healthy participants' activations were on average more similar to the control group's activations in all the contrasts and for all the Hb response types. The between-group difference was only significant in the Language Comprehension contrast ($p < 0.0005$ for all Hb types); ***Between-contrast:*** In both groups, similarity scores were highest in the sound Perception and lowest in the Language Comprehension. In both groups, Language Comprehension similarities significantly differed from the other two contrasts' similarities.
(The purple bars represent the 95% confidence interval for the average HbO/HbR similarities)

3.5 Group-level comparisons

A fixed-effect unbalanced three-way ANOVA ($Group \times Contrast \times Hb$) was performed (type III sum of squares) on the individual-group similarities. The Hb factor had three levels: HbO, HbR, and average HbO/HbR (i.e., 'Hb types'). The model also included the interactions between each of the factors. Based on the ANOVA results, multiple comparisons were made to evaluate the significant differences (corrected for multiple comparisons via Dunn and Sidak's approach).

The three-way ANOVA revealed a main effect of Group and Contrast. The individual-group similarities were significantly different between the healthy participants and the patients ($F(1,324) = 38.52, p < 0.0001, \eta^2 = 0.10$). Compared to the patients ($mean = 0.25, std = 0.19$), the healthy participants' brain responses ($mean = 0.40, std = 0.24$) correlated 60% more with the control group's pattern of activation ($95\%\ CI = [0.1, 0.2], p < .0001$).

Although none of the interactions were significant, simple effects were explored via post-hoc Welch's t-tests (5000 permutations, controlled for family-wise error rate at $\alpha = 0.05$). The independent sample Welch's t-tests revealed that, while the healthy group had higher similarity scores in all contrasts and Hb types than patients, the between-group differences did not reach significance in any of the Hb types within the Sound and Speech Perception contrasts. Rather, for the HbR and the average HbO/HbR similarities, the difference *approached* significance in the Speech Perception contrast ($p < 0.09$ and $p < 0.06$, respectively). However, the between-group difference within the Language Comprehension contrast was significant for all the Hb types ($p < 0.0005$ for all).

Paired sample Welch's t-tests revealed that, in both groups and for all Hb types, the highest individual-group similarities were in the Sound Perception contrast, followed by the Speech perception and Language Comprehension contrasts. In both groups, the similarities within the Language Comprehension contrast were significantly lower than the Sound Perception and Speech Perception similarities for all Hb types ($p < 0.0005$ for all six comparisons within the healthy group and $p < 0.005$ for all six comparisons

within the patient group). Within the control group, the difference between the Sound Perception and Speech Perception similarities was not significant for the average HbO/HbR responses, but the difference approached significance for the HbO and HbR responses themselves ($p < 0.08$ and $p < 0.06$, respectively). However, within the patient group, the Sound Perception and Speech Perception similarities were very close for all the Hb types ($p < 0.8$ for the HbO, $p < 0.8$ for the HbR, and $p < 0.9$ for the average HbO/HbR).

3.6 Subject-level rankings

The individuals (healthy participants and patients) were compared by ranking them based on the following criteria:

- **Within-contrast individual-group similarity** (three rankings): In each contrast, the individuals were ranked according to their average HbO/HbR similarity to the group.
- **Overall individual-group similarity** (three rankings): Individuals were ranked based on their overall similarity to the group *across* contrasts.

For this purpose, an "Overall score" measure was defined, reflecting an individual's overall function in the auditory processing hierarchy. The Overall score had two adjustable parameters per contrast: the Hb type and its weight. In the Balanced overall score, the average HbO/HbR was a priori selected as the Hb type within all contrasts, and equal weights were given to all contrasts. As described in 2.7.3.2, to determine each individual's Specific and Sensitive overall scores, the parameters were set based on the between-groups dissimilarity effect sizes specific to that individual following a leave-one-out approach.

Figure 3.19 demonstrates the Glass' Δ between-group effect sizes of the *quantile-normalized* similarity scores (all individuals included). As evidenced, the effect sizes varied based on the contrast and Hb response type. The Language Comprehension contrast had the largest effect sizes across the contrasts for all the Hb response types. The largest effect size in the Sound Perception contrast was observed in the HbR response.

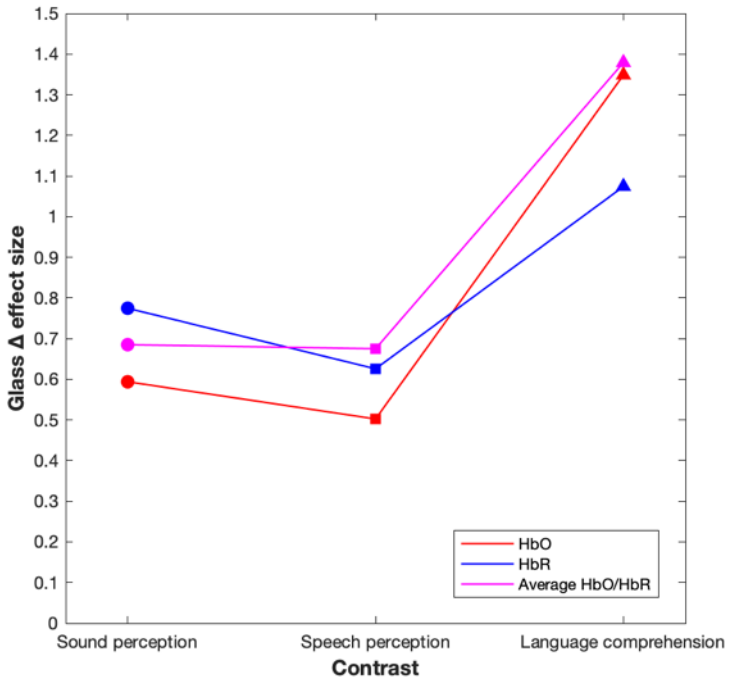

Figure 3.19 Between-group Glass' Δ effect sizes for each Hb response per contrast. The maximum effect sizes were for the average HbO/HbR response in all but the Sound Perception contrast in which the HbR response had the maximum effect size. The minimum effect sizes were for the HbO response in all but the Language Comprehension contrast in which the HbR response had the minimum effect size.

However, the maximum effect sizes in the Speech Perception and Language Comprehension contrasts were seen in the average HbO/HbR response. The minimum effect sizes in the Sound Perception and Speech Perception contrasts were seen in the HbO response. In contrast, the HbR response had the smallest effect size in the Language Comprehension contrast.

The resulting parameters for patients are presented in Table 3.1. Two main patterns were evident in the results. First, for all patients, the Language Comprehension contrast received the highest and the lowest weights by a factor of ~2 and ~0.5, respectively, in the Specific overall and Sensitive overall scores. Second, with a few exceptions (3/24), HbO was not selected as the specific Hb type. Instead, HbR was selected for the Sound Perception contrast, and average HbO/HbR was chosen for the other two contrasts. Conversely, average HbO/HbR was never selected as the sensitive Hb type. Rather, HbO was selected for the Sound and Speech Perception contrasts, and HbR was chosen for the Language comprehension contrast.

	Specific overall score			Sensitive overall score		
	Sound Per.	Speech Per.	Language Comp.	Sound Per.	Speech Per.	Language Comp.
Patient #1	1	1	1.8	1.5	2.0	1
Patient #2	1	1.1	2.2	1.5	1.6	1
Patient #3	1.1	1	2.2	1.5	2.1	1
Patient #4	1.5	1	2.2	1.1	1.6	1
Patient #5	1.2	1	1.7	1.5	1.8	1
Patient #6	1.2	1	2.4	2.1	2.5	1
Patient #7	1.3	1	2.4	1.7	1.9	1
Patient #8	1	1	1.9	1.9	1.8	1

Table 3.1 The Sensitive and Specific overall scores' parameters. The numbers represent the weight of each contrast in the respective overall score. The numbers' color represents the selected Hb response type: red=HbO; blue=HbR; purple=average HbO/HbR. (The healthy participants' parameters are not shown)

3.6.1 Rankings

The six following rankings (Figures 3.20 to 3.25) make it possible to compare the individuals based on their individual-group similarity in a single contrast or across contrasts. The rankings are preceded by Table 3.2, which summarizes the findings.

- Sound Perception (Fig. 3.20): The highest similarity scores within the healthy (C) individuals and patients (P) were 1.02 (C #18, 1st) and 0.74 (P #4, 6th), respectively. The groups' lowest scores were 0.18 (C #9, 37th) and 0.14 (P #6, 38th). The patients' second and third highest scores were 0.65 (P #5, 12th) and 0.37 (P #1, 26th).
- Speech Perception (Fig. 3.21): The highest similarity scores within the healthy participants and patients were 0.81 (C #20, 1st) and 0.43 (P #5, 15th), respectively. The groups' lowest scores were 0.12 (C #23, 38th) and 0.18 (P #6, 37th). The patients' second and third highest scores were 0.38 (P #1, 18th) and 0.37 (P #8, 20th).
- Language Comprehension (Fig. 3.22): The highest similarity scores within the healthy participants and patients were 0.61 (C #4, 1st) and 0.11 (P #4, 24th),

respectively. The groups' lowest scores were -0.01 (C #1, 37th) and -0.02 (P #5, 38th). The patients' second and third highest scores were 0.09 (P #2, 26th) and 0.07 (P #7, 29th).

- Balanced overall score (Fig. 3.23): The highest overall similarity scores within the healthy participants and patients were 0.60 (C #18, 1st) and 0.37 (P #4, 19th), respectively. The groups' lowest scores were 0.17 (C #6, 37th) and 0.11 (P #6, 38th). The patients' second and third highest scores were 0.31 (P #5, 24th) and 0.26 (P #1, 28th).
- Specific overall score (Fig. 3.24): The highest overall similarity scores within the healthy participants and patients were 0.60 (C #18, 1st) and 0.36 (P #4, 17th), respectively. The groups' lowest scores were 0.17 (C #6, 37th) and 0.11 (P #6, 38th). The patients' second and third highest scores were 0.31 (P #5, 25th) and 0.26 (P #1, 28th).
- Sensitive overall score (Fig. 3.25): The highest overall similarity scores within the healthy participants and patients were 0.60 (C #22, 1st) and 0.36 (P #4, 15th), respectively. The groups' lowest scores were 0.20 (C #9, 37th) and 0.10 (P #6, 38th). The patients' second and third highest scores were 0.31 (P #5, 23rd) and 0.26 (P #8, 26th).

3.6.1.1 Groups' average rank

The patients' best placings were, on average, in the Sound Perception and Speech Perception contrasts (25.5 in both), followed by the Sensitive Overall score (28.1). Their lowest average placing was in the Language Comprehension contrast (31.5), followed by the Specific overall score (30.3) and Balanced overall score (30.1).

In parallel, the healthy participants had their highest average placing in the Language Comprehension contrast (16.3) followed by the Specific overall score (16.6) and the Balanced overall score (16.7). Their lowest placings were, on average, in the Sound Perception and Speech Perception contrasts (17.9 in both), followed by the Sensitive Overall score (17.1).

3.6.1.2 Patients' rank

Patients could be split into two groups with respect to the resulting overall scores:

- Patients whose rank in *at least two* of the overall scores was *5th or worse* among themselves (i.e., 3rd and 4th quartile patients): patient #2, patient #3, patient #6, and patient #7. All of these patients underwent WLST due to assumed poor prognosis.
- Patients whose rank in at least two of the overall scores was 4th or better among themselves (i.e., 1st and 2nd quartile patients): Two of these four patients gained responsiveness and partial functional recovery (patient #4 and patient #8), one deceased due to medical complications (patient #1), and one due to WLST (patient #5).

A results description of the latter group of patients follows. The (second) number in the parentheses refers to the rank among the patients unless implied otherwise.

Patient #1 (pontine stroke, deceased): The patient, who was a potential but unconfirmed case of locked-in syndrome, ranked 26th (3rd) and 18th (2nd), respectively, in the Sound Perception and Speech Perception contrasts; however, the patient's Language Comprehension rank was 35th (6th). For this reason, although the patient was ranked below 30 in the Balanced (28th, 3rd) and Sensitive (28th, 4th) overall scores, their Specific (35th, 7th) overall rank was poor.

Patient #4 (GBS, good outcome): The patient was placed first among the patients in all the rankings except Speech Perception contrast (5th). The patient stood very high among all in the Sound Perception contrast (6th) and had a remarkable rank in the Language Comprehension contrast (24th). The patient's best overall rank was in the Sensitive score (15th), followed by the specific (17th) and Balanced (19th) scores (all very remarkable).

Patient #5 (hepatic encephalopathy, WLST): The patient ranked highly in the Sound Perception (12th, 2nd) and Speech Perception (15th, 1st) contrasts but very poorly in the Language Comprehension contrast (38th, 8th). The patient had the second-best overall scores among the patients; among all, the best placing was in the Sensitive score (23rd), followed by the Balanced (24th) and Specific (25th) scores (all remarkable).

Patient #8 (cardiac arrest, recovered but largely dependent): The patient was ranked 20th (3rd) in the Speech Perception contrast; however, the patient's Sound Perception and Language Comprehension placings were 32nd (6th) and 34th (5th), respectively. The patient's best overall rank was in the Sensitive score (28th, 3rd), followed by the Balanced (31st, 4th) and Specific (32nd, 5th) scores.

3.6.2 Prognostic utility

The Specific overall score ranking was the only ranking with significant prognostic utility ($r = 0.73, p = 0.04$). The rankings based on the Balanced ($r = 0.62, p = 0.10$) and Sensitive ($r = 0.60, p = 0.12$) overall scores had the next two highest prognostic utilities. Among the single-contrast rankings, Language Comprehension ($r = 0.50, p = 0.21$) similarity scores had the highest prognostic utility, followed by the Sound Perception ($r = 0.42, p = 0.30$) and Speech Perception ($r = 0.38, p = 0.35$) contrasts.

	Rank (among all, among patients)								Average rank		Prognostic utility	
	P #1 (PS, d)	P #2 (CA, d)	P #3 (CA, d)	P #4 (GBS, r)	P #5 (HE, d)	P #6 (CA, d)	P #7 (CA, d)	P #8 (CA, r)	Controls	Patients	r	p
Sound Per.	26, 3	33, 7	31, 5	6, 1	12, 2	38, 8	27, 4	32, 6	17.9	25.5	0.42	0.30
Speech Per.	18, 2	24, 4	32, 6	25, 5	15, 1	37, 8	33, 7	20, 3	17.9	25.5	0.38	0.35
Language Comp.	35, 6	26, 2	30, 4	24, 1	38, 8	36, 7	29, 3	34, 5	16.3	31.5	0.50	0.21
Overall (Balanced)	28, 3	32, 5	35, 7	19, 1	24, 2	38, 8	34, 6	31, 4	16.7	30.1	0.62	0.10
Overall (Specific)	35, 7	33, 5	34, 6	17, 1	25, 2	38, 8	32, 4	28, 3	16.6	30.3	0.73	0.04
Overall (Sensitive)	28, 4	26, 3	33, 6	15, 1	23, 2	36, 8	35, 7	32, 5	17.1	28.5	0.60	0.12

Table 3.2 Summary of the rankings and their prognostic utility.

d= deceased, r= recovered; green= ranked in the top 30 *and* patients' Q1, no color highlight= ranked in the top 30 but not in the patients' Q1, yellow= ranked worse than 30th but within the patients' Q2, red= ranked worse than 30th and within the patients' Q3 or Q4

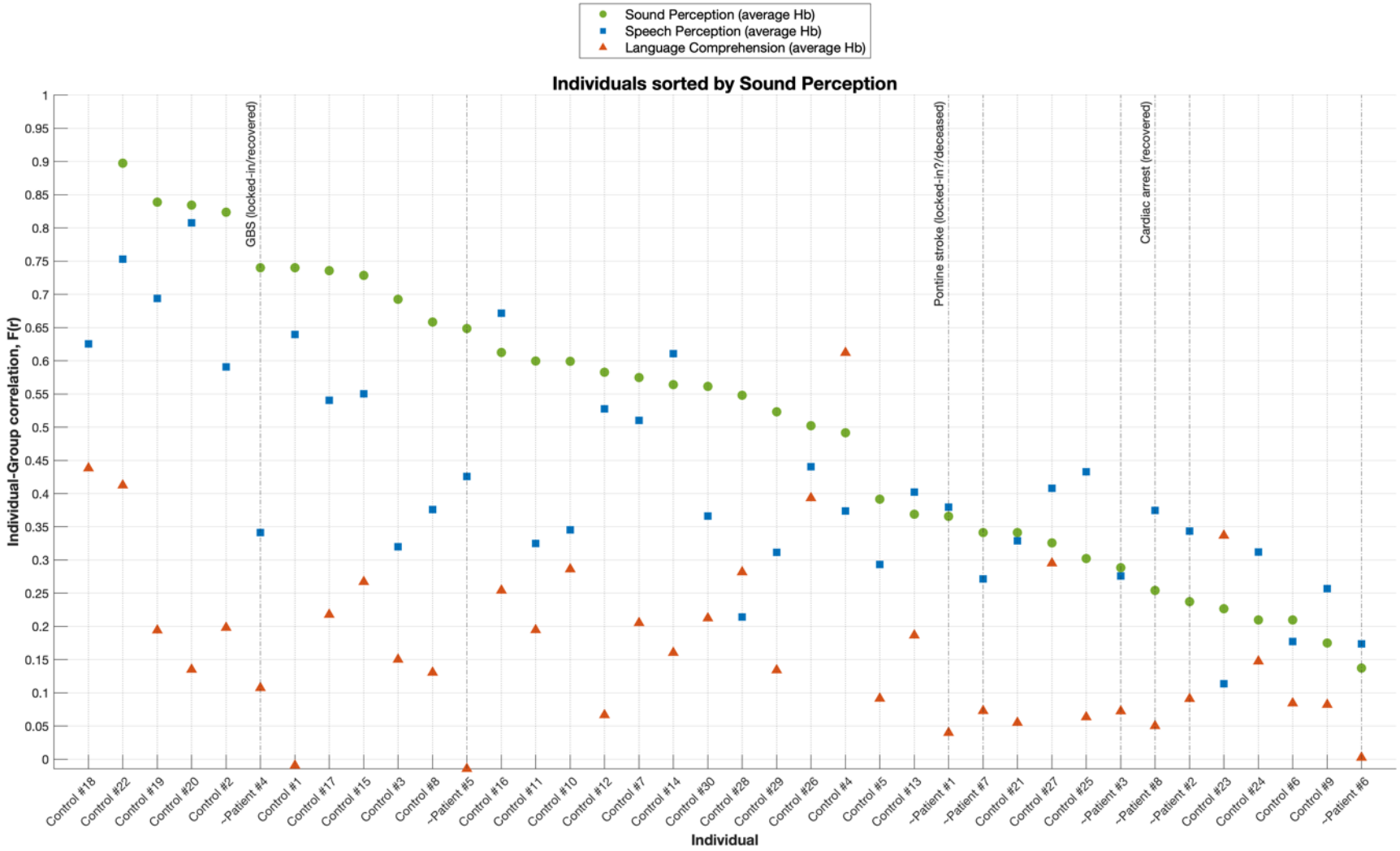

Figure 3.20 Sound Perception similarity scores ranking (average HbO/HbR)

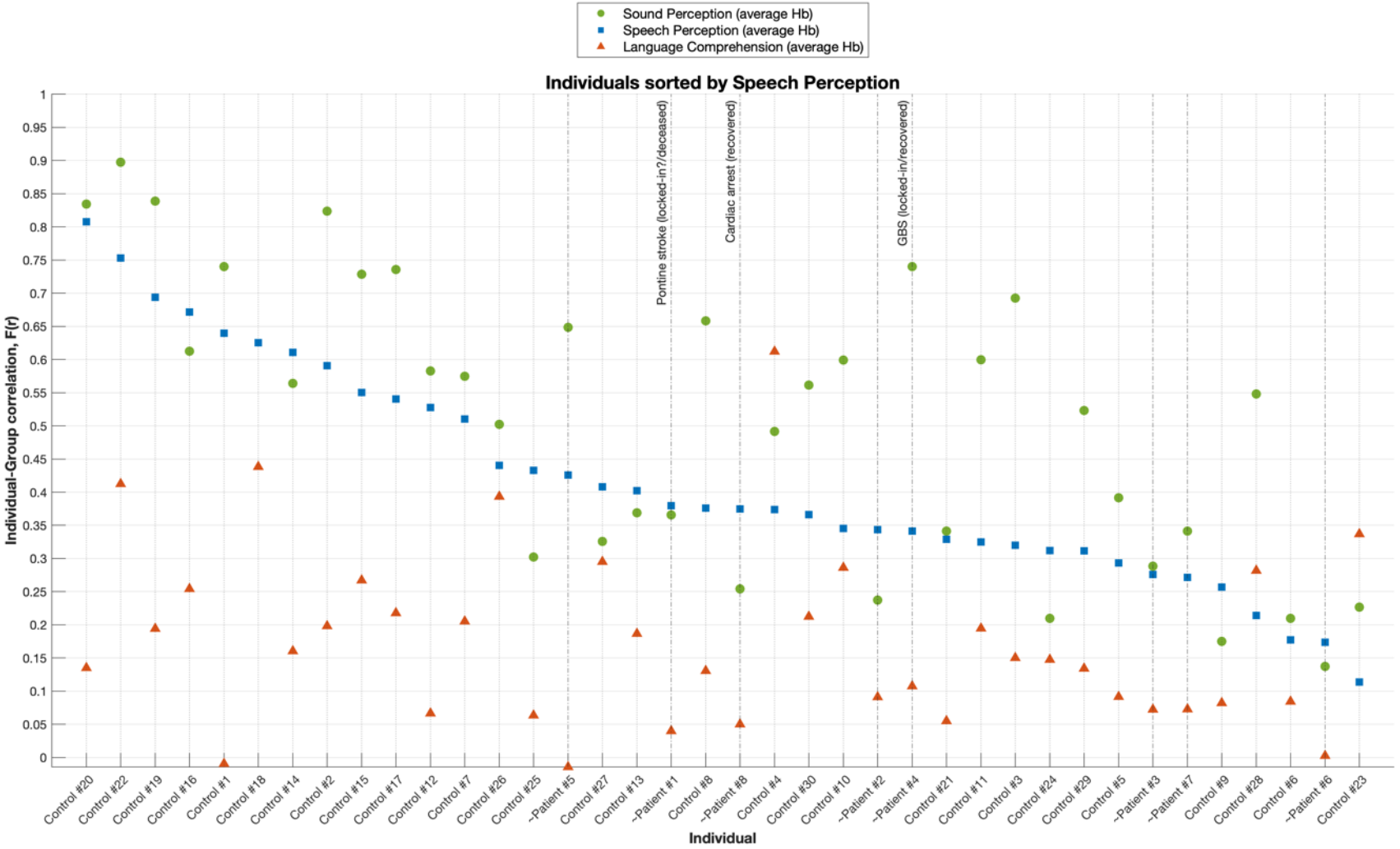

Figure 3.21 Speech Perception similarity scores ranking (average HbO/HbR)

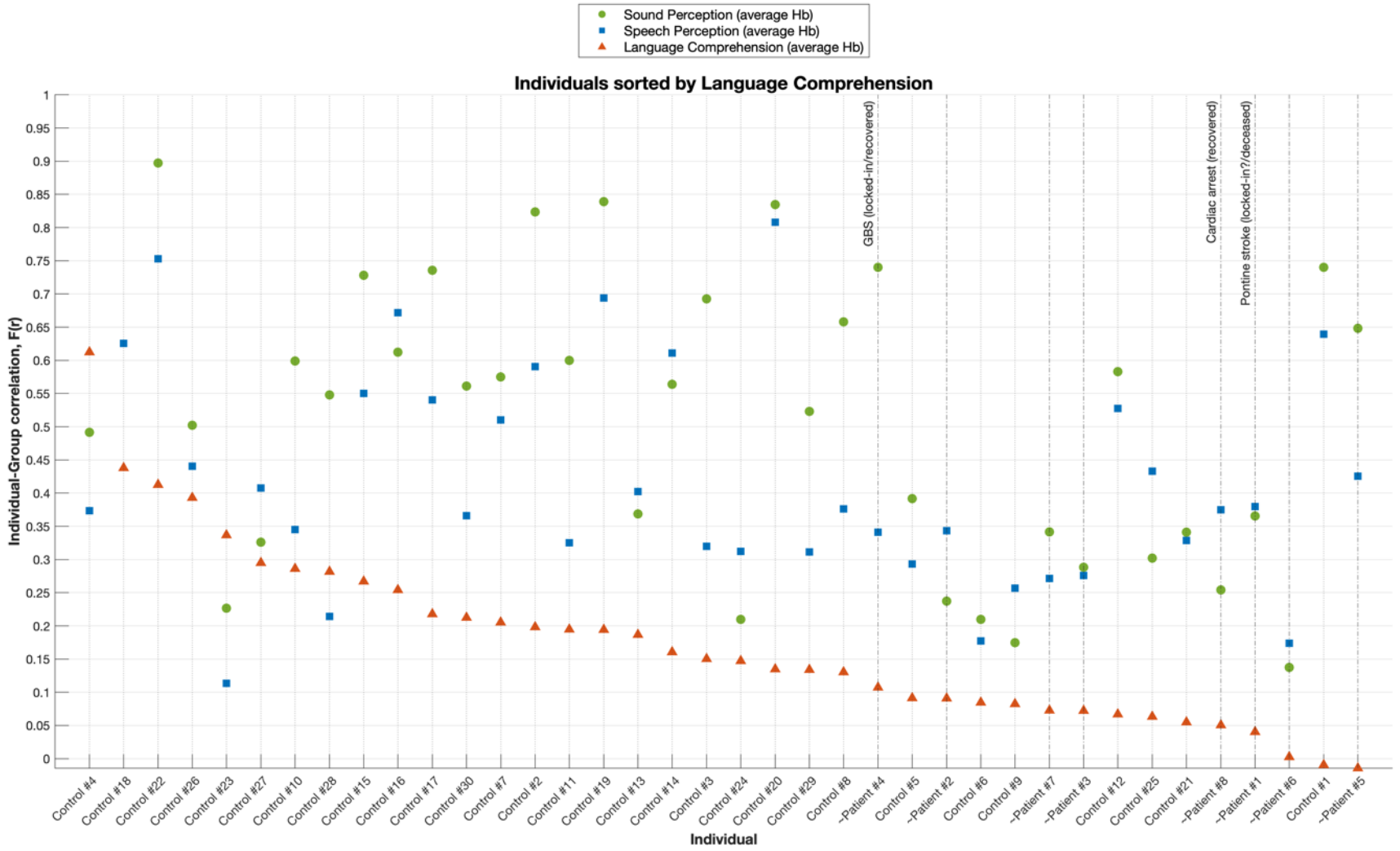

Figure 3.22 Language Comprehension similarity scores ranking (average HbO/HbR)

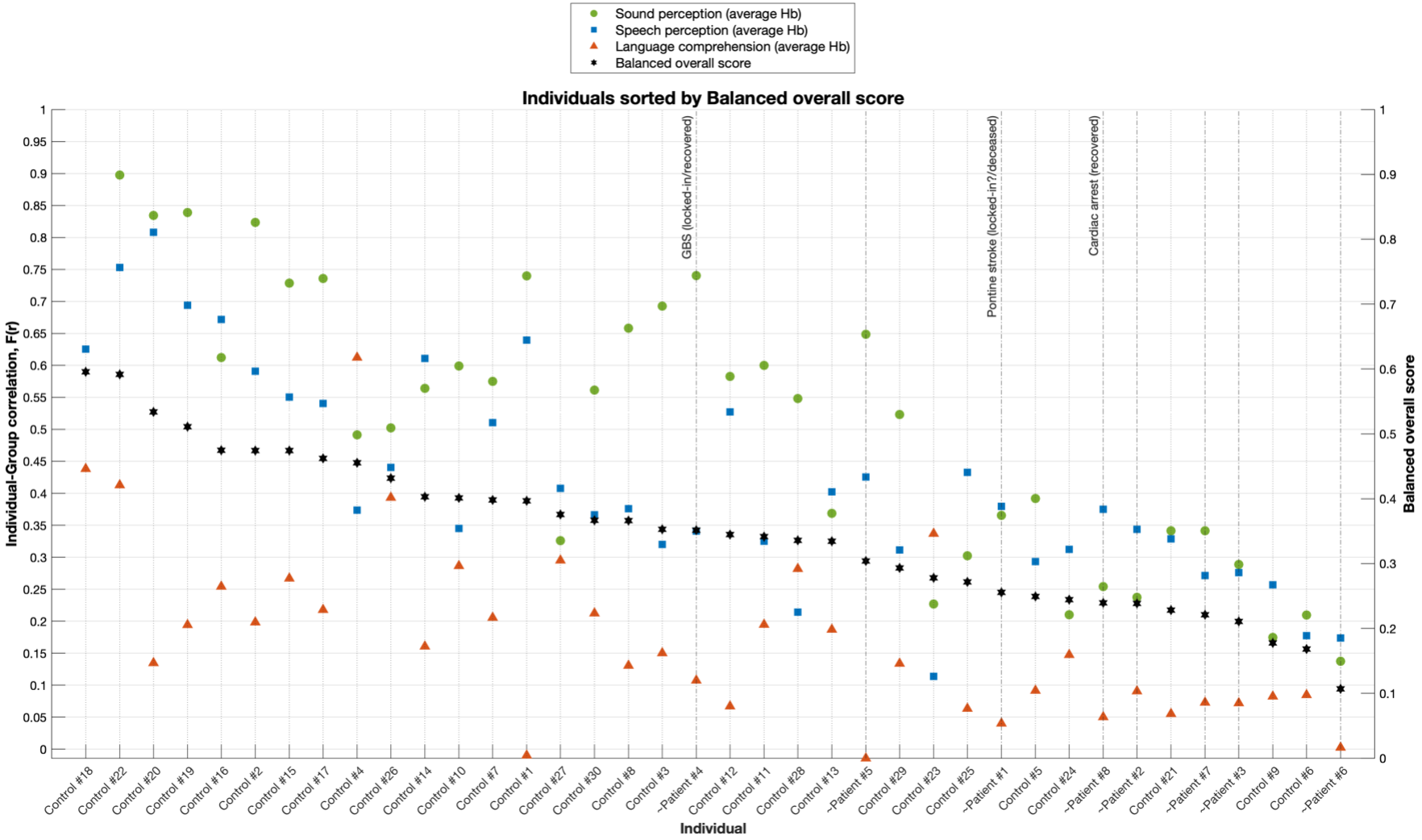

Figure 3.23 Balanced overall scores ranking (average HbO/HbR)

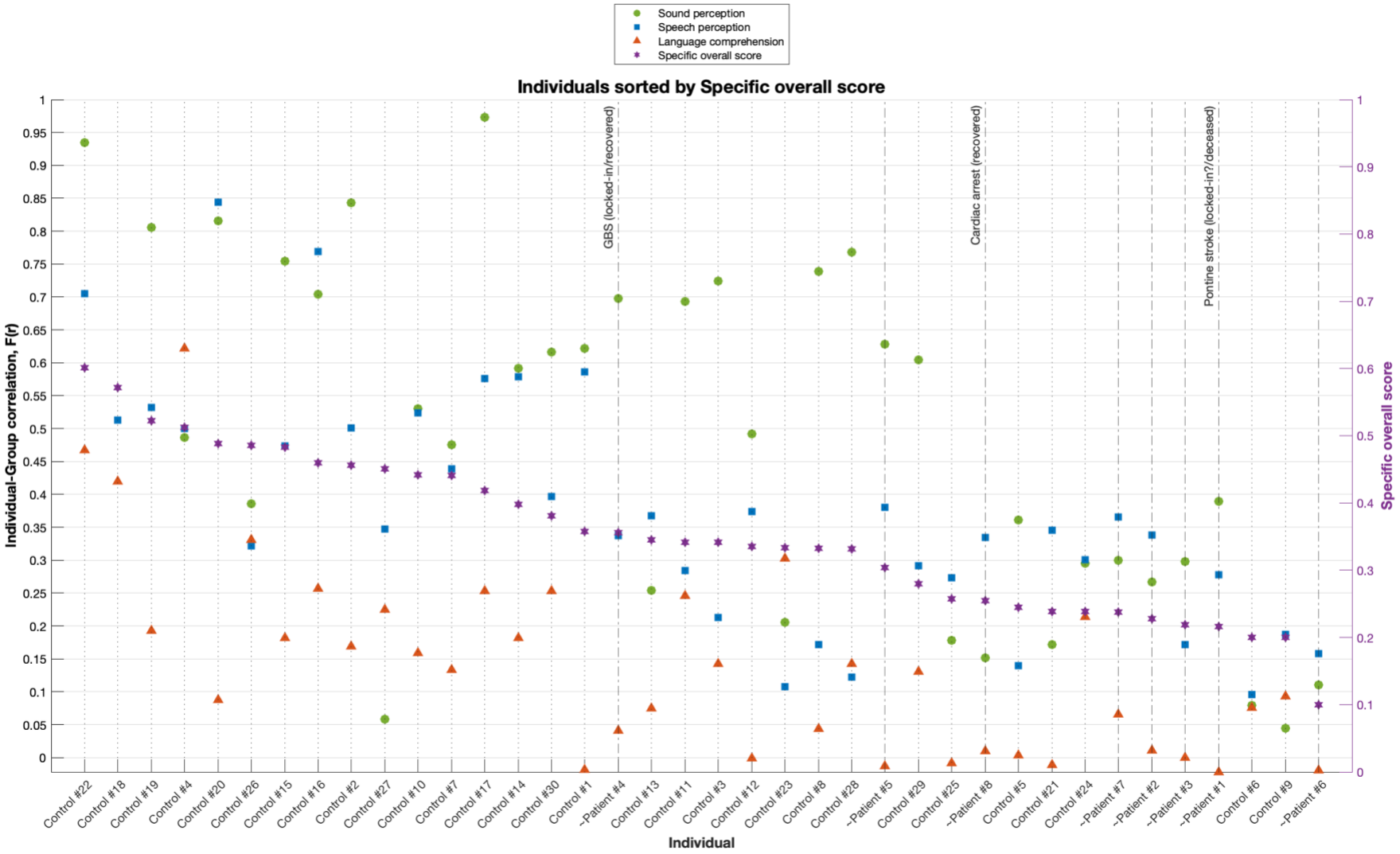

Figure 3.24 Specific overall scores ranking

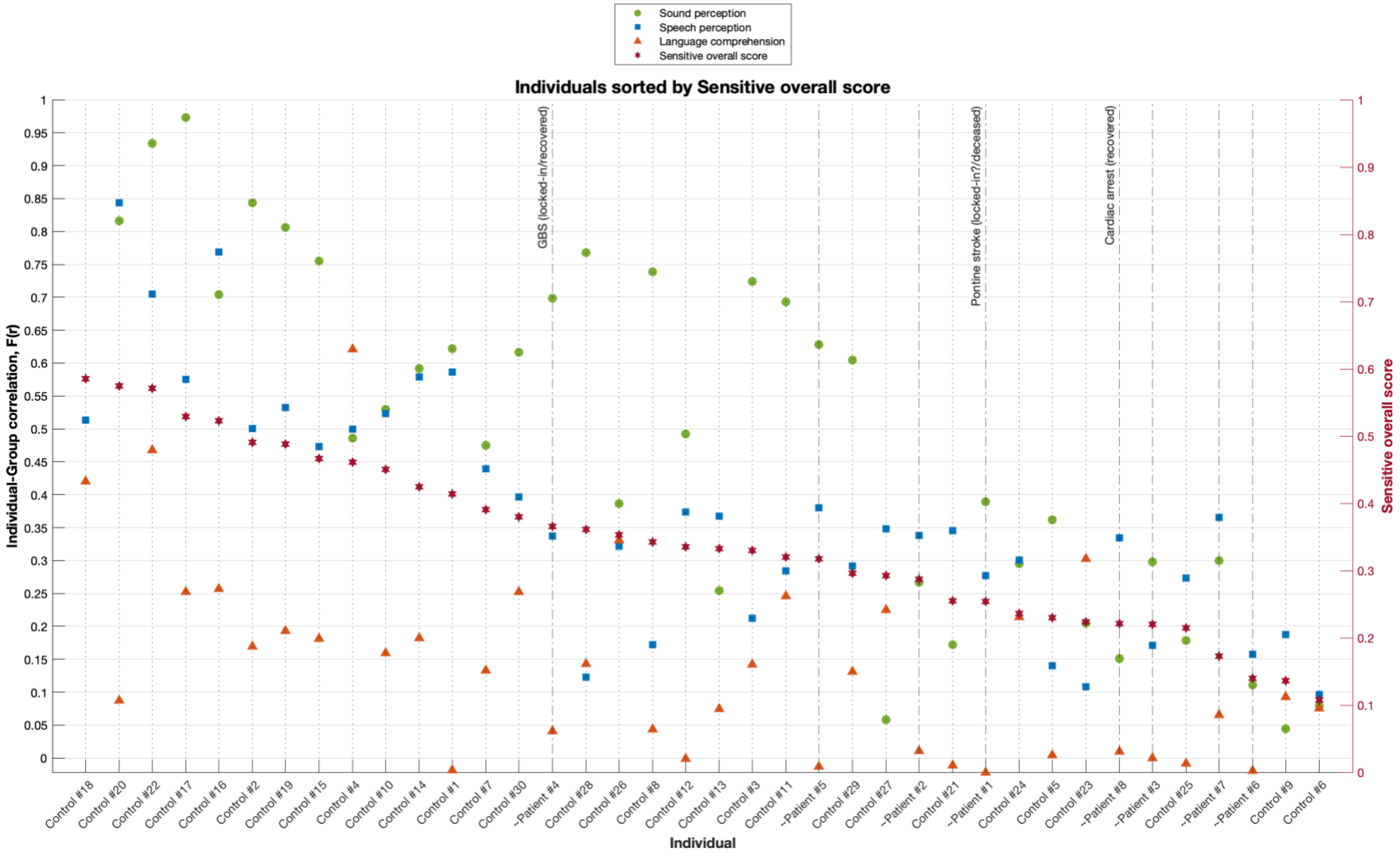

Figure 3.25 Sensitive overall scores ranking

Chapter 4

4 Discussion

Estimation of prognosis of the recovery outcome is just challenging as it is crucial to the treatment and goal-of-the-care decisions for comatose patients (Fischer et al., 2022). Functional neuroimaging can assess the residual brain function in behaviorally unresponsive patients, as is shown in studies on patients with chronic DoC. The accumulated knowledge and methods developed in chronic DoC studies can now be translated into the context of acute brain injury. However, due to several practical and medical constraints, many comatose patients cannot be tested with fMRI, the gold-standard neuroimaging method commonly used in chronic DoC studies. These constraints emphasize the need for a bedside neuroimaging tool, with EEG being the traditional option that has its own advantages and limitations.

As an emerging functional neuroimaging technique with advantageous features, fNIRS is a promising candidate for use at the bedside in the ICUs. I used fNIRS to test 30 healthy participants and eight unresponsive patients for neural correlates of auditory processing at three levels. The employed auditory task originated from auditory neuroscience research Davis & Johnsrude, 2003; Rodd et al., 2005; Uppenkamp et al., 2006) and fMRI studies on patients with *chronic* DoC (Coleman et al., 2007; Davis et al., 2007; Owen et al., 2002, 2006). More recently, the task was adapted for use in the context of *acute* brain injury with encouraging results (Norton, 2017; Norton et al., 2023).

The first goal of this study was to investigate the feasibility of utilizing fNIRS to reliably detect brain activations associated with acoustic, phonetic, and semantic levels of auditory processing. The second goal was to examine if there was a direct relationship between patients' coma outcomes and the degree to which their brain activations resembled the healthy control group's activation patterns. To quantify the similarities, I developed a scoring method tailored to the multi-dimensionality of auditory assessments and the duality of the fNIRS measurements. As my third goal, I explored a data-driven approach to increase the sensitivity and specificity of the assessments.

4.1 Validation against fMRI in healthy participants

fNIRS has a lower signal-to-noise ratio and spatial resolution than fMRI. Consequently, my attempt to replicate fMRI findings required addressing these limitations in the research methodology. I implemented several measures to achieve acceptable spatial resolution by using an optical montage of 121 channels with full head coverage but higher temporal lobe densities, especially in the left hemisphere. The additional sources or detectors added 18 channels to the left and 13 channels to the right hemisphere (=31 in total). Additionally, several measures were taken simultaneously to improve the signal-to-noise ratio of the measurements: Systemic extracerebral blood flow was recorded via eight short-distance channels and regressed from the cortical measurements confounded by the systemic physiology. A state-of-the-art data analysis pipeline was employed to reduce the impact of physiological confounds in the subject- and group-level analyses, as discussed in detail in sections 2.4.2 and 2.4.3. As another measure, 30-second intertrial intervals were added to the original fMRI stimulus design to allow for the recovery of the hemodynamic response before the onset of the subsequent trial. Having implemented all these measures, the replicability of fMRI findings with fNIRS is detailed below.

In the Sound Perception contrast, the fMRI study (Norton, 2017) found bilateral temporal lobe activation along STG with peaks in the primary auditory cortices, where 92% (13/14) of the participants showed activity. In line with the fMRI findings, in my study, bilateral activity in the STG and MTG and additional activation in the left upper ventral SMC were detected at the group level. The activation included five channels in the left and four in the right hemisphere. Twenty-nine participants (97%) showed at least one common activated channel with the group's nine channels. In this contrast, two of the additional 31 channels (#48 and #108) were among the group's nine activated channels. Nevertheless, these two channels did not contribute to the subject-level sensitivity since none of the 12 participants with (one or both of) these channels activated were distinct from the participants under the other seven channels.

In the Speech Perception contrast, the fMRI study (Norton, 2017) found bilateral activity in the STG with peaks in the anterior STG at the group level. Thirteen (92%) of the participants exhibited bilateral STG activity. fNIRS similarly detected activity in the

temporal lobe bilaterally in addition to the left frontoparietal junction. The activation in the right temporal lobe included one channel in the anterior temporal lobe. In the left hemisphere, however, the activation was within a four-channel narrow ventrodorsal strip encompassing the mid-MTG, mid-STG, supramarginal gyrus, and ventral SMC. The *anterior* temporal lobe in the *left* hemisphere also showed activation; however, it was not strong enough to survive FDR correction for multiple comparisons when compared to the rest of the activations (uncorrected results were not reported). One potential explanation for this finding is the inhomogeneous sensitivity of the optical montage used in the study. As seen in Figure 2.1, the optical montage had no sensitivity in the bilateral temporal poles and lower sensitivity in the anterior temporal lobes compared to the rest of the temporal lobe, where the optical montage's coverage was dense. Therefore, it is possible that the left anterior temporal lobe was highly active but only partially detected due to the limited sensitivity of the optical montage in this area

Matching the fMRI's sensitivity, 93% (28/30) of the healthy participants exhibited at least one commonly activated channel with the group's five channels. One of the additional channels (#43) was among the five activated channels at the group level. Among 13 participants that had this channel activated, only two of them were distinct from the participants under the other four channels.

In contrast to the present study, the fMRI study (Norton, 2017) did not report SMC activity in either Sound or Speech Perception contrasts. However, based on the fact that SMC is known to be involved in both speech production *and* perception (D'Ausilio et al., 2009; Iacoboni, 2008; Pardo et al., 2021; Schomers & Pulvermüller, 2016; Wilson & Iacoboni, 2006), I propose that the robust sensorimotor activation detected by fNIRS in the Speech Perception contrast should not be considered a false positive. As a related example, premotor cortex activation has been reported in response to "synthetic vowels vs. nonspeech sound" (Uppenkamp et al., 2006), a contrast which resembles the Speech Perception contrast here. Activation in the motor area has also been reported while passively listening to monosyllables (Wilson et al., 2004; Watkin & Paus, 2004), a condition that is closer to the Sound Perception contrast in the present study.

In the Language Comprehension contrast, the fMRI study found a *strongly left-lateralized* activation within the angular, posterior inferior temporal, and parahippocampal gyri. Consistent with fMRI, fNIRS detected *entirely left-lateralized* activity in the posterior temporal lobe (ITG, MTG, and STG) and angular gyrus. Given the limited depth sensitivity of fNIRS, however, detecting activity from the parahippocampal gyrus, which is a deeper cortical region, was highly unlikely (Liu et al., 2015). To the best of my knowledge, detection of activity in this region has not been reported in any fNIRS study. The parahippocampal gyrus is involved in the encoding, storage, retrieval of episodic memories, and spatial navigation. While its role in semantic processing is recognized (Binder et al., 2009), the current limitation would not pose any challenge to the validity of the method. This is because major temporal, frontal, and parietal cortical regions involved in semantic processing (i.e., posterior ITG, IFG, temporoparietal junction, and frontoparietal junction) (Hickok & Poeppel, 2007) are all within the depth-sensitivity range of fNIRS.

The Language Comprehension contrast designed to capture the neural activity underlying semantic processing has proven challenging for previous fMRI studies (Norton, 2017) due to the subtle linguistic differences between complex language and meaningless sounds. In fact, the original fMRI study (Norton, 2017) only achieved a low sensitivity of 43% (6/14) in this contrast, even when not correcting for multiple comparisons in the subject's activation maps to account for the small effect size. Relatedly, several other fMRI studies that relied on ambiguity resolution (i.e., “ambiguous sentences vs. unambiguous sentences”) adopted an *ROI* approach instead of whole brain analysis either with (Davis et al., 2007) or without (Coleman et al., 2007, 2009) correction for multiple comparisons. In the same vein, Davis and Johnsrude (2003) omitted correction for multiple comparisons in detecting neural correlates of distortion compensation (i.e., “distorted speech vs. intelligible speech”).

Using fNIRS, 65% (17/30) of participants showed at least one commonly activated channel with the group's only two channels, while the correction for multiple comparisons was made at the subject but not the group level. This was a significant achievement, especially given that the sensitivity was based on two channels covering the

posterior left temporal lobe and angular gyrus, whereas the fMRI's sensitivity was based on ROIs extracted from the Neurosynth database (Yarkoni et al., 2011), which included four additional regions along with the left temporal lobe (i.e., bilateral ventral IFG; left MFG; right temporal pole).

In the Language Comprehension contrast, *one of the two* activated channels of the group (#62) was from the additional channels, and *five out of 11* participants with this channel activated were distinct from the participants under the other channel. This amounted to ~30% of the participants who shared one channel with the group in this contrast, highlighting the importance of increased optical montage density in this subtle contrast.

While the use of a high-density optical montage substantially enhanced sensitivity in the Language Comprehension contrast, it alone cannot explain why fNIRS achieved a higher sensitivity than fMRI, despite the latter having a far better spatial resolution. As one possibility, it can be claimed that the fMRI sensitivity and the fNIRS sensitivity, as formulated here, are incommensurable in the first place. Although such a possibility cannot be decisively ruled out, a likely alternative explanation for this observation is the negative impact of the lack of intertrial intervals on the fMRI study's sensitivity in this contrast (Norton, 2017). It is well established that by allowing time for physiological signals to stabilize and averaging out random noise across time points, an optimal intertrial interval can reduce noise. Additionally, an appropriate intertrial interval can improve the detection of task-related neural activity by allowing the hemodynamic response to return to baseline before the next stimulus presentation, avoiding an overlap of the hemodynamic response from succeeding stimulus trials. Reduced signal-to-noise ratio due to the lack of intertrial interval might also explain why fMRI did not detect SMC activity in the Speech perception contrast.

Based on the current findings, it can be concluded that fNIRS did replicate the fMRI results of Norton (2017) at the group level within its depth sensitivity limits. Furthermore, at the single participant level, I demonstrated that fNIRS sensitivity was not lower than fMRI sensitivity in the current task. However, as stated earlier, it should be noted that the sensitivity analysis in the present study differed from that of the original

fMRI study (Norton, 2017). While the sensitivity analysis in the present study was based on having at least *one common channel* with the *group*, the fMRI study relied on overlapping with the *mask* extracted from *Neurosynth*. Adopting the fMRI study's method would require going from channel-space to brain-space, and this, in turn, would require anatomical registration of fNIRS measurements, a feature that was unavailable in the present study (see section 4.8 for details). However, considering that anatomical registration reduces variability and enhances subject-level sensitivity (Ayaz et al., 2022; Novi et al., 2020a), the potential of fNIRS may be underestimated in the current study. These differences in sensitivity analysis methods across studies should not be considered a major issue when interpreting the results and drawing conclusions.

In addition to broadly replicating the earlier fMRI findings, two other observations provided further support for the validity of the employed fNIRS method. One observation concerned an expected trend in the between-group comparison results, but the more important and compelling observation was the cross-validated detection of cognitive-motor dissociation in an unresponsive patient with severe GBS. Details on both observations are provided in the following two sections.

4.2 Between-group comparison results

A three-way ANOVA ($Group \times Contrast \times Hb\ type$) was performed on the similarity scores. The ANOVA yielded a large effect size ($\eta^2 = 0.10$) for the $Group$ factor ($p < 0.0001$), indicating that the dissimilarity between the healthy participants and patients (across the contrasts and Hb types) was statistically significant. Post-hoc comparisons revealed that healthy participants had higher similarity scores in all three contrasts (i.e., auditory processing levels) than patients, which was an expected effect.

While no significant $Group \times Contrast$ interaction was found, the analysis of between-group simple effects in each contrast revealed an interesting trend: The between-group difference was more statistically significant at higher levels of auditory processing. In other words, the difference between patients and healthy controls was less statistically pronounced in lower levels of auditory processing, suggesting that patients retained sensory and perceptual aspects of sound processing to some extent but had major deficits

in processing the semantics of speech. Specifically, between-group differences were significant only in the Language Comprehension contrast ($p < 0.0005$ for HbO, HbR, and average HbO/HbR), where the next most significant difference was observed in the HbR responses within the Speech Perception contrast ($p < 0.06$).

The observed trend is consistent with our current understanding of the cognitive deficit profile that typically follows a severe brain injury (Aubinet et al., 2022a, 2022b). This understanding is primarily informed by studies conducted on patients with chronic DoC, but also includes research on patients with acute severe brain injury. In particular, Norton et al. (2023) reported that the neural correlates of Language Comprehension were only detected in 5 of the 14 acute patients (=36%), whereas activations linked to sound and speech perception were observed in 12 patients (=86%). In this sense, the observed trend aligns with our prior expectation and, therefore, can be viewed as a "reality check" for the validity of the employed method. Admittedly, since the $Group \times Contrast$ interaction was not statistically significant, nothing more can be inferred from this observation. However, it is worth noting that the non-significance of the interaction could simply be due to the small sample size (especially in the patient group) since it has been shown that at least four times the sample size is needed to estimate an interaction than to estimate a main effect (Leon & Heo, 2009).

4.3 Single-case cross-validation

Patient #4, a 63-year-old female, was clinically diagnosed with severe GBS, an autoimmune condition that affects the peripheral nervous system and leads to sensory disturbances and motor weakness. In its severe forms, the syndrome can cause complete motor paralysis, resulting in a cognitive-motor dissociation state where the patient has preserved cognitive function and awareness but no detectable motor response. This was the case for patient #4, who was admitted to the ICU with rapidly progressive motor and sensory impairment, resulting in a minimum GCS score of 3 on the seventh day after admission, the day on which she was tested with the auditory task.

The auditory assessments for this patient were remarkable, as she was rated in the range of healthy controls and indistinguishable from them in all rankings: In the Sound

Perception contrast, the patient showed bilateral temporal lobe activation closely resembling the control group's activation pattern. In addition, the patient exhibited activity in the lateral frontopolar cortex bilaterally and the middle frontal gyrus in the left hemisphere, anterior to the control group's activation in the SMC. The high degree of similarity between the patient's activation pattern and that of the control group was striking in this contrast, resulting in the patient being ranked 6th among all 38 participants. In the Speech Perception contrast, the patient ranked 25th by demonstrating activation in the regions activated by the group (bilateral temporal lobes and left frontoparietal junction) as well as other language-related regions associated with language (bilateral frontal lobe and right frontoparietal junction). This score is on the low side, but importantly, it is well within the range of healthy participant values.

Most importantly, in the Language Comprehension contrast, the patient had one activated channel slightly posterior to, but still partially overlapping with the control group's two activated channels in the posterior temporal lobe. A channel in the left lateral frontopolar cortex and another in the right dorsolateral prefrontal cortex was also activated, possibly reflecting the differential involvement of high-order cognitive processes in comprehending short stories compared to pseudowords. The patient was ranked 24th in this contrast, which is low, but still well within the range of healthy participant values. The patient's overall ratings were accordingly impressive, with no rank lower than 19 (Balanced score) and the best of 15 (Sensitive score). She ranked first among the patients in all but one of the rankings (Speech Perception). Consistent with the clinical diagnosis, these results suggested that the patient retained auditory function, including higher-level semantic processing.

In addition to the passive auditory processing paradigm, patient #4 was evaluated with a battery of other tasks, including movie listening and command following, using fNIRS and EEG (these results are not reported in this thesis). The results from both modalities showed that the patient could engage in the movie's narrative and willfully modulate her brain activity in response to the verbal commands. These results were confirmed when the patient regained behavioral responsiveness and had recollections of the other testing sessions.

The convergence of auditory assessment results with other tasks and modality assessments in this rare GBS case can be interpreted as evidence for the validity of the employed method. To the best of my knowledge, this is the first report of using CW-fNIRS for detection of intact cognitive function in an unresponsive patients. Prior to this, only one study using time-domain fNIRS detected cognitive-motor dissociation in a GBS patient (Abdalmalak et al., 2017).

4.4 Prognostic utility

The present study began investigating the utility of fNIRS-based neuro-auditory assessments for prediction of recovery outcomes in acute DoC. The results were based on a small patient cohort with a low rate (2/8) of a good outcome (i.e., an unbalanced sample). These preliminary results, however, can be informative, especially since, to the best of my knowledge, no published study has yet utilized *fNIRS* for such a purpose in *acute* DoC. Among the handful of fNIRS studies on *chronic* DoC (Abdalmalak et al., 2020; Kempny et al., 2016; Kurz et al., 2018; Molteni et al., 2013; Zhang et al., 2017), only one recent study by Si et al., (2023) investigated the association between results of a mental imagery task with the level of consciousness (CRS-R) six months after the test with no positive findings.

However, in line with recent auditory-based EEG (Claassen et al., 2019; Sokoliuk et al., 2021) and fMRI (Norton, 2017a; Norton et al., 2023) studies, I found a significant association between the patients' coma outcome as measured by GOSE and their multi-level auditory function as measured by the Specific overall score ($r = 0.73, p < 0.05$). Although the association did not reach significance in Balanced ($r = 0.62, p < 0.10$) and Sensitive ($r = 0.60, p < 0.12$) overall scores, they were all found to be better outcome predictors than the within-contrast scores. In other words, more comprehensive neuroauditory assessments, which considered patients' performance at all three levels of auditory processing, yielded better predictions, which is an expected and meaningful observation.

Among the within-contrast scores, the Language Comprehension evaluations had the strongest association with the outcome ($r = 0.50, p < 0.21$), followed by Sound

Perception ($r = 0.42, p < 0.30$) and then Speech Perception ($r = 0.38, p < 0.35$) contrasts. At first glance, this might seem counterintuitive that the prognostic utility of Sound Perception was higher than Speech Perception's, as neural correlates of higher levels of cognition are expected to be better predictors of good functional recovery. This observation is partly due to the small sample size and vulnerability of Pearson correlations to outliers in small samples. The GBS patient scored very high in the Sound Perception contrast (6^{th} among 38), which leveraged the contrasts' prognostic utility.

However, I propose that even if a larger and more balanced sample yielded the same patterns for prognostic purposes, it would not necessarily be a problem: The Sound Perception contrast measures the brain's response to *all* sound conditions (vs. silence), not just the non-speech sound condition (noise). Therefore, the elicited brain response is likely to reflect both higher-order auditory functions and basic sensory processes. The healthy group results were consistent with this view. As demonstrated in section 3.2.1, the activation in the Sound Perception contrast was not limited to the (middle part of) STG, the closest lateral region to the deeper primary auditory cortex. Instead, the activations extended to the SMC and posterior temporal lobe, the higher order regions activated in the Speech Perception (see 3.2.2) and Language Comprehension (see 3.2.3) contrasts, respectively.

As a side note, in light of the above argument, it may be more appropriate to refer to the "noise vs. silence" contrast as the basic auditory processing level instead of the Sound Perception contrast. This suggestion is consistent with several previous studies that have used the "noise vs. silence" contrast as the fundamental auditory processing level in the context of chronic DoC or altered states of consciousness (Davis et al., 2007; de Jong et al., 1997; Owen et al., 2002, 2006).

It is important to acknowledge that establishing the *true* validity of a (novel) prognostic test is not feasible, as there is no defenitive "ground truth" about a patient's *likely* outcome to which we can compare our predictions. Instead, the *actual* outcomes we observe are influenced by decisions made for patients based on the *predicted* outcome, including the choice of treatments, rehabilitative plans, and the critical decision to

withdrawal life support. In particular, poor outcomes observed in a study may be partially due to a *bias* towards predicting a poor outcome, which can lead to the premature withdrawal of life support. Critically, it is impossible to know if such bias has impacted the outcomes, since it cannot be determined whether a patient would have had a good outcome if life support had not been withdrawn. Consequently, this bias can inflate the resulting prognostic utility by steering outcomes towards the predictions, an issue known as "self-fulfilling prophecy" (Becker et al., 2001).

Although the results of the current study were not used to make decisions for the patients, including those that resulted in life support withdrawal for five of the study participants, it is possible that biases in the guidelines or decision-making processes could have affected the observed prognostic utilities. Therefore, the probable impact of such biases on our results must be taken into account. To this end, we can examine statistics on long-term outcomes in societies like Japan, where withdrawal of life-sustaining treatment for patients with a poor prognosis is uncommon.

In a recent study (Egawa et al., 2022), the long-term outcomes of 40 stroke patients in Japan with a prognosis of no "meaningful recovery" were examined. Among the 15 patients alive at six months, only eight had GOSE scores available. Of these eight patients, six had a GOSE of two or three (indicating a vegetative state or severe disability with full dependency), one patient had a GOSE of four, and another had a GOSE of five (good outcome). For the seven patients whose GOSE scores were unavailable, five were living in long-term care hospitals, which in Japan is reserved for patients who are not expected to regain functional recovery. No data was available from the other two patients. Even if we assume that the two patients without data had a good outcome, less than 10% (3/40) of the patients with a poor prognosis showed meaningful recovery.

Since the majority of patients in the present study also had a stroke as the etiology of their injury, it is reasonable to extrapolate the findings from the Japanese cohort to some extent. Based on this, it can be inferred that, at most, only one out of the five patients who underwent WLST could have had a good outcome. This potential outcome is unlikely to significantly impact the observed prognostic utility in the current study. While the

generalizability assumption may be debatable, its implication is that the self-fulfilling prophecy does not invalidate the findings of the present study, which suggests the applicability of fNIRS-based auditory assessments for prognosis in acute severe brain injury.

It is worth noting that biased poor prognoses leading to premature WLST could result in underestimating the utility of an independent biomarker rather than overestimating it. For example, patient #5 in the study had high scores in all rankings except for the Language Comprehension contrast, where no activity was observed. Despite this, the patient's overall scores suggested a good outcome was likely. However, since the patient's life support was withdrawn, it is impossible to objectively determine the accuracy of this prediction. If the patient could have had a good outcome if not for the WLST, the current prognostic utility would have been even higher. To further clarify, note that cases like patient #5 arise because the current study's findings were not used to inform decision-making. Underestimation of prognostic utility is unlikely when a biomarker's predictions are actually used to inform decisions because if a good prognosis is predicted, the WLST is delayed.

4.5 Scoring method

The prognostic utility analysis in the previous fMRI studies (Coleman, 2009; Norton, 2017; Norton et al., 2023) used a coarse-grained scoring method, where patients were clustered into sub-groups based on their achieved level in the auditory processing and command-following hierarchy. Higher levels were assigned higher numeric scores, and Spearman's rank-order correlation was used to determine the association between the outcome and the assigned scores

The binary clustering scoring method only concerned the *absence* or *presence* of a response from patients within ROIs defined by healthy group results. Consequently, the activations outside the ROIs (i.e., activation specificity) and the strength of activity with respect to the distribution of other patients and healthy controls (i.e., inter-subject variability) were not taken into account. These important pieces of information could otherwise be used to obtain a better sense of patients' auditory functions and quantify

them more informatively. In addition, using Spearman's correlation meant that only the order of the scores and not their numeric value mattered, leading to further loss of valuable information.

In contrast, I developed a fuzzier yet more nuanced approach for prognostic utility analysis which differed from the above approach in two important ways. First, for quantifying the auditory assessment results, instead of binary *clustering*, I used a similarity-based scoring method which allowed for *ranking* patients in the distribution of healthy participants. Second, Pearson correlation was used to derive the association between patients' assessment scores (i.e., their ranks among healthy participants) and their recovery outcome.

The developed method involved ranking the individuals within each and across all contrasts based on the extent of their brain activation similarity to the control group's activation pattern. A weighted averaging scheme was employed to assign individuals an overall score that subsumed their performance across all contrasts. Weights of the contrasts and Hb types (i.e., HbO, HbR, and average HbO/HbR) were determined either a priori or a posteriori (data-driven approach). For a priori weighting, equal weights were given to the contrasts, and in all contrasts, the average HbO/HbR measurements were used.

This scoring method allowed for a one-to-one comparison of all individuals, whether patient or healthy, at a certain level of auditory processing or overall (inter-subject comparison). It also allowed for a detailed comparison of an individual's performance across the levels (within-subject comparison). However, the critical advantage of my proposed scoring method was that it enabled quantifying patients' results in light of the inevitable variability of subject-level results by including the healthy controls in the similarity rankings. In addition, including healthy controls in the rankings widened the range of possible scores available to the patients and consequently enhanced the scores' sensitivity to individual differences between patients themselves. In short, compared to the previous method, the resulting scores were closely informed by the healthy control

subject-level results and also contained more information regarding patients' individual differences.

The use of the proposed fine-grained scoring method and Pearson correlation to derive the prognostic utility was intended to enhance the accuracy of the analysis result. However, given the absence of ground truth for patient outcomes, as discussed earlier, it is impossible to empirically evaluate the success of this method in its expected impact. Nonetheless, it can be argued that the weighted averaging scheme of the scoring method was well-suited to the multi-dimensional nature of the assessments, i.e., having three contrasts and duality of the hemodynamic response measurements in fNIRS differentiating it and fMRI, which has only one measurement output (BOLD signal). Additionally, it is reasonable to assume that by placing patients within the context of healthy controls in the scoring process, the analysis is likely less vulnerable to inter-subject variability, which is a common limitation of fNIRS. Therefore, the proposed scoring method can be viewed as an analytical arrangement to tailor the method to the specific characteristics and limitations of fNIRS.

4.6 Data-driven approach

The weighted averaging scheme of the scoring method also made it possible to explore improving the sensitivity and specificity of the rankings by adjusting the dimensions' weights. To this end, I developed an exploratory data-driven method with a leave-one-out distance minimizing/maximizing logic. My conception of increasing the rankings' specificity involved the following assumption: maximizing the between-group distances should improve the healthy participants' rank and worsen the patients' rank; therefore, if a patient is ranked in the range of healthy controls when the distance between the two groups is maximized, then our certainty in attributing a good outcome to that patient increases. On the other hand, the between-group distances were minimized to increase the rankings' sensitivity, which was expected to improve patients' rankings compared to their specific and a priori rankings. This was assumed to lead to the best ranking that the available data allowed for a given patient. Therefore, in my conception, a good outcome was not likely for a patient whose a priori and sensitive rankings were both unremarkable.

The data-driven method improved the prognostic utility from a non-significant association in the Balanced overall score ($r = 0.62, p < 0.10$) to a significant association in the Specific overall score ($r = 0.73, p < 0.05$). As the two most considerable changes, increasing the specificity interestingly improved the rank of patient #8, one of the two recovered patients, from 31 to 28; on the other hand, patient #1's rank fell from 28 to 35. This patient was the only one who died due to complications and not WLST, and based on his pontine stroke etiology, the possibility of being locked-in was considered for him. As anticipated, the ranks of a large percentage of patients (six out of eight) improved in the Sensitive overall score compared to the Balanced overall score, but no improvement in the prognostic utility resulted.

The lack of ground truth regarding patients' outcomes also poses an obstacle to examining the true effectiveness of the data-driven approach for increasing sensitivity and specificity. However, I argue that, regardless of the performance of the *current* data-driven method, the proposed *idea* of having *complementary* sensitive and specific scores is valuable; in principle, these complementary measures can add perspective to the interpretation of a priori score and consequently increase the reliability of decisions.

In addition to providing complementary measures, the data-driven approach enabled exploring the dimensions' *differential* contribution to the rankings. As a clear example, a meaningful pattern was observed in the weights of the contrasts: for all individuals, the Language Comprehension contrast received the maximum weight (by a factor of ~2) in the Specific overall score, and the minimum weight (by a factor of ~0.5) in the Sensitive overall score. In each case, the weights of the other two contrasts did not substantially differ from each other across individuals. This indicates that the Language Comprehension contrast at the top of the auditory processing hierarchy had the greatest influence on maximizing the rankings' specificity and sensitivity and hence, can be considered the "principal component" in the contrast dimension. Given that the Language Comprehension contrast had the highest prognostic utility among the contrasts (see 4.4 above), this was an expected yet informative finding enhancing our understanding of auditory processing deficits in acute DoC.

As fNIRS provides measurements of both HbO and HbR, the differential contribution analysis can also be extended to the Hb dimension. Notably, the selected Hb type varied mostly across contrasts, but also within contrasts in both data-driven scores. However, a larger sample size is needed for this analysis, as there is more variability to be explained in the Hb type dimension. The result of such an analysis could enhance our understanding of the neurologic underpinnings of auditory function deficiencies in acute DoC, as hemodynamic response is linked to neurovascular coupling.

While much has been discussed about the sensitivity and specificity of biomarkers, and the use of data-driven approaches for diagnostic and prognostic purposes in DoC is rapidly rising, I have not yet encountered a study in the fMRI literature of DoC where the idea of having complementary sensitive and specific scores is presented. The proposed data-driven approach was designed with the characteristics of the task and fNIRS in mind, and used innovatively to add depth to the auditory assessments. With further development, this approach has the potential to improve the reliability of auditory assessments and enhance our understanding of auditory function in severe brain injury.

4.7 Applicability and methodological implications

fNIRS has several advantageous features for testing patients at the bedside in the ICUs: portability, cost-effectiveness, and robustness against motion artifacts and electromagnetic noise. However, while fNIRS offers several advantages as a prognosis aid compared to fMRI and EEG, it also has some limitations, including a lower signal-to-noise ratio and spatial resolution compared to fMRI. In addition, due to the novelty of fNIRS relative to EEG and fMRI, data analysis methods are not well-established or widely validated and are still in development.

The limitations of fNIRS are particularly relevant for applications that require high sensitivity at the individual subject level, such as the present study. To address these limitations, it is crucial to implement methodological measures, such as using a stimulus design optimized for fNIRS, a high-density optical montage, regression of physiological confounds, and up-to-date preprocessing and statistical techniques. These measures can

help mitigate fNIRS's limitations and improve the accuracy and reliability of measurments.

The current study implemented several methodological measures to mitigate the limitations of fNIRS, including using an optical montage with high temporal lobe density and adding intertrial intervals to the stimulus design to enhance the signal-to-noise ratio of the measurements. Short channel regression was necessary to obtain reliable measurements, as sensitivity was drastically lower without it (results not reported). The added crossing channels in the optical montage enhanced the sensitivity in the Language Comprehension contrast by approximately 30%, which is particularly noteworthy given the challenges of this contrast, even for fMRI. Moreover, the minimal modification of the stimulus design allowed for the detection of activation in language-related regions that were not detected in the fMRI study, in addition to enabling the replication of fMRI group results with a comparable or better degree of inter-subject sensitivity.

The promising results obtained in this study were not restricted to healthy controls, as the method was reliable enough to detect preserved auditory function in an entirely unresponsive patient with severe GBS. This finding was consistent with the patient's clinical diagnosis and validated using active tasks with both EEG and fNIRS. Additionally, a positive correlation was observed between the auditory function scores of a small group of patients and their recovery outcomes, although the validity of this finding was difficult to verify due to uncertainties surrounding patient outcomes.

Taken together, these findings highlight the potential of fNIRS as a bedside neurofunctional assessment tool while emphasizing the importance of methodology in achieving high subject-level sensitivity, a critical requirement for any tool used in outcome prognosis. As fNIRS continues to evolve, it is poised to become a formidable neuroimaging instrument for clinical neuroimaging purposes. However, the fNIRS device used must be complemented with appropriate methods to achieve the necessary reliability for critical applications. Based on the results of the present study, two pivotal methodological recommendations can be made to help unlock the full potential of fNIRS.

As discussed earlier, the higher density of the optical montage in the posterior temporal lobe was effective in achieving a higher sensitivity in the challenging Language Comprehension contrast. However, it had a negligible effect on the already high sensitivities observed in the other two contrasts. The redundancy of additional channels in the less challenging contrasts resulted in increased setup time with no gain, which is a crucial factor to consider in ICU settings. Thus, finding an optimal number of channels that balances practicality with sensitivity enhancement is important.

Based on the current study's findings, I propose the removal of all additional sources and detectors except for detector #10 and its counterpart in the right hemisphere. This detector forms four channels with surrounding sources, covering the mid-to-posterior region of the left temporal lobe. Specifically, one of these four channels (#62) was critical in the Language Comprehension contrast, while another (#43) was beneficial in the Speech Perception contrast. I have shown that the remaining 23 additional channels can be removed without impacting inter-subject sensitivity, and additional coverage can be provided for language-related areas with already low sensitivity (bilateral anterior temporal lobe) or areas with a high potential of enhancing the sensitivity in the Language Comprehension contrast (left posterior temporal lobe, left temporoparietal junction, and bilateral ventral IFG). Notably, the present study detected left frontal components of the language network, albeit at a reduced significance level of $p < 0.1$. Therefore, adding coverage in this region is expected to be beneficial at the group level and, in turn, influential for the subject-level sensitivity.

As discussed earlier, the added intertrial intervals also effectively enhanced the method's sensitivity. Further improvements can be made in the stimulus design to achieve higher reliability. First, the rest periods should be jittered to mitigate the interference of the periodic physiological confounds with the stimulus-evoked brain responses, enhancing the signal-to-noise ratio of the measurements. Second, the number of block repetitions should be at least doubled to 10 to increase the statistical power of the experimental design. Obviously, doing so would double the task duration, which is an undesired outcome. The duration of rest and non-rest trials can be shortened as a solution. the optimal duration can be determined based on the results of the current study.

As presented in sections 3.2.1 through 3.2.3, the highly activated channels' hemodynamic responses reached their maximum ~10 seconds after the onset of the stimulus and declined a few seconds later. Therefore, a trial duration of longer than ~15 seconds is not optimal. Thus, the duration of short stories and pseudowords can be reduced to 15 seconds. The noise trials can be considerably shorter (~7 seconds), especially considering the habituation effect when listening to noise. Additionally, it would be beneficial to jitter non-rest periods and randomly switch the condition order within a block to control for participant anticipation and trial order effects. Implementing these changes will result in a *slow* event-related design with a much faster pace than the current design. The increased stimulation pace would have two other benefits: First, it takes advantage of the higher temporal resolution of fNIRS over fMRI. Second, it increases the stimulation frequency of the task reducing the interference of the task-related components with systemic-physiology-driven very-low-frequency noises, allowing for the use of a high pass filter. The current study did not use a high pass filter (signals were only detrended) since the stimulus frequency was very low (~0.005 Hz).

Making such extensive modifications to the stimulus design in the present study would have made it even more challenging to compare fNIRS and fMRI results. Furthermore, an informed and structured optimization of the stimulus design requires prior experimentation to assess the time and frequency profiles of hemodynamic responses, which can now be extracted from the current study. Therefore, it was decided not to make any further modifications to the fMRI design beyond adding intertrial intervals.

4.8 Limitations and future directions

A notable limitation of the present study concerning the comparison between fMRI and fNIRS is that a reliable direct comparison necessitates the concurrent assessment of the same participants using both modalities. This is unless independently tested sample sizes are significantly large. Given the practical challenges of obtaining such extensive samples for a valid comparison, a future study that combines fMRI and fNIRS concurrently is essential to precisely assess the sensitivities of these modalities within the employed paradigm.

In addition to the overarching limitation discussed above, the lack of anatomical co-registration was a considerable limitation in the current study, particularly for the subject-level sensitivity and similarity analyses. fNIRS is blind to brain anatomy; therefore, the implicit assumption regarding the consistent placement of optical montage relative to the underlying brain anatomy is limited unless a procedure similar to fMRI for anatomical registration and spatial normalization is pursued. Alignment inconsistencies can occur for various reasons, including experimental error in placing the cap (relative to the anatomical landmarks) and differences in the participants' head shape and/or brain anatomy. The probable misalignment between the optical montage's intended coverage and a patient's brain anatomy limits the method's reliability (Novi et al., 2020a).

This issue can be addressed by co-registering the optical montage with each individual's brain anatomy, which requires acquiring anatomical scans from the participants and digitizing the optodes' exact location on their heads. The optodes' exact locations and the anatomical scan can be used to individualize the sensitivity profile of the optical montage for each patient via photon migration Monte Carlo simulation. The individualized sensitivity profiles would enable direct comparison of fNIRS and fMRI results in voxel space. A voxel-wise analysis would then allow for a direct and accurate comparison of fNIRS and fMRI results. Additionally, it would enhance the subject-level sensitivity due to the prevention of anatomical misalignment across individuals.

In the present study, anatomical scans were not acquired and optodes' locations were not digitized. Consequently, a sensitivity profile was created based on default optodes' locations and a standard brain atlas, and was used for all individuals, which may have led to inaccuracies.

A lack of anatomical co-registration is not only a problem for healthy control results, but more importantly, it undermines the reliability of similarity analysis, which is critical for patients whose similarity scores are used for prognosis. Note that cap placement error is more likely to happen for intubated, comatose patients in the ICU due to external factors like time and space restrictions. On the other hand, it can be justifiably argued that acquiring anatomical scans from patients defeats the whole purpose of developing a

bedside neuroimaging method. This, however, does not prevent using patients' anatomical scans if already acquired for clinical purposes. In the absence of anatomical scans, optodes' locations should still be digitized and then used with a standard brain model to produce semi-individualized sensitivity profiles, as a way to *partially* mitigate the anatomical co-registration issue.

However, a computationally intensive yet effective solution to the problem would be to go beyond one standard brain model and instead use a large number of anatomical scans from available databases in conjunction with the digitized optodes' locations to create a series of sensitivity profiles and voxel-wise activation maps. Next, an analytical or machine learning approach could be used to make statistical inferences based on the similarity scores from all these activation maps. That said, acquiring anatomical scans and digitized optodes' locations from *healthy* participants should be a priority in the future to create an accurate activation map for the control group.

Neither the present fNIRS study nor the original fMRI study (Norton, 2017) conducted test-retest reproducibility examinations, which limits the validity of the subject-level sensitivity results. The overlap of an individual's activation map with the ROI is not sufficient to guarantee a reliable assessment, as the degree of overlap could vary greatly across tests. To address this issue, future studies should include a within-subject reproducibility measure by conducting the experiment over multiple sessions. A comprehensive reliability analysis, such as the interclass correlation method (Li et al., 2015), should then be used to assess the consistency of the results across the sessions and participants.

The other limitation of the current study concerns the groups' sample sizes. This is particularly important for the Language Comprehension contrast and the prognostic utility analysis results. As seen in the Language Comprehension contrast's activation frequency map (Figure 3.13), the top four channels with the highest activation frequencies were all in the left hemisphere around the posterior temporal lobe; however, there were a large number of channels with relatively high activation frequencies widely distributed in the frontal and parietal lobes bilaterally. This was clearly different from the

other two contrasts, where the distribution of frequently activated channels was highly localized around the most frequently activated channels. The wide distribution of frequently activated channels in the Language comprehension contrast aligned with the distributed dual stream model of speech processing, requiring a larger number of healthy controls to achieve the statistical power already existing in the other contrasts. In addition, considering that handedness is directly linked to language lateralization in the brain, enhancing the ecological validity of the group and individual subject levels in this contrast requires testing healthy participants who are not exclusively right-handed.

In the present study, based on a small patient cohort, we began to investigate the applicability of fNIRS as a bedside neuroassessment tool. In addition to its small size, the tested sample was unbalanced regarding the outcome, as six out of eight patients deceased. Consequently, the generalizability of our findings, particularly the prognostic utility results, is limited. Future studies should utilize larger and more heterogeneous patient samples to better assess the present methods' prognostic utility.

The present study focused on detecting brain responses to auditory stimuli using the GLM approach. Complementary analyses can be performed to enhance the reliability of neuroauditory assessments. In particular, analyzing the flow of information in the brain (e.g., via Granger causal connectivity analysis) will add a new dimension to our understanding of auditory processing in a coma. Auditory processing can also be viewed from the angle of brain activity synchronization (via inter-subject correlation analysis): Since semantic processing yields a higher synchronization across individuals than basic acoustic processing, patients' synchronization profiles can be used to assess their auditory processing function.

Finally, extending the tests beyond one session is a critical issue that should be considered in the future. Repeated measurements and diversified analyses can take advantage of machine learning approaches to enhance the sensitivity and specificity of the outcome predictions. Higher prognosis accuracies will be achieved when the current neuroauditory test is administered in a battery of other passive (e.g., tactile stimulus) and

active (e.g., command following) tasks and repeated with EEG, the alternative bedside modality.

4.9 Conclusion

This proof-of-concept study was a first step towards developing and validating an fNIRS-based method for bedside assessment of auditory function in severe acute brain injury. In this study, the promise of fNIRS for such an application and the criticality of methodologic considerations, particularly optical montage and stimulus design, were demonstrated. Based on the results, specific recommendations were made to improve the optical montage and stimulus design.

A weighted averaging scoring method was proposed to provide a fine-grained index of auditory function. The method was well-suited to the hierarchical structure of the auditory assessments and limitations and characteristics of fNIRS. In line with several recent fMRI and EEG studies, an association was found between the fNIRS-based neuroauditory assessments and patients' coma outcomes. Expectedly, higher prognostic utilities resulted when the neuroauditory evaluations subsumed information from all three levels of auditory processing.

Additionally, a data-driven approach for increasing the specificity and sensitivity of the outcome predictions was explored. Increasing the specificity of the assessments enhanced their prognostic utility to a statistically significant degree. Semantic processing assessments contributed the most to the predictions' sensitivity and specificity, in line with its higher prognostic utility than the other two contrasts.

Probable misalignments between the optical montage's intended coverage and the individuals' brain anatomy undermine the method's reliability. Possible solutions to this issue, including co-registration with clinical anatomical imaging, were discussed. Repeating the measurements (test-retest) was recommended to improve the sensitivity analysis in healthy controls and the predictions' reliability in patients.

To validate fNIRS as a prognosis aid and assess the effectiveness of the proposed data-driven approach in enhancing prediction sensitivity and specificity, larger studies with

improved experimental designs are necessary. An accurate coma outcome prediction would require machine learning methods trained with data from several tasks, repetitions, and analyses. Although substantial experimental, methodological, and analytical work is required for enhancing the reliability of fNIRS, this study highlighted the promising potential of fNIRS as a bedside functional neuroimaging tool.

References

Aasted, C. M., Yücel, M. A., Cooper, R. J., Dubb, J., Tsuzuki, D., Becerra, L., Petkov, M. P., Borsook, D., Dan, I., & Boas, D. A. (2015). Anatomical guidance for functional near-infrared spectroscopy: AtlasViewer tutorial. *Neurophotonics*, *2*(2). https://doi.org/10.1117/1.NPh.2.2.020801

Abdalmalak, A., Laforge, G., Yip, L. C. M., Milej, D., Gonzalez-Lara, L. E., Anazodo, U., Owen, A. M., & St. Lawrence, K. (2020). Shining Light on the Human Brain: An Optical BCI for Communicating with Patients with Brain Injuries. *2020 IEEE International Conference on Systems, Man, and Cybernetics (SMC)*, 502–507. https://doi.org/10.1109/SMC42975.2020.9283123

Abdalmalak, A., Milej, D., Norton, L., Debicki, D. B., Owen, A. M., & Lawrence, K. St. (2021). The Potential Role of fNIRS in Evaluating Levels of Consciousness. *Frontiers in Human Neuroscience*, *15*. https://www.frontiersin.org/article/10.3389/fnhum.2021.703405

Abdalmalak, A., Milej, D., Norton, L., Debicki, D., Gofton, T., Diop, M., Owen, A. M., & Lawrence, K. S. (2017). Single-session communication with a locked-in patient by functional near-infrared spectroscopy. *Neurophotonics*, *4*(4), 040501. https://doi.org/10.1117/1.NPh.4.4.040501

Abdalmalak, A., Novi, S. L., Kazazian, K., Norton, L., Benaglia, T., Slessarev, M., Debicki, D. B., Lawrence, K. St., Mesquita, R. C., & Owen, A. M. (2022). Effects of Systemic Physiology on Mapping Resting-State Networks Using Functional Near-Infrared Spectroscopy. *Frontiers in Neuroscience*, *16*. https://www.frontiersin.org/articles/10.3389/fnins.2022.803297

Andrews, K., Murphy, L., Munday, R., & Littlewood, C. (1996). Misdiagnosis of the vegetative state: Retrospective study in a rehabilitation unit. *BMJ*, *313*(7048), 13–16. https://doi.org/10.1136/bmj.313.7048.13

Arridge, S. R., Schweiger, M., Hiraoka, M., & Delpy, D. T. (1993). A finite element approach for modeling photon transport in tissue. *Medical Physics*, *20*(2), 299–309. https://doi.org/10.1118/1.597069

Aubinet, C., Chatelle, C., Gosseries, O., Carrière, M., Laureys, S., & Majerus, S. (2022a). Residual implicit and explicit language abilities in patients with disorders of consciousness: A systematic review. *Neuroscience & Biobehavioral Reviews*, *132*(Complete), 391–409. https://doi.org/10.1016/j.neubiorev.2021.12.001

Aubinet, C., Schnakers, C., & Majerus, S. (2022b). Language Assessment in Patients with Disorders of Consciousness. *Seminars in Neurology*, *42*(3), 273–282. https://doi.org/10.1055/s-0042-1755561

Ayaz, H., Baker, W. B., Blaney, G., Boas, D. A., Bortfeld, H., Brady, K., Brake, J., Brigadoi, S., Buckley, E. M., Carp, S. A., Cooper, R. J., Cowdrick, K. R., Culver, J. P., Dan, I., Dehghani, H., Devor, A., Durduran, T., Eggebrecht, A. T., Emberson, L. L., … Zhou, W. (2022). Optical imaging and spectroscopy for the study of the human brain: Status report. *Neurophotonics*, *9*(S2), S24001. https://doi.org/10.1117/1.NPh.9.S2.S24001

Barker, J. W., Aarabi, A., & Huppert, T. J. (2013). Autoregressive model based algorithm for correcting motion and serially correlated errors in fNIRS. *Biomedical Optics Express*, *4*(8), 1366–1379. https://doi.org/10.1364/BOE.4.001366

Bauer, G., Gerstenbrand, F., & Rumpl, E. (1979). Varieties of the locked-in syndrome. *Journal of Neurology, 221*(2), 77–91. https://doi.org/10.1007/BF00313105

Becker, K. J., Baxter, A. B., Cohen, W. A., Bybee, H. M., Tirschwell, D. L., Newell, D. W., Winn, H. R., & Longstreth, W. T. (2001). Withdrawal of support in intracerebral hemorrhage may lead to self-fulfilling prophecies. *Neurology, 56*(6), 766–772. https://doi.org/10.1212/WNL.56.6.766

Beckmann, C. F., Jenkinson, M., & Smith, S. M. (2003). General multilevel linear modeling for group analysis in FMRI. *NeuroImage*, *20*(2), 1052–1063. https://doi.org/10.1016/S1053-8119(03)00435-X

Binder, J. R., Desai, R. H., Graves, W. W., & Conant, L. L. (2009). Where Is the Semantic System? A Critical Review and Meta-Analysis of 120 Functional Neuroimaging Studies. *Cerebral Cortex (New York, NY)*, *19*(12), 2767–2796. https://doi.org/10.1093/cercor/bhp055

Boly, M., Coleman, M. R., Davis, M. H., Hampshire, A., Bor, D., Moonen, G., Maquet, P. A., Pickard, J. D., Laureys, S., & Owen, A. M. (2007). When thoughts become action: An fMRI paradigm to study volitional brain activity in non-communicative brain injured patients. *NeuroImage*, *36*(3), 979–992. https://doi.org/10.1016/j.neuroimage.2007.02.047

Boly, M., Faymonville, M.-E., Peigneux, P., Lambermont, B., Damas, P., Del Fiore, G., Degueldre, C., Franck, G., Luxen, A., Lamy, M., Moonen, G., Maquet, P., & Laureys, S. (2004). Auditory Processing in Severely Brain Injured Patients: Differences Between the Minimally Conscious State and the Persistent Vegetative

State. *Archives of Neurology*, *61*(2), 233–238. https://doi.org/10.1001/archneur.61.2.233

Brigadoi, S., Ceccherini, L., Cutini, S., Scarpa, F., Scatturin, P., Selb, J., Gagnon, L., Boas, D. A., & Cooper, R. J. (2014). Motion artifacts in functional near-infrared spectroscopy: A comparison of motion correction techniques applied to real cognitive data. *NeuroImage*, *85*(0 1), 10.1016/j.neuroimage.2013.04.082. https://doi.org/10.1016/j.neuroimage.2013.04.082

Brigadoi, S., & Cooper, R. J. (2015). How short is short? Optimum source–detector distance for short-separation channels in functional near-infrared spectroscopy. *Neurophotonics*, *2*(2), 025005. https://doi.org/10.1117/1.NPh.2.2.025005

Bruno, M.-A., Vanhaudenhuyse, A., Thibaut, A., Moonen, G., & Laureys, S. (2011). From unresponsive wakefulness to minimally conscious PLUS and functional locked-in syndromes: Recent advances in our understanding of disorders of consciousness. *Journal of Neurology*, *258*(7), 1373–1384. https://doi.org/10.1007/s00415-011-6114-x

Buxton, R. B., Uludağ, K., Dubowitz, D. J., & Liu, T. T. (2004). Modeling the hemodynamic response to brain activation. *NeuroImage*, *23*, S220–S233. https://doi.org/10.1016/j.neuroimage.2004.07.013

Chen, W.-L., Wagner, J., Heugel, N., Sugar, J., Lee, Y.-W., Conant, L., Malloy, M., Heffernan, J., Quirk, B., Zinos, A., Beardsley, S. A., Prost, R., & Whelan, H. T. (2020). Functional Near-Infrared Spectroscopy and Its Clinical Application in the Field of Neuroscience: Advances and Future Directions. *Frontiers in Neuroscience*, *14*, 724. https://doi.org/10.3389/fnins.2020.00724

Chiarelli, A. M., Perpetuini, D., Filippini, C., Cardone, D., & Merla, A. (2019). Differential pathlength factor in continuous wave functional near-infrared spectroscopy: Reducing hemoglobin's cross talk in high-density recordings. *Neurophotonics*, *6*(3), 035005. https://doi.org/10.1117/1.NPh.6.3.035005

Childs, N. L., Mercer, W. N., & Childs, H. W. (1993). Accuracy of diagnosis of persistent vegetative state. *Neurology*, *43*(8), 1465–1467. https://doi.org/10.1212/wnl.43.8.1465

Claassen, J., Doyle, K., Matory, A., Couch, C., Burger, K. M., Velazquez, A., Okonkwo, J. U., King, J.-R., Park, S., Agarwal, S., Roh, D., Megjhani, M., Eliseyev, A., Connolly, E. S., & Rohaut, B. (2019). Detection of Brain Activation in

Unresponsive Patients with Acute Brain Injury. *New England Journal of Medicine*, *380*(26), 2497–2505. https://doi.org/10.1056/NEJMoa1812757

Coleman, M. R., Davis, M. H., Rodd, J. M., Robson, T., Ali, A., Owen, A. M., & Pickard, J. D. (2009). Towards the routine use of brain imaging to aid the clinical diagnosis of disorders of consciousness. *Brain*, *132*(9), 2541–2552. https://doi.org/10.1093/brain/awp183

Coleman, M. R., Rodd, J. M., Davis, M. H., Johnsrude, I. S., Menon, D. K., Pickard, J. D., & Owen, A. M. (2007). Do vegetative patients retain aspects of language comprehension? Evidence from fMRI. *Brain*, *130*(10), 2494–2507. https://doi.org/10.1093/brain/awm170

Cooper, R., Selb, J., Gagnon, L., Phillip, D., Schytz, H., Iversen, H., Ashina, M., & Boas, D. (2012). A Systematic Comparison of Motion Artifact Correction Techniques for Functional Near-Infrared Spectroscopy. *Frontiers in Neuroscience*, *6*. https://www.frontiersin.org/articles/10.3389/fnins.2012.00147

Cruse, D., Chennu, S., Chatelle, C., Bekinschtein, T. A., Fernández-Espejo, D., Pickard, J. D., Laureys, S., & Owen, A. M. (2011). Bedside detection of awareness in the vegetative state: A cohort study. *The Lancet*, *378*(9809), 2088–2094. https://doi.org/10.1016/S0140-6736(11)61224-5

D'Ausilio, A., Pulvermüller, F., Salmas, P., Bufalari, I., Begliomini, C., & Fadiga, L. (2009). The Motor Somatotopy of Speech Perception. *Current Biology*, *19*(5), 381–385. https://doi.org/10.1016/j.cub.2009.01.017

Davis, M. H., Coleman, M. R., Absalom, A. R., Rodd, J. M., Johnsrude, I. S., Matta, B. F., Owen, A. M., & Menon, D. K. (2007). Dissociating speech perception and comprehension at reduced levels of awareness. *Proceedings of the National Academy of Sciences*, *104*(41), 16032–16037. https://doi.org/10.1073/pnas.0701309104

Davis, M. H., & Johnsrude, I. S. (2003). Hierarchical Processing in Spoken Language Comprehension. *Journal of Neuroscience*, *23*(8), 3423–3431. https://doi.org/10.1523/JNEUROSCI.23-08-03423.2003

de Jong, B. M., Willemsen, A. T. M., & Paans, A. M. J. (1997). Regional cerebral blood flow changes related to affective speech presentation in persistent vegetative state. *Clinical Neurology and Neurosurgery*, *99*(3), 213–216. https://doi.org/10.1016/S0303-8467(97)00024-3

Delpy, D. T., & Cope, M. (1997). Quantification in tissue near-infrared spectroscopy. *Philosophical Transactions of the Royal Society B: Biological Sciences*, *352*(1354), 649–659. https://doi.org/10.1098/rstb.1997.0046

Edlow, B. L., Chatelle, C., Spencer, C. A., Chu, C. J., Bodien, Y. G., O'Connor, K. L., Hirschberg, R. E., Hochberg, L. R., Giacino, J. T., Rosenthal, E. S., & Wu, O. (2017). Early detection of consciousness in patients with acute severe traumatic brain injury. *Brain: A Journal of Neurology*, *140*(9), 2399–2414. https://doi.org/10.1093/brain/awx176

Edlow, B. L., Claassen, J., Schiff, N. D., & Greer, D. M. (2020). Recovery from disorders of consciousness: Mechanisms, prognosis and emerging therapies. *Nature Reviews Neurology*, 1–22. https://doi.org/10.1038/s41582-020-00428-x

Egawa, S., Ader, J., Shen, Q., Nakagawa, S., Fujimoto, Y., Fujii, S., Masuda, K., Shirota, A., Ota, M., Yoshino, Y., Amai, H., Miyao, S., Nakamoto, H., Kuroda, Y., Doyle, K., Grobois, L., Vrosgou, A., Carmona, J. C., Velazquez, A., … Claassen, J. (2022). Long-Term Outcomes of Patients with Stroke Predicted by Clinicians to have no Chance of Meaningful Recovery: A Japanese Cohort Study. *Neurocritical Care*. https://doi.org/10.1007/s12028-022-01644-7

Fernández-Espejo, D., & Owen, A. M. (2013). Detecting awareness after severe brain injury. *Nature Reviews Neuroscience*, *14*(11), Article 11. https://doi.org/10.1038/nrn3608

Fischer, D., Edlow, B. L., Giacino, J. T., & Greer, D. M. (2022). Neuroprognostication: A conceptual framework. *Nature Reviews. Neurology*, *18*(7), 419–427. https://doi.org/10.1038/s41582-022-00644-7

Friederici, A. D. (2006). What's in control of language? *Nature Neuroscience*, *9*(8), Article 8. https://doi.org/10.1038/nn0806-991

Giacino, J. T., Ashwal, S., Childs, N., Cranford, R., Jennett, B., Katz, D. I., Kelly, J. P., Rosenberg, J. H., Whyte, J., Zafonte, R. D., & Zasler, N. D. (2002). The minimally conscious state: Definition and diagnostic criteria. *Neurology*, *58*(3), 349–353. https://doi.org/10.1212/wnl.58.3.349

Giacino, J. T., Fins, J. J., Laureys, S., & Schiff, N. D. (2014). Disorders of consciousness after acquired brain injury: The state of the science. *Nature Reviews Neurology*, *10*(2), 99–114. https://doi.org/10.1038/nrneurol.2013.279

Giacino, J. T., Katz, D. I., Schiff, N. D., Whyte, J., Ashman, E. J., Ashwal, S., Barbano, R., Hammond, F. M., Laureys, S., Ling, G. S. F., Nakase-Richardson, R., Seel, R.

T., Yablon, S., Getchius, T. S. D., Gronseth, G. S., & Armstrong, M. J. (2018). Practice guideline update recommendations summary: Disorders of consciousness. *Neurology*, *91*(10), 450–460. https://doi.org/10.1212/WNL.0000000000005926

Gill-Thwaites, H. (2006). Lotteries, loopholes and luck: Misdiagnosis in the vegetative state patient. *Brain Injury*, *20*(13–14), 1321–1328. https://doi.org/10.1080/02699050601081802

Glover, G. H. (2011). Overview of Functional Magnetic Resonance Imaging. *Neurosurgery Clinics*, *22*(2), 133–139. https://doi.org/10.1016/j.nec.2010.11.001

Gofton, T. E., Chouinard, P. A., Young, G. B., Bihari, F., Nicolle, M. W., Lee, D. H., Sharpe, M. D., Yen, Y.-F., Takahashi, A. M., & Mirsattari, S. M. (2009). Functional MRI study of the primary somatosensory cortex in comatose survivors of cardiac arrest. *Experimental Neurology*, *217*(2), 320–327. https://doi.org/10.1016/j.expneurol.2009.03.011

Green, S. M. (2011). Cheerio, Laddie! Bidding Farewell to the Glasgow Coma Scale. *Annals of Emergency Medicine*, *58*(5), 427–430. https://doi.org/10.1016/j.annemergmed.2011.06.009

Hawkes, M. A., & Rabinstein, A. A. (2019). Neurological Prognostication After Cardiac Arrest in the Era of Target Temperature Management. *Current Neurology and Neuroscience Reports*, *19*(2), 10. https://doi.org/10.1007/s11910-019-0922-2

Hertrich, I., Dietrich, S., & Ackermann, H. (2020). The Margins of the Language Network in the Brain. *Frontiers in Communication*, *5*. https://www.frontiersin.org/articles/10.3389/fcomm.2020.519955

Hickok, G., & Poeppel, D. (2007). The cortical organization of speech processing. *Nature Reviews Neuroscience*, *8*(5), 393–402. https://doi.org/10.1038/nrn2113

Huppert, T. J. (2016a). Commentary on the statistical properties of noise and its implication on general linear models in functional near-infrared spectroscopy. *Neurophotonics*, *3*(1), 010401. https://doi.org/10.1117/1.NPh.3.1.010401

Huppert, T. J. (2016b). Commentary on the statistical properties of noise and its implication on general linear models in functional near-infrared spectroscopy. *Neurophotonics*, *3*(1), 010401. https://doi.org/10.1117/1.NPh.3.1.010401

Huppert, T. J., Diamond, S. G., Franceschini, M. A., & Boas, D. A. (2009). HomER: A review of time-series analysis methods for near-infrared spectroscopy of the

brain. *Applied Optics*, *48*(10), D280–D298. https://doi.org/10.1364/AO.48.00D280

Iacoboni, M. (2008). The role of premotor cortex in speech perception: Evidence from fMRI and rTMS. *Journal of Physiology-Paris*, *102*(1), 31–34. https://doi.org/10.1016/j.jphysparis.2008.03.003

Jennett, B., & Bond, M. (1975). Assessment of outcome after severe brain damage. *Lancet (London, England)*, *1*(7905), 480–484. https://doi.org/10.1016/s0140-6736(75)92830-5

Jennett, B., & Plum, F. (1994). Medical Aspects of the Persistent Vegetative State. *New England Journal of Medicine*, *330*(21), 1499–1508. https://doi.org/10.1056/NEJM199405263302107

Jöbsis, F. F. (1977). Noninvasive, Infrared Monitoring of Cerebral and Myocardial Oxygen Sufficiency and Circulatory Parameters. *Science*, *198*(4323), 1264–1267.

Kamps, M. J. A., Horn, J., Oddo, M., Fugate, J. E., Storm, C., Cronberg, T., Wijman, C. A., Wu, O., Binnekade, J. M., & Hoedemaekers, C. W. E. (2013). Prognostication of neurologic outcome in cardiac arrest patients after mild therapeutic hypothermia: A meta-analysis of the current literature. *Intensive Care Medicine*, *39*(10), 1671–1682. https://doi.org/10.1007/s00134-013-3004-y

Kazazian, K., Norton, L., Laforge, G., Abdalmalak, A., Gofton, T. E., Debicki, D., Slessarev, M., Hollywood, S., Lawrence, K. St., & Owen, A. M. (2021). Improving Diagnosis and Prognosis in Acute Severe Brain Injury: A Multimodal Imaging Protocol. *Frontiers in Neurology*, *12*. https://www.frontiersin.org/articles/10.3389/fneur.2021.757219

Kempny, A. M., James, L., Yelden, K., Duport, S., Farmer, S., Playford, E. D., & Leff, A. P. (2016). Functional near infrared spectroscopy as a probe of brain function in people with prolonged disorders of consciousness. *NeuroImage. Clinical*, *12*, 312–319. https://doi.org/10.1016/j.nicl.2016.07.013

Ketteler, D., Kastrau, F., Vohn, R., & Huber, W. (2008). The subcortical role of language processing. High level linguistic features such as ambiguity-resolution and the human brain; an fMRI study. *NeuroImage*, *39*(4), 2002–2009. https://doi.org/10.1016/j.neuroimage.2007.10.023

Kirilina, E., Jelzow, A., Heine, A., Niessing, M., Wabnitz, H., Brühl, R., Ittermann, B., Jacobs, A. M., & Tachtsidis, I. (2012). The physiological origin of task-evoked

systemic artefacts in functional near infrared spectroscopy. *NeuroImage*, *61*(1), 70–81. https://doi.org/10.1016/j.neuroimage.2012.02.074

Koenig, M. A., Holt, J. L., Ernst, T., Buchthal, S. D., Nakagawa, K., Stenger, V. A., & Chang, L. (2014). MRI Default Mode Network Connectivity is Associated with Functional Outcome after Cardiopulmonary Arrest. *Neurocritical Care*, *20*(3), 348–357. https://doi.org/10.1007/s12028-014-9953-3

Kondziella, D., Bender, A., Diserens, K., van Erp, W., Estraneo, A., Formisano, R., Laureys, S., Naccache, L., Ozturk, S., Rohaut, B., Sitt, J. D., Stender, J., Tiainen, M., Rossetti, A. O., Gosseries, O., Chatelle, C., & the EAN Panel on Coma, D. of C. (2020). European Academy of Neurology guideline on the diagnosis of coma and other disorders of consciousness. *European Journal of Neurology*, *27*(5), 741–756. https://doi.org/10.1111/ene.14151

Kondziella, D., Friberg, C. K., Frokjaer, V. G., Fabricius, M., & Møller, K. (2016). Preserved consciousness in vegetative and minimal conscious states: Systematic review and meta-analysis. *Journal of Neurology, Neurosurgery & Psychiatry*, *87*(5), 485–492. https://doi.org/10.1136/jnnp-2015-310958

Kurz, E.-M., Wood, G., Kober, S. E., Schippinger, W., Pichler, G., Müller-Putz, G., & Bauernfeind, G. (2018). Towards using fNIRS recordings of mental arithmetic for the detection of residual cognitive activity in patients with disorders of consciousness (DOC). *Brain and Cognition*, *125*, 78–87. https://doi.org/10.1016/j.bandc.2018.06.002

Laureys, S., Faymonville, M. E., Degueldre, C., Fiore, G. D., Damas, P., Lambermont, B., Janssens, N., Aerts, J., Franck, G., Luxen, A., Moonen, G., Lamy, M., & Maquet, P. (2000). Auditory processing in the vegetative state. *Brain: A Journal of Neurology*, *123 (Pt 8)*, 1589–1601. https://doi.org/10.1093/brain/123.8.1589

Laureys, S., Faymonville, M. E., Peigneux, P., Damas, P., Lambermont, B., Del Fiore, G., Degueldre, C., Aerts, J., Luxen, A., Franck, G., Lamy, M., Moonen, G., & Maquet, P. (2002). Cortical Processing of Noxious Somatosensory Stimuli in the Persistent Vegetative State. *NeuroImage*, *17*(2), 732–741. https://doi.org/10.1006/nimg.2002.1236

Laureys, S., Owen, A. M., & Schiff, N. D. (2004). Brain function in coma, vegetative state, and related disorders. *The Lancet. Neurology*, *3*(9), 537–546. https://doi.org/10.1016/S1474-4422(04)00852-X

Laureys, S., Pellas, F., Van Eeckhout, P., Ghorbel, S., Schnakers, C., Perrin, F., Berré, J., Faymonville, M.-E., Pantke, K.-H., Damas, F., Lamy, M., Moonen, G., & Goldman, S. (2005). The locked-in syndrome: What is it like to be conscious but paralyzed and voiceless? *Progress in Brain Research*, *150*, 495–511. https://doi.org/10.1016/S0079-6123(05)50034-7

Leon, A. C., & Heo, M. (2009). Sample Sizes Required to Detect Interactions between Two Binary Fixed-Effects in a Mixed-Effects Linear Regression Model. *Computational Statistics & Data Analysis*, *53*(3), 603–608. https://doi.org/10.1016/j.csda.2008.06.010

Li, L., Zeng, L., Lin, Z.-J., Cazzell, M., & Liu, H. (2015). Tutorial on use of intraclass correlation coefficients for assessing intertest reliability and its application in functional near-infrared spectroscopy–based brain imaging. *Journal of Biomedical Optics*, *20*(5), 050801. https://doi.org/10.1117/1.JBO.20.5.050801

Liu, N., Cui, X., Bryant, D. M., Glover, G. H., & Reiss, A. L. (2015). Inferring deep-brain activity from cortical activity using functional near-infrared spectroscopy. *Biomedical Optics Express*, *6*(3), 1074–1089. https://doi.org/10.1364/BOE.6.001074

Marino, M. H., Koffer, J., & Nalla, S. (2023). Update on Disorders of Consciousness. *Current Physical Medicine and Rehabilitation Reports*, *11*(1), 62–73. https://doi.org/10.1007/s40141-023-00384-9

Mark, N. M., Rayner, S. G., Lee, N. J., & Curtis, J. R. (2015). Global variability in withholding and withdrawal of life-sustaining treatment in the intensive care unit: A systematic review. *Intensive Care Medicine*, *41*(9), 1572–1585. https://doi.org/10.1007/s00134-015-3810-5

Menon, D. K., Owen, A. M., Williams, E. J., Minhas, P. S., Allen, C. M. C., Boniface, S. J., & Pickard, J. D. (1998). Cortical processing in persistent vegetative state. *The Lancet*, *352*(9123), 200. https://doi.org/10.1016/S0140-6736(05)77805-3

Molteni, E., Arrigoni, F., Bardoni, A., Galbiati, S., Villa, F., Colombo, K., & Strazzer, S. (2013). Bedside assessment of residual functional activation in minimally conscious state using NIRS and general linear models. *Annual International Conference of the IEEE Engineering in Medicine and Biology Society. IEEE Engineering in Medicine and Biology Society. Annual International Conference*, *2013*, 3551–3554. https://doi.org/10.1109/EMBC.2013.6610309

Monti, M. M., Vanhaudenhuyse, A., Coleman, M. R., Boly, M., Pickard, J. D., Tshibanda, L., Owen, A. M., & Laureys, S. (2010). Willful Modulation of Brain Activity in Disorders of Consciousness. *New England Journal of Medicine*, *362*(7), 579–589. https://doi.org/10.1056/NEJMoa0905370

Moritz, C. H., Rowley, H. A., Haughton, V. M., Swartz, K. R., Jones, J., & Badie, B. (2001). Functional MR imaging assessment of a non-responsive brain injured patient. *Magnetic Resonance Imaging*, *19*(8), 1129–1132. https://doi.org/10.1016/s0730-725x(01)00432-5

Mummery, C. J., Ashburner, J., Scott, S. K., & Wise, R. J. (1999). Functional neuroimaging of speech perception in six normal and two aphasic subjects. *The Journal of the Acoustical Society of America*, *106*(1), 449–457. https://doi.org/10.1121/1.427068

Murakami, T., Kell, C. A., Restle, J., Ugawa, Y., & Ziemann, U. (2015). Left Dorsal Speech Stream Components and Their Contribution to Phonological Processing. *Journal of Neuroscience*, *35*(4), 1411–1422. https://doi.org/10.1523/JNEUROSCI.0246-14.2015

Nippert, A. R., Biesecker, K. R., & Newman, E. A. (2018). Mechanisms Mediating Functional Hyperemia in the Brain. *The Neuroscientist: A Review Journal Bringing Neurobiology, Neurology and Psychiatry*, *24*(1), 73–83. https://doi.org/10.1177/1073858417703033

Norton, L. (2017). *Functional Magnetic Resonance Imaging as an Assessment Tool in Critically Ill Patients* [PhD Dissertation, Western University]. Electronic Thesis and Dissertation Repository. https://ir.lib.uwo.ca/etd/4812

Norton, L., Hutchison, R. M., Young, G. B., Lee, D. H., Sharpe, M. D., & Mirsattari, S. M. (2012). Disruptions of functional connectivity in the default mode network of comatose patients. *Neurology*, *78*(3), 175–181. https://doi.org/10.1212/WNL.0b013e31823fcd61

Norton, L., Kazazian, K., Gofton, T., Debicki, D. B., Fernandez-Espejo, D., Peelle, J. E., Al Thenayan, E., Young, G. B., & Owen, A. M. (2023). Functional Neuroimaging as an Assessment Tool in Critically Ill Patients. *Annals of Neurology*, *93*(1), 131–141. https://doi.org/10.1002/ana.26530

Novi, S. L., Forero, E. J., Rubianes Silva, J. A. I., de Souza, N. G. S. R., Martins, G. G., Quiroga, A., Wu, S.-T., & Mesquita, R. C. (2020a). Integration of Spatial Information Increases Reproducibility in Functional Near-Infrared Spectroscopy.

Frontiers in Neuroscience, *14*. https://www.frontiersin.org/articles/10.3389/fnins.2020.00746

Novi, S. L., Roberts, E., Spagnuolo, D., Spilsbury, B. M., Price, D. C., Imbalzano, C. A., Forero, E., Yodh, A. G., Tellis, G. M., Tellis, C. M., & Mesquita, R. C. (2020b). Functional near-infrared spectroscopy for speech protocols: Characterization of motion artifacts and guidelines for improving data analysis. *Neurophotonics*, *7*(1), 015001. https://doi.org/10.1117/1.NPh.7.1.015001

Okada, K., Rong, F., Venezia, J., Matchin, W., Hsieh, I.-H., Saberi, K., Serences, J. T., & Hickok, G. (2010). Hierarchical Organization of Human Auditory Cortex: Evidence from Acoustic Invariance in the Response to Intelligible Speech. *Cerebral Cortex*, *20*(10), 2486–2495. https://doi.org/10.1093/cercor/bhp318

Owen, A. M. (2019). The Search for Consciousness. *Neuron*, *102*(3), 526–528. https://doi.org/10.1016/j.neuron.2019.03.024

Owen, A. M. (2020). Improving diagnosis and prognosis in disorders of consciousness. *Brain*, *143*(4), 1050–1053. https://doi.org/10.1093/brain/awaa056

Owen, A. M., & Coleman, M. R. (2008). Detecting Awareness in the Vegetative State. *Annals of the New York Academy of Sciences*, *1129*(1), 130–138. https://doi.org/10.1196/annals.1417.018

Owen, A. M., Coleman, M. R., Boly, M., Davis, M. H., Laureys, S., & Pickard, J. D. (2006). Detecting Awareness in the Vegetative State. *Science*, *313*(5792), 1402–1402. https://doi.org/10.1126/science.1130197

Owen, A. M., Coleman, M. R., Menon, D. K., Johnsrude, I. S., Rodd, J. M., Davis, M. H., Taylor, K., & Pickard, J. D. (2005). Residual auditory function in persistent vegetative state: A combined pet and fmri study. *Neuropsychological Rehabilitation*, *15*(3–4), 290–306. https://doi.org/10.1080/09602010443000579

Owen, A. M., Menon, D. K., Johnsrude, I. S., Bor, D., Scott, S. K., Manly, T., Williams, E. J., Mummery, C., & Pickard, J. D. (2002). Detecting Residual Cognitive Function in Persistent Vegetative State. *Neurocase*, *8*(5), 394–403. https://doi.org/10.1076/neur.8.4.394.16184

Pardo, J. S., Nygaard, L. C., Remez, R. E., & Pisoni, D. B. (2021). *The Handbook of Speech Perception*. John Wiley & Sons.

Patil, A. V., Safaie, J., Moghaddam, H. A., Wallois, F., & Grebe, R. (2011). Experimental investigation of NIRS spatial sensitivity. *Biomedical Optics Express*, *2*(6), 1478–1493. https://doi.org/10.1364/BOE.2.001478

Paulmann, S., Ott, D. V. M., & Kotz, S. A. (2011). Emotional Speech Perception Unfolding in Time: The Role of the Basal Ganglia. *PLOS ONE*, *6*(3), e17694. https://doi.org/10.1371/journal.pone.0017694

Pinti, P., Scholkmann, F., Hamilton, A., Burgess, P., & Tachtsidis, I. (2019). Current Status and Issues Regarding Pre-processing of fNIRS Neuroimaging Data: An Investigation of Diverse Signal Filtering Methods Within a General Linear Model Framework. *Frontiers in Human Neuroscience*, *12*. https://www.frontiersin.org/article/10.3389/fnhum.2018.00505

Pinti, P., Tachtsidis, I., Hamilton, A., Hirsch, J., Aichelburg, C., Gilbert, S., & Burgess, P. W. (2020). The present and future use of functional near-infrared spectroscopy (fNIRS) for cognitive neuroscience. *Annals of the New York Academy of Sciences*, *1464*(1), 5–29. https://doi.org/10.1111/nyas.13948

Posner, J. B., Saper, C. B., Schiff, N. D., & Claassen, J. (2019). *Plum and Posner's Diagnosis and Treatment of Stupor and Coma*. Oxford University Press. https://doi.org/10.1093/med/9780190208875.001.0001

Price, C. J. (2012). A review and synthesis of the first 20 years of PET and fMRI studies of heard speech, spoken language and reading. *Neuroimage*, *62*(2), 816–847. https://doi.org/10.1016/j.neuroimage.2012.04.062

Rodd, J. M., Davis, M. H., & Johnsrude, I. S. (2005). The Neural Mechanisms of Speech Comprehension: FMRI studies of Semantic Ambiguity. *Cerebral Cortex*, *15*(8), 1261–1269. https://doi.org/10.1093/cercor/bhi009

Rupawala, M., Dehghani, H., Lucas, S. J. E., Tino, P., & Cruse, D. (2018). Shining a Light on Awareness: A Review of Functional Near-Infrared Spectroscopy for Prolonged Disorders of Consciousness. *Frontiers in Neurology*, *9*, 350. https://doi.org/10.3389/fneur.2018.00350

Sandroni, C., D'Arrigo, S., Cacciola, S., Hoedemaekers, C. W. E., Kamps, M. J. A., Oddo, M., Taccone, F. S., Di Rocco, A., Meijer, F. J. A., Westhall, E., Antonelli, M., Soar, J., Nolan, J. P., & Cronberg, T. (2020). Prediction of poor neurological outcome in comatose survivors of cardiac arrest: A systematic review. *Intensive Care Medicine*, *46*(10), 1803–1851. https://doi.org/10.1007/s00134-020-06198-w

Santosa, H., Zhai, X., Fishburn, F., Sparto, P. J., & Huppert, T. J. (2020). Quantitative comparison of correction techniques for removing systemic physiological signal in functional near-infrared spectroscopy studies. *Neurophotonics*, *7*(3), 035009. https://doi.org/10.1117/1.NPh.7.3.035009

Sanz, L. R. D., Thibaut, A., Edlow, B. L., Laureys, S., & Gosseries, O. (2021). Update on neuroimaging in disorders of consciousness. *Current Opinion in Neurology, Publish Ahead of Print*. https://doi.org/10.1097/WCO.0000000000000951

Schiff, N. D. (2015). Cognitive Motor Dissociation Following Severe Brain Injuries. *JAMA Neurology*, *72*(12), 1413–1415. https://doi.org/10.1001/jamaneurol.2015.2899

Schnakers, C., Vanhaudenhuyse, A., Giacino, J., Ventura, M., Boly, M., Majerus, S., Moonen, G., & Laureys, S. (2009). Diagnostic accuracy of the vegetative and minimally conscious state: Clinical consensus versus standardized neurobehavioral assessment. *BMC Neurology*, *9*(1), 35. https://doi.org/10.1186/1471-2377-9-35

Scholkmann, F., Kleiser, S., Metz, A. J., Zimmermann, R., Mata Pavia, J., Wolf, U., & Wolf, M. (2014). A review on continuous wave functional near-infrared spectroscopy and imaging instrumentation and methodology. *NeuroImage*, *85*, 6–27. https://doi.org/10.1016/j.neuroimage.2013.05.004

Scholkmann, F., Spichtig, S., Muehlemann, T., & Wolf, M. (2010). How to detect and reduce movement artifacts in near-infrared imaging using moving standard deviation and spline interpolation. *Physiological Measurement*, *31*(5), 649–662. https://doi.org/10.1088/0967-3334/31/5/004

Scholkmann, F., & Wolf, M. (2013). General equation for the differential pathlength factor of the frontal human head depending on wavelength and age. *Journal of Biomedical Optics*, *18*(10), 105004. https://doi.org/10.1117/1.JBO.18.10.105004

Schomers, M. R., & Pulvermüller, F. (2016). Is the Sensorimotor Cortex Relevant for Speech Perception and Understanding? An Integrative Review. *Frontiers in Human Neuroscience*, *10*. https://www.frontiersin.org/articles/10.3389/fnhum.2016.00435

Shibasaki, H. (2008). Human brain mapping: Hemodynamic response and electrophysiology. *Clinical Neurophysiology: Official Journal of the International Federation of Clinical Neurophysiology*, *119*(4), 731–743. https://doi.org/10.1016/j.clinph.2007.10.026

Si, J., Yang, Y., Xu, L., Xu, T., Liu, H., Zhang, Y., Jing, R., Li, J., Wang, D., Wu, S., & He, J. (2023). Evaluation of residual cognition in patients with disorders of consciousness based on functional near-infrared spectroscopy. *Neurophotonics*, *10*(2), 025003. https://doi.org/10.1117/1.NPh.10.2.025003

Singh, A. K., & Dan, I. (2006). Exploring the false discovery rate in multichannel NIRS. *NeuroImage*, *33*(2), 542–549. https://doi.org/10.1016/j.neuroimage.2006.06.047

Smith, E., & Delargy, M. (2005). Locked-in syndrome. *BMJ*, *330*(7488), 406–409. https://doi.org/10.1136/bmj.330.7488.406

Sokoliuk, R., Degano, G., Banellis, L., Melloni, L., Hayton, T., Sturman, S., Veenith, T., Yakoub, K. M., Belli, A., Noppeney, U., & Cruse, D. (2021). Covert Speech Comprehension Predicts Recovery From Acute Unresponsive States. *Annals of Neurology*, *89*(4), 646–656. https://doi.org/10.1002/ana.25995

Stevens, R. D., & Sutter, R. (2013). Prognosis in severe brain injury. *Critical Care Medicine*, *41*(4), 1104–1123. https://doi.org/10.1097/CCM.0b013e318287ee79

Tak, S., Uga, M., Flandin, G., Dan, I., & Penny, W. D. (2016). Sensor space group analysis for fNIRS data. *Journal of Neuroscience Methods*, *264*, 103–112. https://doi.org/10.1016/j.jneumeth.2016.03.003

Teasdale, G., & Jennett, B. (1974). Assessment of coma and impaired consciousness. A practical scale. *Lancet (London, England)*, *2*(7872), 81–84. https://doi.org/10.1016/s0140-6736(74)91639-0

Teasdale, G., Maas, A., Lecky, F., Manley, G., Stocchetti, N., & Murray, G. (2014). The Glasgow Coma Scale at 40 years: Standing the test of time. *The Lancet Neurology*, *13*(8), 844–854. https://doi.org/10.1016/S1474-4422(14)70120-6

Turgeon, A. F., Lauzier, F., Burns, K. E. A., Meade, M. O., Scales, D. C., Zarychanski, R., Moore, L., Zygun, D. A., McIntyre, L. A., Kanji, S., Hébert, P. C., Murat, V., Pagliarello, G., Fergusson, D. A., & Group, for the C. C. C. T. (2013). Determination of Neurologic Prognosis and Clinical Decision Making in Adult Patients With Severe Traumatic Brain Injury: A Survey of Canadian Intensivists, Neurosurgeons, and Neurologists*. *Critical Care Medicine*, *41*(4), 1086–1093. https://doi.org/10.1097/CCM.0b013e318275d046

Turgeon, A. F., Lauzier, F., Simard, J.-F., Scales, D. C., Burns, K. E. A., Moore, L., Zygun, D. A., Bernard, F., Meade, M. O., Dung, T. C., Ratnapalan, M., Todd, S., Harlock, J., Fergusson, D. A., & Canadian Critical Care Trials Group. (2011). Mortality associated with withdrawal of life-sustaining therapy for patients with

severe traumatic brain injury: A Canadian multicentre cohort study. *CMAJ: Canadian Medical Association Journal = Journal de l'Association Medicale Canadienne*, *183*(14), 1581–1588. https://doi.org/10.1503/cmaj.101786

Uppenkamp, S., Johnsrude, I. S., Norris, D., Marslen-Wilson, W., & Patterson, R. D. (2006). Locating the initial stages of speech–sound processing in human temporal cortex. *NeuroImage*, *31*(3), 1284–1296. https://doi.org/10.1016/j.neuroimage.2006.01.004

Vigneau, M., Beaucousin, V., Hervé, P. Y., Duffau, H., Crivello, F., Houdé, O., Mazoyer, B., & Tzourio-Mazoyer, N. (2006). Meta-analyzing left hemisphere language areas: Phonology, semantics, and sentence processing. *NeuroImage*, *30*(4), 1414–1432. https://doi.org/10.1016/j.neuroimage.2005.11.002

Watkins, K., & Paus, T. (2004). Modulation of motor excitability during speech perception: the role of Broca's area. *Journal of Cognitive Neuroscience*, 16(6), 978-987.

Weijer, C. (2019). Imaging in the acute brain injured state; Ethical considerations. *Journal of the Neurological Sciences*, *405*, 56. https://doi.org/10.1016/j.jns.2019.10.157

Weijer, C., Bruni, T., Gofton, T., Young, G. B., Norton, L., Peterson, A., & Owen, A. M. (2016). Ethical considerations in functional magnetic resonance imaging research in acutely comatose patients. *Brain: A Journal of Neurology*, *139*(Pt 1), 292–299. https://doi.org/10.1093/brain/awv272

Wijdicks, E. F. M., Hijdra, A., Young, G. B., Bassetti, C. L., & Wiebe, S. (2006). Practice Parameter: Prediction of outcome in comatose survivors after cardiopulmonary resuscitation (an evidence-based review): Report of the Quality Standards Subcommittee of the American Academy of Neurology. *Neurology*, *67*(2), 203–210. https://doi.org/10.1212/01.wnl.0000227183.21314.cd

Wilson, J. T., Pettigrew, L. E., & Teasdale, G. M. (1998). Structured interviews for the Glasgow Outcome Scale and the extended Glasgow Outcome Scale: Guidelines for their use. *Journal of Neurotrauma*, *15*(8), 573–585. https://doi.org/10.1089/neu.1998.15.573

Wilson, S. M., & Iacoboni, M. (2006). Neural responses to non-native phonemes varying in producibility: Evidence for the sensorimotor nature of speech perception. *NeuroImage*, *33*(1), 316–325. https://doi.org/10.1016/j.neuroimage.2006.05.032

Wilson, S. M., Saygin, A. P., Sereno, M. I., & Iacoboni, M. (2004). Listening to speech activates motor areas involved in speech production. *Nature Neuroscience*, *7*(7), 701–702. https://doi.org/10.1038/nn1263

Wyser, D. G., Kanzler, C. M., Salzmann, L., Lambercy, O., Wolf, M., Scholkmann, F., & Gassert, R. (2022). Characterizing reproducibility of cerebral hemodynamic responses when applying short-channel regression in functional near-infrared spectroscopy. *Neurophotonics*, *9*(1), 015004. https://doi.org/10.1117/1.NPh.9.1.015004

Yarkoni, T., Poldrack, R. A., Nichols, T. E., Van Essen, D. C., & Wager, T. D. (2011). Large-scale automated synthesis of human functional neuroimaging data. *Nature Methods*, *8*(8), 665–670. https://doi.org/10.1038/nmeth.1635

Young, G. B. (2009a). Coma. *Annals of the New York Academy of Sciences*, *1157*(1), 32–47. https://doi.org/10.1111/j.1749-6632.2009.04471.x

Young, G. B. (2009b). Neurologic Prognosis after Cardiac Arrest. *New England Journal of Medicine*, *361*(6), 605–611. https://doi.org/10.1056/NEJMcp0903466

Young, G. B., & Schiff, N. D. (2014). Disorders of consciousness. In M. Filippi & J. H. Simon (Eds.), *Imaging Acute Neurologic Disease: A Symptom-Based Approach* (pp. 1–18). Cambridge University Press. https://doi.org/10.1017/CBO9781139565653.002

Yücel, M. A., Selb, J., Aasted, C. M., Lin, P.-Y., Borsook, D., Becerra, L., & Boas, D. A. (2016). Mayer waves reduce the accuracy of estimated hemodynamic response functions in functional near-infrared spectroscopy. *Biomedical Optics Express*, *7*(8), 3078–3088. https://doi.org/10.1364/BOE.7.003078

Zhang, Y., Yang, Y., Si, J., Xia, X., He, J., & Jiang, T. (2017). Influence of inter-stimulus interval of spinal cord stimulation in patients with disorders of consciousness: A preliminary functional near-infrared spectroscopy study. *NeuroImage : Clinical*, *17*, 1–9. https://doi.org/10.1016/j.nicl.2017.09.017

Appendices

Appendix A

Western Research

Date: 7 February 2020

To: Dr. Adrian M. Owen

Project ID: 114967

Study Title: Improving Diagnosis and Prognosis in Acute Brain Injury: A Multimodal Imaging Approach (MIMIC Study - Multimodal IMaging in Intensive Care)

Application Type: HSREB Initial Application

Review Type: Full Board

Meeting Date: November 19, 2019

Date Approval Issued: 07/Feb/2020

REB Approval Expiry Date: 07/Feb/2021

Dear Dr. Adrian M. Owen

The Western University Health Science Research Ethics Board (HSREB) has reviewed and approved the above mentioned study as described in the WREM application form, as of the HSREB Initial Approval Date noted above. This research study is to be conducted by the investigator noted above. All other required institutional approvals must also be obtained prior to the conduct of the study.

Documents Approved:

Document Name	Document Type	Document Date	Document Version
Assent_V3	Assent Form	20/Jan/2020	3
Improving Diagnosis and Prognosis in Acute Brain Injury_ A Multimodal Imaging Approach V1_final	Protocol	04/Nov/2019	
LOI-control-v3	Written Consent/Assent	20/Jan/2020	3
LOI-patient-v4	Written Consent/Assent	29/Jan/2020	4
MIMIC CRF-v1	Other Data Collection Instruments	05/Nov/2019	1
MIMIC Scales	Other Data Collection Instruments	Received January 30, 2020	
PDF For recruitment BrainsCan	Email Script	Received January 30, 2020	
reminder email script	Email Script	Received January 30, 2020	

No deviations from, or changes to, the protocol or WREM application should be initiated without prior written approval of an appropriate amendment from Western HSREB , except when necessary to eliminate immediate hazard(s) to study participants or when the change(s) involves only administrative or logistical aspects of the trial.

REB members involved in the research project do not participate in the review, discussion or decision.

The Western University HSREB operates in compliance with, and is constituted in accordance with, the requirements of the TriCouncil Policy Statement: Ethical Conduct for Research Involving Humans (TCPS 2); the International Conference on Harmonisation Good Clinical Practice Consolidated Guideline (ICH GCP); Part C Division 5 of the Food and Drug Regulations; Part 4 of the Natural Health Products Regulations; Part 3 of the Medical Devices Regulations and the provisions of the Ontario Personal Health Information Protection Act (PHIPA 2004) and its applicable regulations. The HSREB is registered with the U.S. Department of Health & Human Services under the IRB registration number IRB 00000940.

Please do not hesitate to contact us if you have any questions.

Sincerely,

Karen Gopaul, Ethics Officer on behalf of Dr. Joseph Gilbert, HSREB Chair

Appendix B

Letter of Information and Consent – Healthy Control Volunteers

Study Title: Improving Diagnosis and Prognosis in Acute Brain Injury: A Multimodal Imaging Approach

Principal Investigator

Dr. Adrian Owen, Ph.D., Professor of Cognitive Neuroscience and Imaging

Department of Physiology and Pharmacology, Western University

London, Ontario, Canada

Funder: Canadian Institute of Health Research Foundation Grant

Conflict of Interest: There are no conflicts of interest to declare related to this study.

Introduction: You are invited to take part in a voluntary research study. Before you make a decision, it is important that you are aware of why the research is being done and what it will involve. The goal of the study is to determine whether certain brain images are useful for the diagnosis of coma (whether or not a patient is conscious) and the prognosis following brain injury (whether or not a patient will have a good outcome). We plan to recruit both patient participants who have sustained a severe brain injury and healthy participants who will be the control group. By comparing a group age-matched healthy participants to unconscious patients, we hope to learn more about how the brain operates to give rise to consciousness and if we can use tests to predict outcomes for patients admitted to the hospital. This letter is for healthy control participants. There is a separate letter for patients.

Why is this study being done?

Advances in life-saving medical technology have increased survival rates for patients after a serious brain injury. The recovery and continued care of these people often require long stays in intensive care units (ICUs), where important treatment decisions are made to increase the chances of regaining awareness and recovering thinking-related ability. The decisions made by the ICU healthcare teams have can affect patients' survival and outcomes. The ability to determine a patient's level of awareness and whether or not a patient will have a good outcome are challenging and treatment decisions are usually based on a patient's behavioral responses which can be unreliable.

In this study we plan to determine if new tools that look at brain images (called fMRI), brain function (fNIRS), and brain wave activity (called EEG) can identify awareness and predict good outcomes in unconscious patients.

How many people will take part in this study?

There will be a total of 700 people enrolled in the study over 7 years. We will recruit 350 participants to our study group who are unconscious and currently in the intensive care units at London Health Sciences Centre and 350 healthy conscious participants from the London community who will be in the control group.

As a healthy control participant, it is expected that study procedures will take approximately 3-4 hrs in total. If you are interested and would prefer to do the tests on two separate days that is possible.

What will happen during this study?

This study will use three different imaging methods (fMRI, fNIRS, EEG) to assess brain activity. You may be eligible for some or all of the imaging methods. FNIRS and EEG testing will occur at the Brain and Mind Institute at Western University while fMRI scanning will occur at Robarts Research Institute or at University or Victoria Hospital.

EEG Recording:

You will be seated a comfortable position while fitted with an electrode cap, which containing 128 electrodes, placed on your head. Fitting the cap will take approximately 20 minutes. After the fitting of the cap, some sounds will be presented over earphones. We will make sure before testing starts that that the volume of the sounds are at a comfortable level. The sounds you hear will be acceptable and will not be emotional (there may be sounds like beeps, sentences, songs, and movie clips). In adults who are part of the study, a somatosensory evoked potential task may be completed, where the nerve at your wrist will be electrical stimulated causing a small twitch in your thumb, and we will record the corresponding electrophysiological response. The total time of the testing will be approximately 60 min.

FNIRS Recording:

FNIRS is a portable imaging tool that measures the way brain activity changes when you perform different tasks by using sensors that record the way that light is absorbed in the brain. An fNIRS cap will be placed on your head and will sit gently on the head surface. You may take part in 6 tasks during the testing time where you will hear different sounds presented to you over earphones that will be acceptable and will not be emotional (there may be sounds like white noise, short stories and movie clips). In some tasks we may also ask you to try to follow an instruction given to you. In adults who are part of the study, a

somatosensory evoked potential task will be completed, where the nerve at your wrist will be electrical stimulated causing a small twitch in your thumb. The total time of the testing will be approximately 60 min.

FMRI Recording:

Eligible participants will also undergo a research fMRI scan, which is a specialized MRI scan that is a noninvasive test that uses a strong magnetic field and radio waves to look at blood flow in the brain to detect areas of activity. These changes in blood flow, which are captured on a computer, help us understand more about how the brain works. The scan allows us to understand the activity in areas of the brain in response to various stimuli (for example, the brain's response to hearing sounds). In adults who are part of the study, a somatosensory evoked potential task will be completed, where the nerve at your wrist will be electrical stimulated causing a small twitch in your thumb. You will be comfortably positioned inside the MRI scanner and the same stimuli presented to you in the fNIRS recordings will be used in the fMRI imaging. The total time of this test will be approximately 60 min.

These are images of the equipment being used in this study.

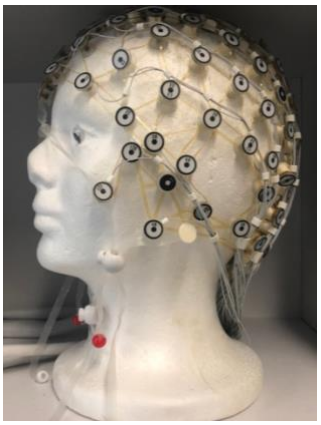

EEG Cap

fNIRS Cap

fMRI Machine

What are the risks and harms of participating in this study?

FMRI: There are no known biological risks associated with MR imaging. Some people cannot have an MRI because they have some type of metal in their body. For instance, if you have a heart pacemaker, artificial heart valves, metal implants such as metal ear implants, bullet pieces, chemotherapy or insulin pumps or any other metal such as metal clips or rings, they cannot have an MRI. During this test, you will lie in a small closed area inside a large magnetic tube. Some people may get scared or anxious in small places (claustrophobic). An MRI may also cause possible anxiety for people due to the loud

banging made by the machine and the confined space of the testing area. You will be given specially designed headphones to help reduce the noise.

EEG: The risks associated with having EEG electrodes placed on the head are minimal and include the potential for slight irritation of the scalp. This irritation will resolve on its own. EEG equipment does not penetrate or abrade the skin. The electrodes are housed in a net which stretches across the head. The correct sized electrode net will be chosen based upon the circumference of the participants head, making it more comfortable for them.

FNIRS: The amount of light that goes into the brain with fNIRS is about the same as the amount of light that goes into the brain when walking outside on a sunny day. The NIRS procedure is non-invasive, painless, and safe. The NIRS system uses a class 1 laser, which is safe for eye and skin exposure. The laser will not emit enough heat to cause any burning or discomfort. The experimenter may need to part small areas of hair using a swab in order for the fNIRS probes to have good contact with participants skin. This may cause mild discomfort, but this will be minimized by using trained experimenters.

What are the benefits?

There will be no direct benefits to you for participating in this study. However, research ultimately derived from this study may be used in establishing new diagnostic and prognostic guidelines for comatose patients after brain injury.

Voluntary Participation

Your participation in this study is voluntary. You may decide not to be in this study, or to be in the study now and then change your mind later. You may leave the study at any time without affecting your care. This form and your permission will never expire unless you change your mind and withdraw it.

What are the rights of participants?

You do not waive any legal right by signing this consent form. If you are harmed as a direct result of taking part in this study, all necessary medical treatment will be made available to you at no cost.

What are the costs to participants? Are participants paid to be in this study?

You will be reimbursed approximately $20 per hour for your participation in this study. This is intended to include your travel costs, parking, all miscellaneous expenses you have from participation. You will not be charged for any tests conducted for this study, including the MRI scan.

Can participants choose to leave the study?

If you decide to withdraw or are withdrawn from the study, the data already collected as part of the study will nonetheless be preserved, analyzed or used to ensure the completeness of the study. You may withdraw your permission by telling the study staff. If you choose to withdraw from the study, no further information will be collected.

How will participant's information be kept confidential?

While you take part in this study, the principal investigator and study staff will collect information about you that is necessary to answer the scientific objectives of the study. The information will be kept in your study file. Any identifying information (for example, your contact and demographic information), will be stored in a secure, password-protected database. Only the local researchers involved in this study at Western University and London Health Sciences Centre will have access to this information.

Personal identifiers collected in this study include full name, age, date of birth, sex, and contact information. All the information collected about you during the study will remain confidential. You will be identified by a numbered code. The key to this code will be kept by the principal investigator, in a locked space. The paper documents will be kept in a locked filing cabinet and the electronic files will be kept on a computer locked with a password and linked to a secure network. The investigators will preserve the data collected during this study indefinitely. The nominative data and codes linking them to you will be preserved for 25 years, and then destroyed. Contact and demographic information (name, sex/gender, age) will be securely stored on the password protected Ripple platform, which is an online platform managed by Western University's BrainsCAN program. Only the researchers of this study and the BrainsCAN coordinator(s), who administers the database system, will have access to your identifiable information as stated above.

The study data could be published in specialized medical journals or shared with others during scientific meetings, but it will be impossible to identify you. If research results are published, your name and other personal information will not be given.

Qualified representatives of the following organizations may look at your medical/clinical study records at the site where these records are held, for quality assurance (to check that the information collected for the study is correct and follows proper laws and guidelines).

- Representatives of Lawson Quality Assurance Education Program

- Representatives of the Western University's Health Sciences Research Ethics Board that oversees the ethical conduct of this study.

Will I know the results of my study tests?

Your individual study results will not be provided to you. If requested you can be sent any publications resulting from the study – in such a case, you will need to provide a mailing address. If study staff note any incidental findings, they will alert your medical care team, to examine the data and treat the findings as is medically necessary.

Whom do participants contact for questions?

If you have any questions about your rights as a research participant or the conduct of this study, you may contact the Patient Experience Office at LHSC or access the online form.

If you have any questions about your rights as a research participant or the conduct of this study, you may contact The Office of Human Research Ethics. The REB is a group of people who oversee the ethical conduct of research studies. The HSREB is not part of the study team. Everything that you discuss will be kept confidential.

Title of research project*:*	Improving Diagnosis and Prognosis in Acute Brain Injury: A Multimodal Imaging Approach

Consent Form – Healthy Controls

Eligible Testing Procedures:

The study team has assessed the participant's eligibility and these tests can be completed:

- ❑ fMRI
- ❑ fNIRS
- ❑ EEG

_____	_____	_____
Print Name of Research Staff	Signature	Date

Participant Consent

This study has been explained to me and any questions I had have been answered.

I know that I may leave the study at any time. I agree to take part in this study.

You agree to the following imaging tests to be completed:

- ❑ fMRI
- ❑ fNIRS
- ❑ EEG

_____	_____	_____
Print Name of Participant	Signature	Date

Person Obtaining Consent:

My signature means that I have explained the study to the individual named above. I have answered all questions.

_____	_____	_____
Print Name of Person	Signature	Date

Obtaining Consent

Appendix C

Letter of Information and Consent - Patient Volunteers

Study Title: Improving Diagnosis and Prognosis in Acute Brain Injury: A Multimodal Imaging Approach

Principal Investigator

Dr. Adrian Owen, Ph.D., Professor of Cognitive Neuroscience and Imaging Department of Physiology and Pharmacology, Western University, London, Ontario, Canada

Funder: Canadian Institute of Health Research Foundation Grant

Conflict of Interest: There are no conflicts of interest to declare related to this study.

Introduction:

NOTE: In this Consent document, "you" always refers to the study participants. If you are a substitute decision maker (SDM) (i.e. someone who makes the decision of participation on behalf of a participant), please remember that "you" refers to the study patient. As the SDM, you will be asked to review and sign this consent form on behalf of the participant. If the participant regains consciousness, they will be asked to sign this consent form.

You are invited to take part in a voluntary research study. Before you make a decision, it is important that you are aware of why the research is being done and what it will involve. The goal of the study is to determine whether certain brain images are useful for the diagnosis of coma (whether or not a patient is conscious) and the prognosis following brain injury (whether or not a patient will have a good outcome).

Why is this study being done?

Advances in life-saving medical technology have increased survival rates for patients after a serious brain injury. The recovery and continued care of these people often require long stays in intensive care units (ICUs), where important treatment decisions are made to increase the chances of regaining awareness and recovering thinking-related ability. The decisions made by the ICU healthcare teams can affect patients' survival and outcomes. The ability to determine a patient's level of awareness and whether or not a patient will have a good outcome are challenging and treatment decisions are usually based on a patient's behavioral responses which can be unreliable.

In this study we plan to determine if new tools that look at brain images (called fMRI), brain function (fNIRS), and brain wave activity (called EEG) can identify consciousness and predict favorable outcomes in unconscious patients.

How many people will take part in this study?

This study is taking place at the London Health Sciences Centre within the Intensive Care Unit at University Hospital, the Critical Care Trauma Centre at Victoria Hospital, and the Pediatric Critical Care Unit at Victoria Hospital. There will be a total of 700 people enrolled in the study over 7 years. We will recruit 350 participants to our study group who are unconscious and 350 healthy conscious participants who will be in the control group. A healthy control group is needed to determine difference between brain activity in people with normal levels of wakefulness compared to the brain activity of unconscious participants.

It is expected that you will be in the study for 1 year.

What will happen during this study?

This study will use three different imaging methods (fMRI, fNIRS, EEG) to assess brain activity and level of consciousness. You may be eligible for some or all of the imaging methods.

<u>EEG Recordings (performed on day 3,5,7 of admission to ICU):</u>

Testing will occur at your bedside and you will remain in their bed in a comfortable position while fitted with an electrode cap, which containing 128 electrodes, placed on your head. Fitting the cap will take approximately 20 minutes. After the fitting of the cap, some sounds will be presented over earphones. We will make sure before testing starts that that the volume of the sounds are at a comfortable level. The sounds you hear will be acceptable and will not be emotional (there may be sounds like beeps, sentences, songs, and movie clips). We will measure your brain waves in response to these sounds. The total time of the testing will be approximately 60 min. In adult patients, you may also have a somatosensory evoked potential test during the recording, where the nerve at your wrist will be electrical stimulated causing a small twitch in your thumb to understand how your brain processes sensations. We will measure the changes in your brain activity to the stimulation.

<u>FNIRS Recordings (performed on day 3,5,7 of admission to ICU):</u>

FNIRS is a portable imaging tool that will be used at your bedside that measures the way brain activity changes when you perform different tasks by using sensors that record the way that light is absorbed in the brain. An fNIRS cap will be placed on your head and will sit gently on the head surface. You may take part in 6 tasks during a 60 minute testing time. You will hear different sounds presented to you over earphones that will be acceptable and

will not be emotional (there may be sounds like white noise, short stories and movie clips). In some tasks we may also ask you to try to follow an instruction given to you. In adult patients, you will also have a somatosensory evoked potential test during the recording, where the nerve at your wrist will be electrical stimulated causing a small twitch in your thumb to understand how your brain processes sensations. We will measure the changes in your brain activity to the stimulation.

FMRI Recordings (performed on day 5 of admission to ICU):

Eligible participants will undergo a research fMRI scan, which is a specialized MRI scan that is a noninvasive test that uses a strong magnetic field and radio waves to look at blood flow in the brain to detect areas of activity. These changes in blood flow, which are captured on a computer, help us understand more about how the brain works. The scan allows us to understand the activity in areas of the brain in response to various stimuli (for example, the brain's response to hearing sounds). When possible, the fMRI scans will be combined with any other MRI imaging your doctor requests for your care. You will be accompanied by a nurse and respiratory technologist during the MRI scanning and you will be comfortably positioned inside the MRI scanner. In adult patients, you will also have a somatosensory evoked potential test during the recording, where the nerve at your wrist will be electrical stimulated causing a small twitch in your thumb to understand how your brain processes sensations. The total time of the study will be approximately 60 min. The same stimuli presented to you in the fNIRS recordings will be used in the fMRI imaging.

Follow-up Testing

During your hospital stay, once you are able to do so, we will ask you to complete computerized tests that assess your cognitive ability, called Cambridge Brain Sciences (www.cambridgebrainsciences.com). This battery of six short tests assesses your memory, attention and language. It will take approximately 20 minutes to complete. A member of the study team will come to your room, with a tablet or laptop, to have you complete the tests. After discharge from the hospital, you will be sent a monthly email invitation to complete the cognitive tests online from home for up to 12 months. If you do not have access to a computer with the internet after discharge, you will be invited to the Western Interdisciplinary Research Building at Western University to complete the online cognitive testing or a member of the research team will make arrangements to visit you.

At 3, 6, and 12 months following discharge from the ICU, you will receive a phone call from a member of the study team. This phone call will last no more than 10 minutes, and its purpose is to assess your level of recovery. If eligible, we may invite you to come back to the hospital at 12 months to repeat the imaging tests you took part in while you were in ICU.

You may also be eligible to enroll in a complementary study, titled "Brain protein microparticles in critical illness" where blood samples will be collected, and the level of proteins found in the blood will be compared to the extent of patient recovery. If eligible, and second letter of information will be presented to you. If and only if you choose to also enroll and consent to the MIMIC study and the microparticles study, we will collect a blood sample on the day of functional MRI imaging.

Summary of Tests and Procedures

	Enrolment	In-hospital testing (days from ICU admission or medically suitable)				Months post injury											
		Day 2-3	Day 4-6	Day7-10	Regain awareness	1	2	3	4	5	6	7	8	9	10	11	12
ENROL:																	
Eligibility Screen	X																
Informed Consent	X																
TESTING:																	
EEG*		x	x	x													x
fNIRS*		x	x	x													x
fMRI*			x														x
ASSESSMENT:																	
Cognitive Tests					x	x	x	x	x	x	x	x	x	x	x	x	x
Phone Interview								x			x						x

* if eligible and willing to participate

What are the risks and harms of participating in this study?

FMRI: There are no known biological risks associated with MR imaging. Some people cannot have an MRI because they have some type of metal in their body. For instance, if you have a heart pacemaker, artificial heart valves, metal implants such as metal ear implants, bullet pieces, chemotherapy or insulin pumps or any other metal such as metal clips or rings, they cannot have an MRI. During this test, you will lie in a small closed area inside a large magnetic tube. Some people may get scared or anxious in small places

(claustrophobic). An MRI may also cause possible anxiety for people due to the loud banging made by the machine and the confined space of the testing area. You will be given specially designed headphones to help reduce the noise. There are rare risks associated with moving outside of the ICU for procedures like MRI imaging. To reduce these risks a physician associated with the study will assess you to make sure you are medical stable for the scan. When possible, the research images will be taken at the same time as the medically required images so you do not need to travel twice to the MRI scanner. A bedside nurse and a respiratory therapist will always travel with you and will monitor you throughout the duration of scanning.

EEG: The risks associated with having EEG electrodes placed on the head are very little and include the possibility of small irritation of the scalp. This irritation will resolve on its own. EEG equipment does not penetrate or scrape the skin. The electrodes are housed in a net which stretches across the head. The correct sized electrode net will be chosen based upon the size of your head, making it more comfortable for you.

FNIRS: The amount of light that goes into the brain with fNIRS is about the same as the amount of light that goes into the brain when walking outside on a sunny day. The NIRS procedure is non-invasive, painless, and safe. The NIRS system uses a class 1 laser, which is safe for eye and skin exposure. The laser will not give off enough heat to cause any burning or discomfort. The experimenter may need to part small areas of hair using a swab in order for the fNIRS probes to have good contact with your skin. This may cause very mild discomfort.

Cognitive Testing: Cambridge Brain Sciences will record your internet protocol (IP) addresses when you complete the thinking-related testing online. Storage of your IP address runs the risk of privacy breaches that is associated with your IP address for example your network, device or service. Your IP address also provides information on the following areas, online services for which an individual has registered; personal interests, based on websites visited; and organizational associations.

What are the benefits?

This study may help determine your level of consciousness. Usually, doctors measure your level of consciousness on how you respond to them at the bedside, but this method may not be able to identify some patients who have an injury to their motor system that causes them to be unable to respond to external stimulation, but are aware. Both fMRI and EEG tests that will be used in this study, have shown that 15%-20% of patients in a vegetative state are misdiagnosed and they are more aware than the doctors can tell with the tools they have at the bedside. It is currently unknown if patients in a coma with a recent injury could have this type of awareness that can't otherwise be detected. This study may be able to find awareness in some brain injured patients and it could help

doctors make a proper finding about your level of consciousness. Additionally, some patients who are aware may be able to use the imaging tasks to communicate their thoughts and needs through using their brain activity.

There will be no direct benefit to patients in terms of prognostication, as the predictive value of the study tests has not been established.

Can participation in this study end early?

You may be taken off the study early if the study doctor no longer feels this is the best option for you, or the Regulatory Authorities research ethics board withdraw permission for this study to continue. If you are removed from this study, the study team will discuss the reasons with you. Your medical care will not change.

Voluntary Participation

Your participation in this study is voluntary. You may decide not to be in this study, or to be in the study now and then change your mind later. You may leave the study at any time without affecting your care. This form and your permission will never expire unless you change your mind and withdraw it.

What are the costs to participants? Are participants paid to be in this study?

If you come back for follow up testing at 12 months, you will be reimbursed for your travel costs, parking, and all miscellaneous expenses you have from participation.

What other choices are there?

An alternative to the procedures described above is not to participate in the study and continue on just as you do now.

What are the rights of participants?

You do not waive any legal right by signing this consent form. If you are harmed as a direct result of taking part in this study, all necessary medical treatment will be made available to you at no cost.

What are the costs to participants? Are participants paid to be in this study?

You will not incur any out-of-pocket expenses while you are in hospital and no compensation will be provided to you while in hospital. If you are eligible, you may return for imaging at 12 months following your injury. At that time you will be compensated for your out-of-pocket expenses (e.g. travel and parking).

Can participants choose to leave the study?

If you decide to withdraw or are withdrawn from the study, the data already collected as part of the study will nonetheless be preserved, analyzed or used to ensure the completeness of the study. If you choose to withdraw from the study, no further information will be collected. You may withdraw your permission by telling the study staff.

How will participant's information be kept confidential?

While you take part in this study, the principal investigator and study staff will collect information about you that is necessary to answer the scientific objectives of the study. The information will be kept in your study file. This information may comprise the details contained in your medical file regarding your past and present medical history, your lifestyle habits and results from exams and procedures, which will be carried out. Any identifying information (for example, your contact and demographic information), will be stored in a secure, password-protected database. Only the local researchers involved in this study at Western University and London Health Sciences Centre will have access to this information.

Personal identifiers collected in this study include full name, hospital number, age, date of birth, sex, and contact information.

All the information collected about you during the study will remain confidential. You will be identified by a numbered code. The key to this code will be kept by the principal investigator, in a locked space. The paper documents will be kept in a locked filing cabinet and the electronic files will be kept on a computer locked with a password and linked to a secure network. The investigators will preserve the data collected during this study indefinitely. The nominative data and codes linking them to you will be preserved for 25 years, and then destroyed. Contact and demographic information (name, telephone number, email, date of birth, date of death, sex/gender, age) will be securely stored on the password protected Ripple platform, which is an online platform managed by Western University's BrainsCAN program. Only the researchers of this study and the BrainsCAN coordinator(s), who administers the database system, will have access to your identifiable information as stated above.

The study data could be published in specialized medical journals or shared with others during scientific meetings, but it will be impossible to identify you. If research results are published, your name and other personal information will not be given.

Qualified representatives of the following organizations may look at your medical/clinical study records at the site where these records are held, for quality

assurance (to check that the information collected for the study is correct and follows proper laws and guidelines).

- Representatives of Lawson Quality Assurance Education Program

- Representatives of the Western University's Health Sciences Research Ethics Board that oversees the ethical conduct of this study.

Will I know the results of my study tests?

Study findings that are relevant to patient care will be given to your doctors. A doctor who understands the study procedures and methods and limitations of the study will interpret the findings and discuss these with you or your family. The test results may either be in alignment with other clinical test results or they could be inconclusive. If requested, you or your family can be sent any publications resulting from the study – in such a case, you will need to provide a mailing address. If study staff note any incidental findings, they will alert your medical care team, to examine the data and treat the findings as is medically necessary.

Whom do participants contact for questions?

If you have any questions about your rights as a research participant or the conduct of this study, you may contact the Patient Experience Office or access the online form.

Title of research project*:* Improving Diagnosis and Prognosis in Acute Brain Injury: A Multimodal Imaging Approach

If you have any questions about your rights as a research participant or the conduct of this study, you may contact The Office of Human Research Ethics. The REB is a group of people who oversee the ethical conduct of research studies. The HSREB is not part of the study team. Everything that you discuss will be kept confidential.

Consent Form

Eligible Testing Procedures:

The study team has assessed the participant's eligibility and these tests can be completed:

- ❑ fMRI
- ❑ fNIRS
- ❑ EEG

_____ _____ _____

Print Name of Research Staff Signature Date

Substitute Decision Maker Consent

Your signature on this form indicates that you are acting as a substitute decision maker(s) for the participant and the study has been explained to you and all your questions have been answered to your satisfaction. You agree to allow the person you represent to take part in the study. You know that the person you represent can leave the study at any time. You agree to the following imaging tests to be completed:

- ❑ fMRI
- ❑ fNIRS
- ❑ EEG

_____ _____ _____

Print Name of Substitute Signature Date

Decision Maker

_____

Relationship to Participant

Person Obtaining Consent:

My signature means that I have explained the study to the individual named above. I have answered all questions.

_____	_____	_____
Print Name of Person	Signature	Date

Obtaining Consent

If applicable (Substitute Decision Maker who cannot read English):
If obtaining verbal consent:

_____	_____
Name of Substitute Decision Maker	Date of Participant Verbal Consent

_____	_____	_____
Name of person obtaining consent	Signature of person obtaining consent	Date

Was the participant assisted during the consent process?

- ❑ Yes
- ❑ No

If YES, please check the relevant box and complete the signature space below:

- ❑ The person signing below acted as a translator for the participant during the consent process and attests that the study as set out in this form was accurately translated and has had any questions answered.

_____	_____	_____
Print Name of Translator	Signature	Date (DD-MM-YYYY)

Title of research project*:*	Improving Diagnosis and Prognosis in Acute Brain Injury: A Multimodal Imaging Approach

Re-Consent of Participant

At the time of enrollment into the study, you were unable to provide consent for the study and your substitute decision maker consented to your participation. You have now regained the capacity to consent and to decide whether to continue to participate in the research study.

This study has been explained to me and any questions I had have been answered.

I know that I may leave the study at any time. I agree to take part in this study.

Participant Consent:

_____	_____	_____
Print Name of Participant	Signature	Date

Person Obtaining Consent:

My signature means that I have explained the study to the participant named above. I have answered all questions.

_____	_____	_____
Print Name of Person	Signature	Date

Obtaining Consent

If applicable (Participant who cannot read English):

Was the participant assisted during the consent process?

- ❑ Yes
- ❑ No

If YES, please check the relevant box and complete the signature space below:

- ❑ The person signing below acted as a translator for the participant during the consent process and attests that the study as set out in this form was accurately translated and has had any questions answered.

_____	_____	_____
Print Name of Translator	Signature	Date (DD-MM-YYYY)

Appendix D

SPRINGER NATURE LICENSE
TERMS AND CONDITIONS

Apr 28, 2023

This Agreement between Reza Moulavi Ardakani ("You") and Springer Nature ("Springer Nature") consists of your license details and the terms and conditions provided by Springer Nature and Copyright Clearance Center.

License Number	5537730309484
License date	Apr 28, 2023
Licensed Content Publisher	Springer Nature
Licensed Content Publication	Nature Reviews Neuroscience
Licensed Content Title	The cortical organization of speech processing
Licensed Content Author	Gregory Hickok et al
Licensed Content Date	Apr 13, 2007
Type of Use	Thesis/Dissertation
Requestor type	non-commercial (non-profit)
Format	electronic
Portion	figures/tables/illustrations
Number of figures/tables/illustrations	1
Would you like a high resolution image with your order?	no

Will you be translating?	no
Circulation/distribution	1 - 29
Author of this Springer Nature content	no
Title	Shedding Light on Hearing in Coma: Investigating the Applicability of fNIRS for Assessing Auditory Processing and Aiding Prognostication in Comatose Patients
Institution name	Western University
Expected presentation date	Jun 2023
Portions	Figure 1

Curriculum Vitae

Name: Reza Moulavi-Ardakani

Post-secondary Education and Degrees:

Isfahan University of Technology
Isfahan, Iran
B.S. in Electrical Engineering, 2006-2011
Final Project: *"Design and MATLAB-Simulation of a Fluency-Aid Device for Stutterers Based on Altered Auditory Feedback"*

Sharif University of Technology
Tehran, Iran
M.A. in Philosophy of Science, 2011-2014
Thesis: *"A Critical Reading of Early Russell on Causation"*

Texas Tech University
Lubbock, TX, USA
M.S. in Physics, 2014-2017
Thesis: *"Time Reversal Invariance in Quantum Mechanics"*